OXFORD

Journal of Petrology, 2025, **66**, egaf053
https://doi.org/10.1093/petrology/egaf053
ADVANCE ACCESS PUBLICATION DATE 27 MAY 2025
Perspectives in Petrology

Melt Inclusions in High-Grade Metamorphic Rocks

BRUNA B. CARVALHO*, OMAR BARTOLI and BERNARDO CESARE

Dipartimento di Geoscienze, Università degli Studi di Padova, Via G. Gradenigo, 6, 35129 Padova, Italy

*Corresponding author. Telephone: (+39)0498279154. E-mail: bruna.borgescarvalho@unipd.it

Melt inclusions (MI) in migmatites and granulites are one of the strongest microstructural criteria for the former presence of melt in high-grade metamorphic rocks and represent fundamental repositories to retrieve the composition of anatectic magmas in the source, as well as the nature of the fluid regime during anatexis. In this 'Perspectives in Petrology' article, we review what has been done on MI in metamorphic rocks in the last 15 years, revisiting the nomenclature and the recommended practices for their successful investigation. Various examples of metamorphic minerals hosting MI are presented, but the main focus is on garnet. Why garnet? Using phase equilibrium modelling, we explore the advantages of this mineral as the ultimate MI host in metamorphic rocks and contemplate what MI teaches us about garnet's suprasolidus behaviour. MI commonly form clusters in the internal part of migmatitic and granulitic garnet, in contrast to phase equilibrium predictions that would indicate the beginning of garnet formation under subsolidus conditions. We present two alternative explanations (growth of garnet highly overstepped vs. complete garnet recrystallization under suprasolidus conditions), concluding that the second one is the most plausible. A complete database of major and trace elements and volatiles of anatectic MI is presented and used to discuss the fluid regime of the deep continental crust and the impact of anatexis on lithosphere differentiation. We also provide new insights into the debate 'conservation vs. depletion' of heat-producing elements (HPE) in the deep crust. Data suggest that only ultrahigh-temperature (UHT) metamorphism and formation of UHT anatectic melts may mobilize sufficient amounts of HPE, resulting in a HPE-depleted residual lower crust. Controversies on the origin of MI by partial melting of pre-existing mineral inclusions are discussed using phase equilibrium modelling. We conclude by proposing some directions to bridge the existing gaps and direct the future studies on this still promising field of research in crustal petrology.

Bruna B. Carvalho is a researcher at the University of Padova (Italy). She earned her PhD at the University of Québec at Chicoutimi (Canada) in 2016. Bruna investigates migmatites and granulites to understand anatexis and fluid regime of the deep continental crust and their impact on granite magmatism and crustal differentiation. Her main interest lies on how crustal magmas are formed and how their composition (major, trace and volatile elements) may change before segregation from the source to form plutons.

Omar Bartoli is an associate professor in Petrology at the University of Padova (Italy). He obtained his PhD at the University of Parma (Italy) in 2012. His work aims at understanding the impact of high-grade metamorphism and granite magmatism on crustal differentiation. The Ivrea-Verbano Zone (NW Italy) is his favourite playground for ongoing studies. Omar is a passionate garnet lover.

Bernardo Cesare is a professor in Petrology at the University of Padova, where he earned his PhD in Earth Sciences in 1992. His works deal with metamorphic petrology, low-pressure – high-temperature metamorphism and anatexis of metapelites; melt and fluid inclusions studies and fluid–rock interactions in graphitic pelites; petrologic mineralogy with special interest in biotite and garnet; alpine metamorphism, geology and geochronology in the eastern Alps (Italy) and in the Betic Cordillera (Spain); Science and Art through rock photomicrography.

Key words: anatectic melts; garnet; high-grade metamorphic rocks; melt inclusions; radiogenic heating

INTRODUCTION AND BACKGROUND

Since the 19th century (Sorby, 1858) melt inclusions (MI), droplets of melt trapped during the growth of minerals from a magma, are recognized as key tools for reconstructing the composition of magmas, their volatile budget and the evolution of igneous systems. Accordingly, there is a considerable literature devoted to review their occurrence, nature, geological significance, as well as the main protocols used to study and characterize them (Roedder, 1979, 1984; Lowenstern, 1995; Frezzotti, 2001; Webster, 2006; Audétat & Lowenstern, 2014; Rose-Koga *et al.*, 2021 and references therein). Melt and fluid inclusions can be called primary and secondary inclusions depending on the timing of entrapment (Bodnar, 2003; Hollister & Crawford, 1981; Roedder, 1984). These different types of inclusions can be determined microstructurally and provide different petrological information. Primary inclusions are entrapped during host mineral growth and may display zonal arrangements or occur as isolated clusters in the host. In contrast, secondary inclusions are formed at any time after host formation

RECEIVED NOVEMBER 8, 2024; **REVISED** MAY 19, 2025; **ACCEPTED** MAY 21, 2025

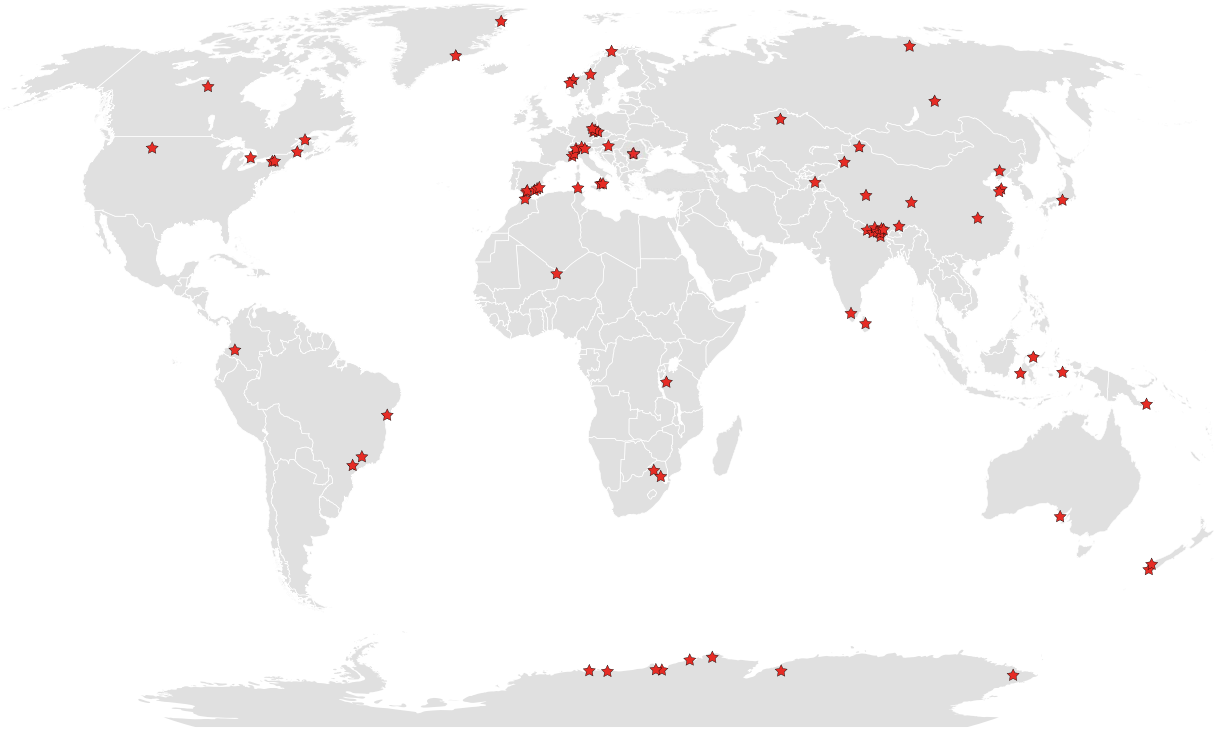

Fig. 1. (a) Global distribution of anatectic MI reported in high-grade metamorphic rocks. Details on the references are presented in Table 1.

and represent former fluids/melts that entered the fractures in the host mineral. After the fracture healing, secondary inclusions form linear trails. Our attention is focused on 'primary' inclusions, i.e. trapped during growth of their mineral host.

In metamorphic rocks, the first unequivocal example of silicate MI in granulitic garnet was reported only in 1990, in a conference abstract by Hartel *et al.* (1990) at the Geological Association of Canada—Mineralogical Association of Canada meeting. Soon after, Cesare *et al.* (1997) also described the presence of glassy MI in all minerals in metapelitic xenoliths from El Hoyazo, Spain. Both works interpreted the inclusions as melt droplets trapped during anatexis (i.e. during partial melting), highlighting their great potential as petrological tools. After these first steps, the subsequent MI studies remained mostly focused on crustal xenoliths (Frezzotti *et al.*, 2004; Chupin *et al.*, 2006), whereas the most targeted inclusions in exposed metamorphic rocks were the so-called multiphase solid inclusions, which were used to shed light on the nature of fluids in subduction zones (Philippot, 1993; Philippot *et al.*, 1995; Fu *et al.*, 2003; Ferrando *et al.*, 2005; Hermann *et al.*, 2006; Korsakov & Hermann, 2006; Malaspina *et al.*, 2006; Frezzotti & Ferrando, 2007; Zhang *et al.*, 2008). For a novel approach to investigate, this type of inclusions we refer the reader to Maffeis *et al.* (2021).

Despite previous reports of MI in regionally metamorphosed terranes (Korsakov & Hermann, 2006), the research on MI in migmatites and granulites only took a leap when Cesare *et al.* (2009a) showed the presence of MI containing both glass and its crystallized counterpart—a cryptocrystalline aggregate of feldspar, quartz and micas—in granulitic garnet from the Kerala Khondalite Belt (India). Because the composition of the glass was granitic and the assemblage found in the crystallized inclusions was quartzo-feldspathic, the authors named these MI '*nanogranites*'. For the sake of clarity, it should be mentioned that despite the microscale size of the inclusions and their crystals, the term '*microgranite*' was already widely used to characterize microcrystalline rocks of granitic composition. Notably, in the term 'nanogranite', the adjective 'nano' refers to the grain size of crystals inside these crystallized MI, which is commonly micrometric (few μm) to submicrometric (hundreds of nm).

Soon after, MI in migmatites and granulites were recognized as one of the strongest microstructural pieces of evidence for the presence of former melt in high-grade rocks (Cesare *et al.*, 2011, 2015; Holness *et al.*, 2011; Ferrero *et al.*, 2012; Bartoli *et al.*, 2016a; Ferrero & Angel, 2018; Bartoli, 2021a), becoming fundamental tools in crustal petrology. Up to now, over one-hundred localities around the globe, with ages from Mesoarchean to Pleistocene, in different tectonic settings, protoliths and P–T–fluid conditions of anatexis have been reported to contain anatectic MI (Figs 1 and 2; Table 1). However, only a quarter of those works were dedicated to the geochemical investigation of the inclusions, as it is a time-consuming approach that often requires the experimental re-homogenization of crystallized inclusions (Bartoli *et al.*, 2013a; Ferrero *et al.*, 2018) and the use of high-resolution, cutting-edge microanalytical techniques. To date, among the works that followed these procedures to recover original composition of the inclusions 17 were focused on sedimentary-derived protoliths, 6 on mafic or ultramafic protoliths and only 2 on granitic protoliths.

As the number of studies increased and the composition of the MI were demonstrated to extend from granite to trondhjemite, granodiorite and tonalite, the term '*nanogranite*' evolved to '*nanogranitoid*' (hereafter NI; see the reviews of Cesare *et al.*, 2015; Bartoli *et al.*, 2016a) and the latter remains as preferred term. It must be noted that although most of the MI found in anatectic rocks are silicic in composition, one case study by Ferrero *et al.* (2016a) demonstrated that carbonatitic MI can also be found in high-grade metamorphic rocks. As a consequence, the term '*nanorocks*' was coined by Bartoli & Cesare (2020) as a comprehensive name for crystallized melt inclusions (MI) of silicic to carbonatitic composition.

Table 1: Occurrences where anatectic MI have been reported (modified after Cesare *et al.*, 2015).

Locality	P (GPa)	T (°C)	Age (Ma)	Rock type	Protolith	Host	MI	FI	Fluid	Geoch. data	Reference
Volcano (Italy)	0.35–0.55	980–1100	<0.09	Quartz xenoliths	Sedimentary rock	Quartz	x			Y	Frezzotti *et al.* (2004)
Lipari (Italy)	0.4–0.45	725–900	0.223–0.127	Felsic granulite (xenolith)	Sedimentary rock	Garnet/Cordierite	x				Cesare *et al.* (2011); Di Martino *et al.* (2011)
Papua New Guinea UHP Terrane	>2.5	825–865	3	Al-rich protolith	Mafic rock	Garnet	x				Baldwin*et al.* (2021)
Thai and Cambodian gem fields	2	>850	3	Eclogite	Mafic rock	Ruby	x				Palke *et al.* (2018)
Mercaderes-Rio Ayo (Colombia)	1.6–1.9	960–1150	5	Mafic granulite	Mafic rock	Garnet, rutile, plagioclase	x			Y	Gianola *et al.* (2023)
Bakony-Balaton Highland (Hungary)	1.2	850–930	8	Mafic granulite	Mafic rock	Clinopyroxene/Garnet/ Ilmenite	x			Y	Németh *et al.* (2021)
Mar Menor (Spain)	0.2–0.3	850–900	9.6	Metapelitic enclave	Sedimentary rock	Cordierite/Plagioclase/ Garnet/Spinel/Andalusite	x				Cesare *et al.* (2008); Álvarez-Valero & Kriegsman (2008); Álvarez-Valero & Kriegsman (2010)
El Hoyazo—Mazarrón (Spain)	0.6	850	9.6	Metapelitic enclave	Sedimentary rock	Garnet/Plagioclase/ Cordierite/Spinel/ Andalusite/Apatite	x	x	COH-N	Y	Cesare *et al.* (1997); Cesare & Maineri (1999); Cesare & Gómez-Pugnaire (2001); Cesare *et al.* (2003a); Cesare *et al.* (2003b); Cesare *et al.* (2005); Álvarez-Valero *et al.* (2005); Álvarez-Valero *et al.* (2007); Acosta-Vigil *et al.* (2007); Cesare *et al.* (2007); Cesare *et al.* (2008); Acosta-Vigil *et al.* (2010); Álvarez-Valero & Kriegsman (2010); Cesare & Acosta-Vigil (2011); Acosta-Vigil *et al.* (2012); Ferrero *et al.* (2011)
La Galite, Maghrebian basement (Tunisia)	0.55	780	12	Felsic granulite	Granitoid	Garnet	x	x	COH-N	Y	Ferrero *et al.* (2014); Ferrero *et al.* (2024)
Higher Himalaya Crystalline (Tibet, China)	0.77–0.82	720–735	16–13	Metapelitic gneiss	Sedimentary rock	Garnet/Monazite	x				Ji *et al.* (2023)
Ama Drime Massif (Nepal)	2	730–770	17–14	Eclogite	Mafic rock	Garnet	x				Liu *et al.* (2023)
Seram (Eastern Indonesia)	0.8	950	16	Felsic granulite	Sedimentary rock	Garnet	x				Pownall *et al.* (2019)
W Sulawesi (Indonesia)	0.8	>700	16	Metapelitic granulite	Sedimentary rock	Garnet	x				Hartel *et al.* (1990)
Central Himalaya	0.7–0.8	880–1000	17–15	Metapelitic granulite	Sedimentary rock	Garnet	x				Zhang *et al.* (2024)
Mugu Karnali transect (Nepal)	1	750	17	Migmatite	Sedimentary rock	Garnet	x				Iaccarino *et al.* (2017)
Nyalam transect (Nepal)	1	700	19	Metapelitic migmatite	Sedimentary rock	Garnet	x				Wang *et al.* (2015)
Kathmandu Nappe, Langtang–Gosainkund–Helambu regions (Nepal)	0.78	780	20–18	Metapelitic migmatite	Sedimentary rock	Garnet	x				Rappa *et al.* (2016)
SE Pamir (Tajikistan)	1.5	1000	18–22	Mafic granulite	Mafic rock	Garnet/Scapolite/ Clinopyroxene/Zircon/ Apatite/Plagioclase	x	x	CO2-rich	Y	Madyukov *et al.* (2011)
Nyalam Valley in the Greater Himalayan Sequence (China)	0.6	725	26–21	Metapelitic migmatite	Sedimentary rock	Garnet/ Zircon	x				Meng *et al.* (2021)
Budhi Gandaki, Manaslu (Nepal)	0.8	700	27–25	Metapelitic migmatite	Sedimentary rock	Garnet	x				Shrestha *et al.* (2019)
Modi Khola Valley (Nepal)	1.1	700	28	Metapelitic migmatite	Sedimentary rock	Garnet	x				Shrestha *et al.* (2020)
Gyirong-Syabrubensi-Langtang transect (Nepal)	0.6–1.2	640–710	29	Metapelitic migmatite	Sedimentary rock	Garnet	x				Khanal *et al.* (2020)
Kangchenjunga (Nepal)	0.74–1.02	680–770	30	Metapelitic migmatite	Sedimentary rock	Garnet	x				Mosca *et al.* (2012)
Barun Gneiss (Himalayas)	0.8	830	30	Migmatite	Sedimentary rock	Garnet	x			Y	Ferrero *et al.* (2012), Groppo *et al.* (2012)
Dinggye, Tibetan Himalaya	1	750–830	30	Migmatite	Sedimentary rock	Monazite	x				Wang *et al.* (2017)
Main Central Thrust Zone (Nepal)	1.1	795	35–13	Migmatite	Sedimentary rock	Garnet	x				Liu *et al.* (2022)
Gruf Complex	0.9	900	33	Granulite	Sedimentary rock	Garnet/Sapphirine	x	x	COH-N	Y	Gianola *et al.* (2021)
Kali Gandaki (Himalayas)	1.05	650–720	38.5	Migmatite	Sedimentary rock	Garnet	x			Y	Bartoli *et al.* (2019); Carosi *et al.* (2015)
Higher Himalaya Crystalline	1.5–1.7	805–840	40–7	Garnet amphibolite	Mafic rock	Garnet	x				Kang *et al.* (2020)
Namche Barwa Complex (Eastern Himalaya)	1.3–1.6	825–900	40	Paragneiss	Sedimentary rock	Garnet	x			Y	Liu *et al.* (2023b)
Yogo Gulch, Montana (USA)	1.2–2.0	811–857	48.4	Al-rich protolith	Mafic rock	Sapphire	x				Palke *et al.* (2016)

Table 1: Continued

Locality	P (GPa)	T (°C)	Age (Ma)	Rock type	Protolith	Host	MI	FI	Fluid	Geoch. data	Reference
Ryoke Belt (Japan)	0.4–0.6	700–750	90	Metapelitic migmatites	Sedimentary rock	Zircon	x				Kawakami *et al.* (2013)
Western Fiordland Orthogneiss (New Zeland)	1.8–2.0	895	125–115	Migmatitic orthogneiss	Granitoid	Garnet	x				Miranda & Klepeis (2016)
Pembroke Valley, Fiordland (New Zealand)	0.8	675–720	126–119	Mafic granulite	Mafic rock	Hornblende	x				Daczko *et al.* (2016); Stuart *et al.* (2018)
Dabie Orogen (China)	3.8–4	800–850	226	Eclogite, Paragneiss	Sedimentary rock	Garnet/Zircon/Epidote	x				Malaspina *et al.* (2006); Liu *et al.* (2013); Liu *et al.* (2014); Gao *et al.* (2014); Chen *et al.* (2015); Liu *et al.* (2020);
Donghai, Sulu (China)	3.5–4.0	>850	230	Quartzite and eclogite	Sedimentary rock	Garnet/Kyanite	x				Ferrando *et al.* (2005)
Sulu Orogen (China)	2.4–3.0	650–830	230	Eclogite, Migmatite, Quartzite	Sedimentary rock	Garnet/Omphacite/ Zircon/ Monazite	x				Zeng *et al.* (2009); Chen *et al.* (2013); Chen *et al.* (2014); Li *et al.* (2016); He *et al.* (2022); Fei & Liu *et al.* (2022)
Jubrique, Betic Cordillera (Spain)	1.3	850	287	Migmatite	Sedimentary rock	Garnet	x	x	CO_2-rich	Y	Barich *et al.* (2014); Massonne (2014); Acosta-Vigil *et al.* (2016)
Ivrea-Verbano Zone (NW Italy)	0.5–1.1	800–900	280	Migmatite	Sedimentary rock	Garnet/Monazite	x	x	COH-N	Y	Bea & Montero (1999); Carvalho *et al.* (2019); Bartoli & Carvalho (2021); Carvalho *et al.* (2023a)
Istán, Ronda (Spain)	0.3–0.35	675–685	280–290	Migmatite	Sedimentary rock	Garnet	x				Acosta-Vigil *et al.* (2014)
Altai orogenic belt (China)	0.8	980	284.1	Metapelitic granulite	Sedimentary rock	Garnet	x				Liu *et al.* (2020)
Ojén, Ronda (Spain)	0.45–0.5	660–780	286	Migmatite	Sedimentary rock	Garnet	x			Y	Cesare & Acosta-Vigil (2011); Bartoli *et al.* (2013a); (2013b); (2013c); (2014); Bartoli *et al.* (2016a); Tacchetto *et al.* (2021)
Tianshan Migmatite Complex (China)	0.47–0.8	682–763	290–270	Mafic migmatite	Mafic rock	Zircon	x				Xia *et al.* (2014)
Valpelline series (Italy)	0.6–0.8	750–850	290–300	Metapelitic migmatite	Sedimentary rock	Garnet	x				Callegari (2018)
Central Rhodope (Bulgaria)	-	-	300	Metapelitic migmatite	Sedimentary rock	Garnet	x				Georgieva *et al.* (2005)
Beni Bousera (Marocco)	1–1.3	900–950	300	Migmatite	Sedimentary rock	Garnet	x				Álvarez-Valero *et al.* (2014); Rossetti *et al.* (2020)
Oberpfalz area (Bohemian Massif)	0.65	800	325	Migmatite	Sedimentary rock	Garnet	x	x	COH-N	Y	Ferrero *et al.* (2016a)
Ulten zone (Italy)	<1	<900	330	Migmatite	Sedimentary rock	Garnet	x				Dalla Brida (2019)
Bavarian Unit (Bohemian Massif)	0.6	870	335	Paragneisse	Sedimentary rock	Garnet	x				Ferrero *et al.* (2019)
Blansky Lés (Bohemian Massif)	2.25	950	335	Felsic granulite	Granitoid	Garnet	x				Ferrero *et al.* (2019)
Hartsteinwerk loja quarry (Bohemian Massif)	0.75	775	335	Paragneiss	Sedimentary rock	Garnet	x				Ferrero *et al.* (2019)
Ktis (Bohemian Massif)	1.8	800	335	Paragneiss	Sedimentary rock	Garnet	x	x	COH-N		Ferrero *et al.* (2019)
Mohsdorf (Bohemian Massif)	1.6	1000	335	Felsic granulite	Granitoid	Garnet	x				Ferrero *et al.* (2019)
Plaimberg (Bohemian Massif)	4.5	1000	335	UHP eclogite	Mafic rock	Garnet	x				Ferrero *et al.* (2019)
Saidenbach (Bohemian Massif)	4.5	1000	335	Felsic granulite	Sedimentary rock	Garnet	x				Stöckhert *et al.* (2001)
Steinaweg (Bohemian Massif)	1.85	825	335	Felsic granulite	Granitoid	Garnet	x				Ferrero *et al.* (2019)
Stuckestein (Bohemian Massif)	0.6	800	335	Migmatite	Sedimentary rock	Garnet	x	x	COH-N		Ferrero *et al.* (2019)
T7 borehole (Bohemian Massif)	4.5	1000	335	Felsic granulite	Sedimentary rock	Garnet	x				Kotkova *et al.* (2014)
Gföhl Unit (Bohemian Massif)	1.5–2.3	800–1000	335–345	Felsic granulite	Sedimentary rock	Garnet	x				Yang *et al.* (2023)
Erzgebirge (Bohemian Massif)	4.5	1000	340	Eclogite, Pyroxenite	Sediment/Mafic rock	Garnet	x			Y	Hwang *et al.* (2001); Stöckhert *et al.* (2001); Stöckhert *et al.* (2009); Borghini *et al.* (2023)
Granulitgebirge (Germany)	2.1	1000	340	Eclogites	Sediment/Mafic rock	Garnet	x			Y	Borghini *et al.* (2018), Borghini *et al.* (2020), Borghini *et al.* (2024)
N Bohemian Massif	-	-	340	UHP Felsic Granulite	Sedimentary rock	Garnet	x				Kotkova *et al.* (2014)
Orlica-Śnieżnik Dome (Bohemian Massif)	2.7	875	340	Felsic granulite	Granitoid	Garnet	x			Y	Ferrero *et al.* (2015)
Drosendorf unit (Bohemian Massif)	0.95–1.1	745–785	343	Paragneiss	Sedimentary rock	Garnet	x				Sorger *et al.* (2020)
NE Greenland	3.6	960	350–360	UHP metapelites	Sedimentary rock	Garnet	x				Lang & Gilotti (2007)
Central Maine terrane (USA)	1.8	1050	379	Felsic granulite	Sedimentary rock	Garnet	x				Axler & Ague (2015), Ferrero *et al.* (2021b)
Gory Sowie (Bohemian Massif)	0.75	950	400	Felsic granulite	Granitoid	Garnet	x				Barnes *et al.* (2022); Słupski *et al.* (2018)
Svartberget, Western Gneiss Region (Norway)	3	750–800	400	UHP Paragneiss	Sedimentary rock	Garnet	x				Ganzhorn *et al.* (2014)

Table 1: Continued

Locality	P (GPa)	T (°C)	Age (Ma)	Rock type	Protolith	Host	MI	FI	Fluid	Geoch. data	Reference
Heia, Artic Caledonides (Norway)	3.7–3.8	840–870	400	UHP Paragneiss	Sedimentary rock	Garnet	x	x	COH-N		Janák *et al.*, 2024
Ulsteinvik metapelite, Western Gneiss Region (Norway)	1	700	400	Paragneiss/Eclogite	Sedimentary rock	Garnet	x				March *et al.* (2022)
Tongbai orogen (China)	0.9–1.1	840–980	440	Felsic granulite	Sedimentary rock	Garnet	x				Zhang *et al.* (2020)
Seve Nappe Complex (Scandinavian Caledonides)	4	835	455	Paragneiss	Sedimentary rock	Garnet	x	x	COH-N		Klonowska *et al.* (2017); Słupski (2023)
Mont Albert Ophiolitic Complex (Canada)	1	850	456	Metapelitic migmatite	Sedimentary rock	Garnet	x				Dubacq *et al.* (2019)
Dulan eclogite-gneiss terrane (China)	1.4–1.8	800–950	470–420	Mafic granulite	Mafic rock	Garnet	x				Yu *et al.* (2019)
South Altyn Tagh (China)	1.7–2.5	710–850	500–486	Mafic granulite	Mafic rock	Garnet	x				Dong *et al.* (2020)
Edixon Metamorphic Complex (Antarctica)	0.8	760	515	Schists	Sedimentary rock	Garnet	x	x	COH-N	Y	Ferri *et al.* (2020)
Kulappara, Kerala Khondalite Belt (India)	0.5	>800	525	Leucocratic vein in UHT migmatite	-	Garnet	x				Harley & Nandakumar (2014)
Kerala Khondalite Belt (India)	0.6	900	525	Migmatite, Felsic Granulite	Sedimentary rock	Garnet/Zircon	x			Y	Cesare & Acosta-Vigil (2011); Cesare *et al.* (2009a); Ferrero *et al.* (2012)
Kokchetav Massif (Kazakhstan)	4.75	975	530	Paragneiss/Eclogite	Sedimentary rock	Garnet	x			Y	Korsakov & Hermann (2006); Stepanov *et al.* (2016)
Dronning Maud Land (Antarctica)	1.55	910	542	Mafic granulite	Mafic rock	Garnet	x			Y	Ferrero *et al.* (2019)
Mather Pensinula (Antarctica)	0.75	850–950	530	Mg-rich granulite	Sedimentary rock	Garnet	x	x		Y	Liu *et al.* (2023a)
Rundvågshetta, Lützow-Holm Complex (Antarctica)	0.8	1000	550	Mg-Al metapelitic granulite	Sedimentary rock	Garnet	x	x		Y	Hiroi *et al.* (2019); Carvalho *et al.* (2023b)
Wanni Complex (Sri Lanka)	0.4–0.6	600–840	560	Metapelitic granulite	Sedimentary rock	Garnet	x				Hirayama *et al.* (2020)
Sør Rondane Mountains (Antarctica)	1.2	900	570	Metapelitic gneiss	Sedimentary rock	Garnet	x				Higashino & Kawakami (2022)
Austhovde, Lützow-Holm Complex (Antarctica)	0.7	800	580	Mafic granulite	Mafic rock	Garnet	x				Hiroi *et al.* (2023)
Central Hoggar (Algeria)	0.55–0.6	800–820	580	Metapelitic Migmatite	Sedimentary rock	Garnet	x				Arab *et al.* (2021)
Ribeira Fold Belt (Brazil)	0.8	850	590–563	Metapelitic Migmatite	Sedimentary rock	Garnet	x	x	COH		Dos Santos *et al.* (2011)
Highland Complex (Sri Lanka)	0.9	950	600–500	Metapelitic granulite	Sedimentary rock	Garnet	x				Hiroi *et al.* (2014); Hiroi *et al.* (2020)
Andrelandia Nappe (Brazil)	1.3	800	618	Metapelitic granulite	Sedimentary rock	Garnet	x	x			Li *et al.* (2021)
Alogonquin Terrane, Greenville Province (Canada)	1.3	920	1100	Eclogite	Mafic rock	Garnet	x				Cao *et al.* (2021)
Gore Mountains, Adirondacks (USA)	1	950	1050	Mafic granulite	Mafic rock	Garnet	x			Y	Darling *et al.* (1997), Ferrero *et al.* (2021), Wannhoff *et al.* (2022)
Hooper Mine, Adirondacks (USA)	1	940	1100	Mafic granulite	Mafic rock	Garnet	x				Ferrero *et al.* (2023)
Port Leyden (USA)	0.66	850	1145	Paragneiss	Sedimentary rock	Garnet	x				Darling (2013)
Black Point, Sleaford Complex (Australia)	0.7–0.9	850	1745	Metapelitic granulite	Sedimentary rock	Garnet	x				This study
Anabar and Aldan Shields, Siberia (Russia)	0.6–0.8	850–950	1800	Metapelitic granulite	Sedimentary rock	Zircon/Kyanite/ Quartz/Garnet	x				Chupin *et al.* (1993)
Alxa Block, North China Craton	0.85–1.0	880–950	1810–1700	Mafic granulite	Mafic rock	Garnet	x				Zou *et al.* (2024)
South Liaohe Group (China)	0.96–1.1	700–750	1880–1820	Metapelitic granulite	Sedimentary rock	Garnet/Monazite	x				Liu *et al.* (2019)
Usagaran belt (Tanzania)	1.5–1.9	750–800	1991	Paragneiss	Sedimentary rock	Garnet	x	x	COH-N	Y	Herms *et al.* (2023)
Salvador-Esplanade Belt (Brazil)	0.7	840–900	2008	Metapelitic granulite	Sedimentary rock	Garnet	x				Goncalves *et al.* (2021)
Athabasca granulite terrane (Canada)	1	875	2580	Felsic granulite	Sedimentary rock	Garnet	x	x	COH-N		Tacchetto *et al.* (2019)
Limpopo belt	1.1	875	2705	Granitoid, Quartzite	Sedimentary rock	Garnet	x	x	COH		Chupin *et al.* (1998), Safonov *et al.* (2020)
Kangerlussuaq basement (Southeast Greenland)	0.7	825	2800	Metapelitic migmatite	Sedimentary rock	Garnet	x	x	COH		Nicoli *et al.* (2022)
Napier Complex (Antarctica)	1	1000	2800	Metapelitic granulite	Sedimentary rock	Garnet	x				Carvalho unpublished
Barberton Grenstone Belt (South Africa)	1.2	800–850	3200	Mafic granulite	Mafic rock	Garnet	x				Bartoli unpublished

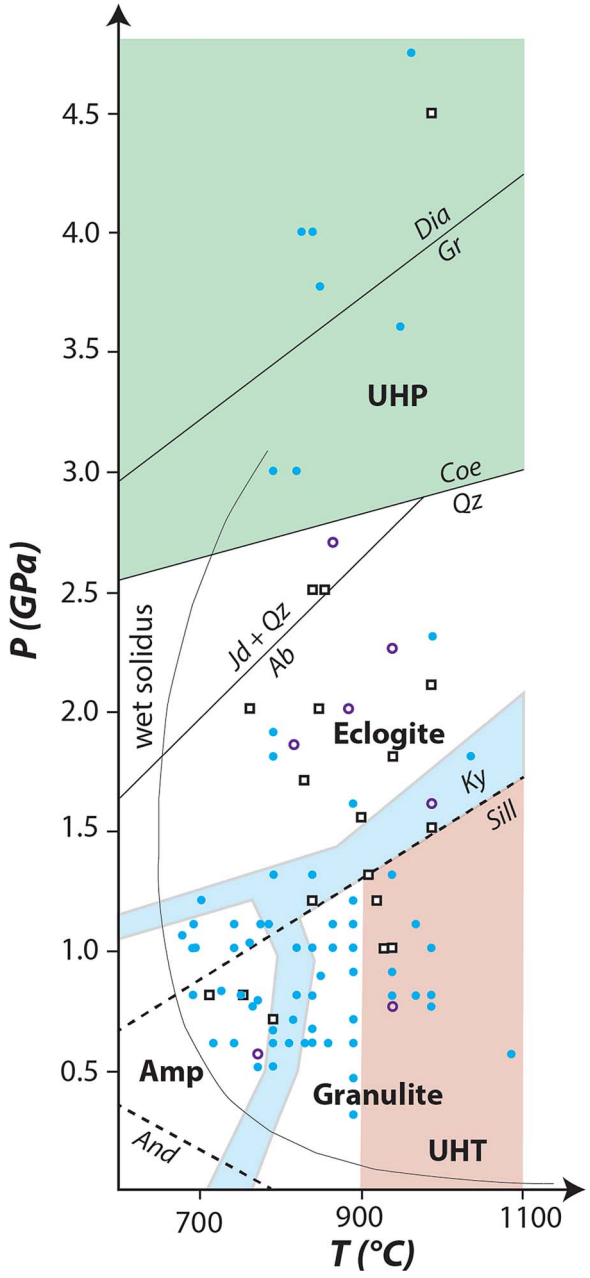

Fig. 2. Pressure–temperature (P–T) diagram depicting the estimated conditions of rocks with anatectic MI from the literature (squares = mafic protoliths; circles = metasedimentary protoliths; empty circles = granitic protoliths). Field of amphibolite (Amp) facies, granulite facies, eclogite facies, ultrahigh temperature (UHT) and ultrahigh pressure (UHP) metamorphism are also highlighted for clarity. Details on the references are presented in Table 1.

Other terms such as '*multiphase solid inclusions*', '*multiphase inclusions*' and '*multiphase fluid inclusions*' (MFI) have also been used to describe polycrystalline inclusions in metamorphic rocks. The term '*multiphase solid inclusions*' (MSI) is most widely used in the literature regarding high pressure to ultrahigh-pressure rocks and denotes 'mineral inclusions that consist of more than one solid mineral phase, with or without a vapour or fluid phase' (Gao *et al.*, 2017). Depending on the work, MSI are interpreted in different ways, among others as being the product of crystallization of anatectic melts or of supercritical fluids (Ferrando *et al.*, 2005; Hermann *et al.*, 2006, 2013; Korsakov & Hermann, 2006; Frezzotti & Ferrando, 2007, 2015; Gao *et al.*, 2013, 2017; Maffeis *et al.*, 2021 and references therein). Conversely, 'multiphase fluid inclusions' and simply 'multiphase inclusions' refer to former fluid inclusions containing, at ambient conditions, both solids and fluids, and usually the fluid is predominant over the solids (Carvalho *et al.*, 2019, 2020, 2023a; Tacchetto *et al.*, 2019; Safonov *et al.*, 2020; Gianola *et al.*, 2021; Bartoli, 2021a; Herms *et al.*, 2023; Liu *et al.*, 2024). In the latter case, the solids are usually 'step-daughter' minerals, i.e. formed from the reaction between the fluid and the host mineral (Roedder, 1984). Given the above somewhat confusing use of different terms to indicate the same microstructures, and the twofold—melt- vs. fluid-dominated—origin of polycrystalline inclusions in high-grade rocks, we propose to use the term nanogranitoid (NI) for all inclusions derived from original droplets of melt, and multiphase fluid inclusions for inclusions that trapped a fluid. A fundamental and easily detectable difference between the two inclusion types is their very different porosity (i.e. volume of inclusion occupied by residual fluid; see more details below), reflecting the contrasting primary volatile contents. When discussing MI in metamorphic rocks, it is important to recall that what happens in the inclusion, mechanically shielded by the host and ideally behaving as an isochoric system, is related to the P–T path of the rock only as concerns the variations of temperature, with pressure behaving as a dependent variable. Therefore, during isobaric cooling of the host rock, the pressure in the MI will decrease, and during near isothermal decompression of the rock, the pressure in the MI will remain approximately constant.

Many fundamental concepts on MI in high-grade metamorphic rocks have been detailed in previous works (Cesare *et al.*, 2011, 2015; Frezzotti & Ferrando, 2015; Bartoli *et al.*, 2016a; Ferrero & Angel, 2018; Bartoli & Cesare, 2020). In this 'Perspectives in Petrology', we provide a review of what has been done on the topic in the last 15 years, revisiting the recommended practices for their investigation, but also focusing on the newest advances on the subject. We also provide the most recent database of major, trace, H_2O and CO_2 contents of anatectic MI. In the discussion, some controversies on the subject are explored. Finally, we propose some directions to bridge the existing gaps and direct the future of this still promising field of research in crustal petrology.

MELT INCLUSIONS IN METAMORPHIC MINERALS

Most literature defines MI as 'droplets of melt trapped in minerals during their growth in a magma' (Audétat & Lowenstern, 2014). This definition is accurate for magmatic rocks, in which the host mineral crystallizes from the magma at any time during its cooling. As a consequence, the MI preserve a wide range of compositions. For instance, MI in early crystallizing minerals from a magma will record more primitive compositions, whereas those in late crystallizing minerals will track the evolved magma (Frezzotti, 2001). Conversely, in anatectic metamorphic rocks, the MI are trapped during the crystallization of minerals in the presence of melt and not (necessarily) from it. To account for this dual origin of MI, Cesare *et al.* (2015) proposed an adaptation to the definition as 'small droplets of melt that are trapped in minerals during their growth or recrystallization in the presence of a melt phase.'

In principle, any mineral crystallizing from or in the presence of melt/magma has the potential to trap and eventually preserve the melt as inclusions. Entrapment of MI is usually favoured by the rapid growth of the host, the presence of fine-grained solids

(e.g. accessory minerals like apatite, zircon, graphite and rutile) in the matrix (see more about accidentally trapped phases below), and by local growth imperfections that create embayments on the advancing crystal faces (Roedder, 1979; Acosta-Vigil *et al.*, 2007; Ferrero *et al.*, 2012).

Most MI in high-grade rocks are hosted in peritectic minerals, the solid phases that grow together with the melt as a result of incongruent partial melting reactions. Therefore, in the following text, 'metamorphic mineral' will refer specifically to the minerals that grow at suprasolidus conditions in metamorphic rocks.

Bulk composition and P–T conditions of melting will define the growing peritectic mineral, and some of the most common simplified reactions are (abbreviations from Whitney & Evans, 2010): Ms + Qz ± Pl = melt + Kfs + Als and Bt + Pl ± Qz + Als = melt + Grt + Kfs ± Crd, in metapelites; Bt + Pl + Qz = melt + Opx + Kfs, in metagreywackes; Hbl + Qz = melt + Opx + Cpx + Pl and Hbl + Pl + Qz = Opx + Cpx ± Grt + melt, in metamafic rocks (Vielzeuf & Holloway, 1988; Waters, 1988; Spear *et al.*, 1999). Therefore, the most common peritectic minerals in crustal protoliths are K-feldspar, garnet, cordierite and orthopyroxene.

In most of the works in the literature (listed in Table 1), the entrapment of MI is inferred to occur when rocks partially melt (i.e. during the prograde path) and both melt and peritectic minerals are formed (Cesare *et al.*, 2015 and references therein). However, MI have also been interpreted to form as result of melt–rock interactions in the lithospheric mantle (Borghini *et al.*, 2018, 2020), and a recent work (Carvalho *et al.*, 2023b) has shown that MI in UHT granulites can be trapped during cooling and residuum–melt interaction (see details below). A fundamental advantage of the entrapment during heating (and not during cooling from a magma) is that the primary anatectic melt has not yet been modified by other processes (i.e. fractional crystallization, volatile degassing, entrapment of xenocrysts) and therefore, its composition is likely to remain preserved in terms of major, trace and volatile contents.

In the literature, many minerals in anatectic rocks are reported to contain MI (see Table 1 and Fig. 3). Below, we highlight some case studies.

MI with well-preserved glass are typical of anatectic xenoliths and enclaves in rapidly cooled lavas. The most studied are the metasedimentary fragments in the dacites of the Neogene Volcanic Province of SE Spain, but there are recent reports also from some pyroxenite xenoliths in the Granatifera Tuffs at Mercaderes, Colombia (Gianola *et al.*, 2023). In the crustal enclaves from El Hoyazo, glassy inclusions have been observed in garnet, biotite, plagioclase, cordierite (Fig. 3a), spinel, corundum, ilmenite, apatite, monazite and zircon (Acosta-Vigil *et al.*, 2007, 2010; Cesare *et al.*, 1997, 2003a, 2003b, 2005, 2007, 2008, 2009b, 2015; Parisatto *et al.*, 2018). Andalusite is a further host for glassy inclusions in the xenoliths at Mazarròn (Cesare *et al.*, 2003b; Fig. 3b). Glassy inclusions have been studied also in crustal enclaves in the granitoids of La Galite, Tunisia (Ferrero *et al.*, 2014) and in the granulitic xenoliths in diatreme pipes in the southeastern Pamir, Tajikistan (Chupin *et al.*, 2006, 2010; Madyukov *et al.*, 2011) and in the Aeolian Arc, Southern Italy (Frezzotti *et al.*, 2004). In the latter case, glass inclusions are hosted in quartz.

Primary MI in ilmenite were observed in the melanosome of migmatites at the contact with the Ronda peridotites (Ferrero *et al.*, 2012; Bartoli *et al.*, 2015). Displaying well-developed negative crystal shapes (i.e. bound by facets representing rational planes of the host mineral; Roedder, 1984) and completely crystallized, these MI contained quartz, plagioclase, biotite and in some cases accessory apatite (Fig. 3c).

Glassy MI have also been described in ilmenite of granulite xenoliths from the Bakony–Balaton Highland Volcanic Field (Németh *et al.*, 2021). Glassy MI containing shrinkage bubbles were detected in rutile in pyroxenite xenoliths of the lower continental arc beneath the Northern Volcanic Zone in Colombia (Gianola *et al.*, 2023; see Fig. 3d). In these case studies, MI in opaque and semi-opaque minerals were identified through careful examination with a scanning electron microscope (SEM).

Glassy MI in corundum can be found both in sapphire (Yogo Gulch, Montana, USA; Palke *et al.*, 2016) and ruby varieties (from Thailand and Cambodia; Palke *et al.*, 2018; see Fig. 3e) of lamprophyres and basalts were, for instance, used as key evidence for the xenocrystic origin of the corundum in those rocks. According to the authors, the formation of peritectic corundum in both case studies occurred by partial melting of Al-rich rocks when the hot mafic magmas ponded at the base of the continental crust (Palke *et al.*, 2018).

MI in pyroxene are common in volcanic rocks (Reubi *et al.*, 2013; Capriolo *et al.*, 2024 and many others). In contrast, despite being a regular mineral in HT-UHT rocks of both sedimentary and mafic origin, this mineral is only rarely a metamorphic MI host. Rare cases can be quoted, for instance Madyukov *et al.* (2011) and Nemeth *et al.* (2021) report glassy MI containing shrinkage bubbles in clinopyroxene from mafic granulites, and Zheng *et al.* (2009) described MI in omphacite. We speculate that a possible reason for the rare presence of MI in metamorphic pyroxenes could be due to slower growth rates of the latter compared to magmatic ones. Further research on the matter is necessary.

Monazite is an extremely valuable geochronometer, and commonly presents very complex zoning patterns that must be carefully identified to couple precise ages and metamorphic constraints (Williams *et al.*, 2022). Index mineral inclusions can help determine textural relationships to place the different domains and ages in the P–T space. Similarly, MI can be useful as they can be linked to periods at which monazite grew at suprasolidus conditions. The work of Wang *et al.* (2017) described NI with well-developed negative crystal shape in monazite, containing K-feldspar + quartz ± plagioclase ± muscovite (Fig. 3f). These NI turned out to be essential to identify subsolidus and suprasolidus domains, and to pinpoint the timing of the metamorphic peak in pelitic granulites from Dinggye, Tibetan Himalaya.

Metamorphic zircon also offers the possibility to link the geochemical composition of the melt with temporal data (Thomas *et al.*, 2003). In particular, regarding periods in which the rock record is scarce, new studies of MI in zircon can provide unique insights into the early stages of Earth's evolution. Chupin *et al.* (1998) was one of the first studies of MI in 3.4 Ga detrital zircons in quartzites, but in that case, the MI were distributed within the inherited cores but not on the metamorphic overgrowths, pointing out their magmatic origin. MI can be investigated in case studies where metamorphic peritectic zircon grows at suprasolidus conditions (either during heating or cooling). In rocks from the Ryoke metamorphic belt in Japan, Kawakami *et al.* (2013) identified a thin annulus containing MI separating inherited cores and metamorphic rims (Fig. 3g), suggesting growth at suprasolidus conditions. More recently, MI in metamorphic zircon are attracting further attention, and new geochemical data are emerging (Tedeschi *et al.*, 2024; Suzuki *et al.*, 2025).

Other examples of metamorphic minerals containing MI are sapphirine (Gianola *et al.*, 2021; Fig. 3h), scapolite (Chupin *et al.*, 2006; Madyukov *et al.*, 2011), kyanite (Chupin *et al.*, 1993), titanite (Madyukov *et al.*, 2011; Li *et al.*, 2016) and diamond (Shatsky *et al.*,

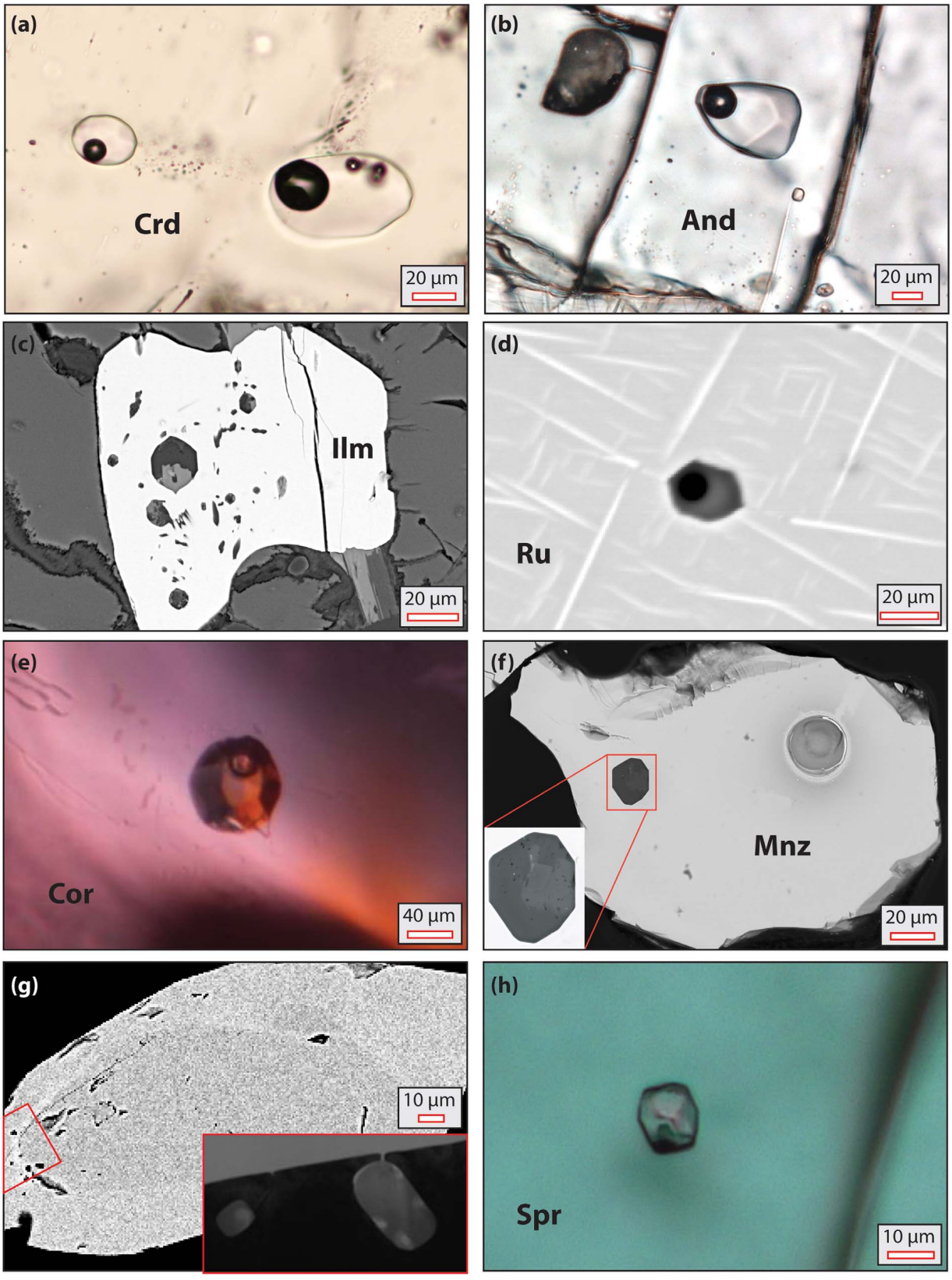

Fig. 3. Examples of MI hosted in metamorphic minerals. (a) Cluster of glassy MI hosted in cordierite in metapelitic xenoliths from El Hoyazo. (b) Glassy MI with faceted shape in andalusite in metapelitic xenoliths from Mazarrón. (c) Cluster of NI in ilmenite from Ronda migmatites (further information in Ferrero *et al.*, 2012 and Bartoli *et al.*, 2015) (d) Bubble-bearing glassy MI in rutile, from pyroxenite xenoliths at Mercaderes (photo courtesy from O. Gianola; see Gianola *et al.*, 2023 for details). (d) Glassy MI in ruby from Cambodia (photo courtesy from A. Palke; see Palke *et al.*, 2018 for more information). (f) Negative crystal shaped NI in monazite from Dinggye, Tibetan Himalaya (photo courtesy from J.-M. Wang; see Wang *et al.*, 2017 for more information). (g) BSE image of zircon containing MI in migmatite from Ryoke Belt (Japan). Inset contains a dark field TEM image depicting glassy MI the metamorphic rim (photo courtesy from T. Kawakami; for further details see Kawakami *et al.*, 2013). (h) Nanogranitoid in sapphirine from Gruf Complex (photo courtesy from O. Gianola, with Permission from John Wiley and Sons; see Gianola *et al.*, 2021 for more information).

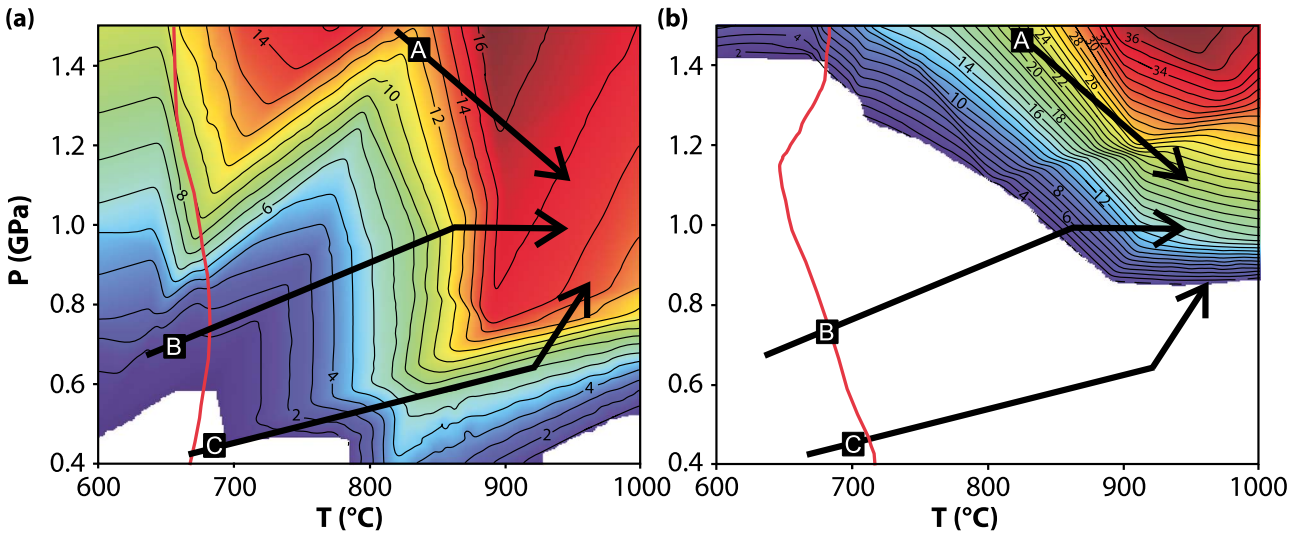

Fig. 4. Calculated isomodes (vol %) of garnet abundance for metapelite (a) and metabasite (b). Calculations were performed by Perple_X software (Connolly, 2009). See Bartoli *et al.* (2024a) and Carvalho *et al.* (2023a) for the selected thermodynamic databases and *a–x* models. Bulk rock compositions from Forshaw & Pattison (2023) and Palin *et al.* (2016). Red curve represents the solidus.

2019). Daczko *et al.* (2016) and Stuart *et al.* (2018) interpreted some polycrystalline aggregates in hornblende as former MI.

BEHAVIOUR OF PERITECTIC GARNET: THE MESSAGE FROM MELT INCLUSIONS

As noted above, any metamorphic mineral crystallizing at suprasolidus conditions has the potential to trap MI, but garnet remains the most common host overall. Garnet is a common peritectic phase in a broad variety of rock compositions, from metamorphosed basalt to metamorphosed granitoids and siliciclastic sediments, and from medium- to high- and ultrahigh-pressure and ultrahigh-temperature conditions (Baxter *et al.*, 2013). For these reasons, we dedicate a section specifically to this mineral.

Metapelite versus metabasite protoliths

Fig. 4 shows the garnet isomodes predicted by phase equilibrium modelling of the median pelite of Forshaw & Pattison (2023) and the average tholeiite of Palin *et al.* (2016). A key difference between the two rock types is the extent of the garnet stability field, much larger in metapelite. Peritectic garnet is not predicted to form at medium pressure (≤0.8–1.0 GPa) in metabasite (Fig. 4b), and this observation is valid also for other metabasic bulk compositions (Palin *et al.*, 2016; Kendrick & Yakymchuk, 2020; Roberts *et al.*, 2024). Considering the large compositional variability of metapelites (Forshaw & Pattison, 2023), it is clear that garnet and, in turn MI, may form over a wide range of P and T conditions. It follows that, since their garnet may trap inclusions of anatectic melt in a wider range of crustal P–T conditions, metapelitic rocks are better candidates for providing a wealth of information on the chemical variability of crustal melts produced in a variety of geodynamic scenarios. The wider stability of suprasolidus garnet predicted for pelitic bulk compositions also explains the much larger number of MI occurrences documented in metapelites rocks compared to metabasites (Table 1). At the same time, this should not lead one to overlook garnet in metabasites, because it could preserve MI that provide important information on lithosphere differentiation (Borghini *et al.*, 2018, 2020, 2023, 2024; Ferrero *et al.*, 2021a; Gianola *et al.*, 2023).

Most *a–x* models for minerals and melts utilized in phase equilibrium modelling of crustal rocks were formally calibrated for pressure < 1.5 GPa (Green *et al.*, 2016). Therefore, phase equilibrium predictions may not be reliable to infer garnet behaviour at higher P. However, experimental studies demonstrated the possibility to form peritectic garnet at higher pressures (Rapp & Watson, 1995) and even at UHP conditions (Auzanneau *et al.*, 2006; Hermann & Spandler, 2008), in agreement with the presence of MI in garnet from UHP rocks (Ferrero *et al.*, 2015; Stepanov *et al.*, 2016; Borghini *et al.*, 2023; Janák *et al.*, 2024).

An important implication of model predictions reported in Fig. 4a is that most UHT (>900°C) melts from metapelitic rocks are unlikely to be trapped, because a net modal increase of peritectic garnet is not expected at these extreme crustal conditions. An exception is the case of a UHT counter-clockwise P–T path at P < 0.8 GPa (path C in Fig. 4a), where most of the garnet growth occurs at T > 900°C and at moderate pressure. Such a P–T evolution has been documented in some UHT terranes (Korhonen *et al.*, 2013). The probability of trapping UHT melts is higher in metabasites (Fig. 4b), but requires greater pressures.

An alternative way to trap UHT MI is when garnet forms as result of melt-consuming reactions during cooling, as documented in Carvalho *et al.* (2023b). In metapelitic rocks from Antarctica, garnet formed via a reaction consuming melt and orthopyroxene during cooling from 1050 to 930°C, trapping melt droplets along with sapphirine + quartz aggregates and rutile grains, the latter recording Zr-in-rutile temperatures in excess of 900°C (see Carvalho *et al.*, 2023b). A process of melt–rock interaction was proposed by Borghini *et al.* (2018, 2020, 2023, 2024) to interpret the formation of MI-bearing garnet from eclogites of the Bohemian Massif. Following this interpretation, the growing garnet formed at >1000°C from interaction of an inhomogeneous peridotitic body and silicate melts derived externally from the surrounding metasediments, trapping remnants of the metasomatizing melt.

As discussed by Carvalho *et al.* (2023b), the ability of peritectic garnet to trap MI at, or near, UHT conditions may be questioned when inferred from phase equilibrium modelling, depending on which dataset is adopted. For instance, using the internally consistent thermodynamic dataset ds62 (Holland & Powell, 2011) and

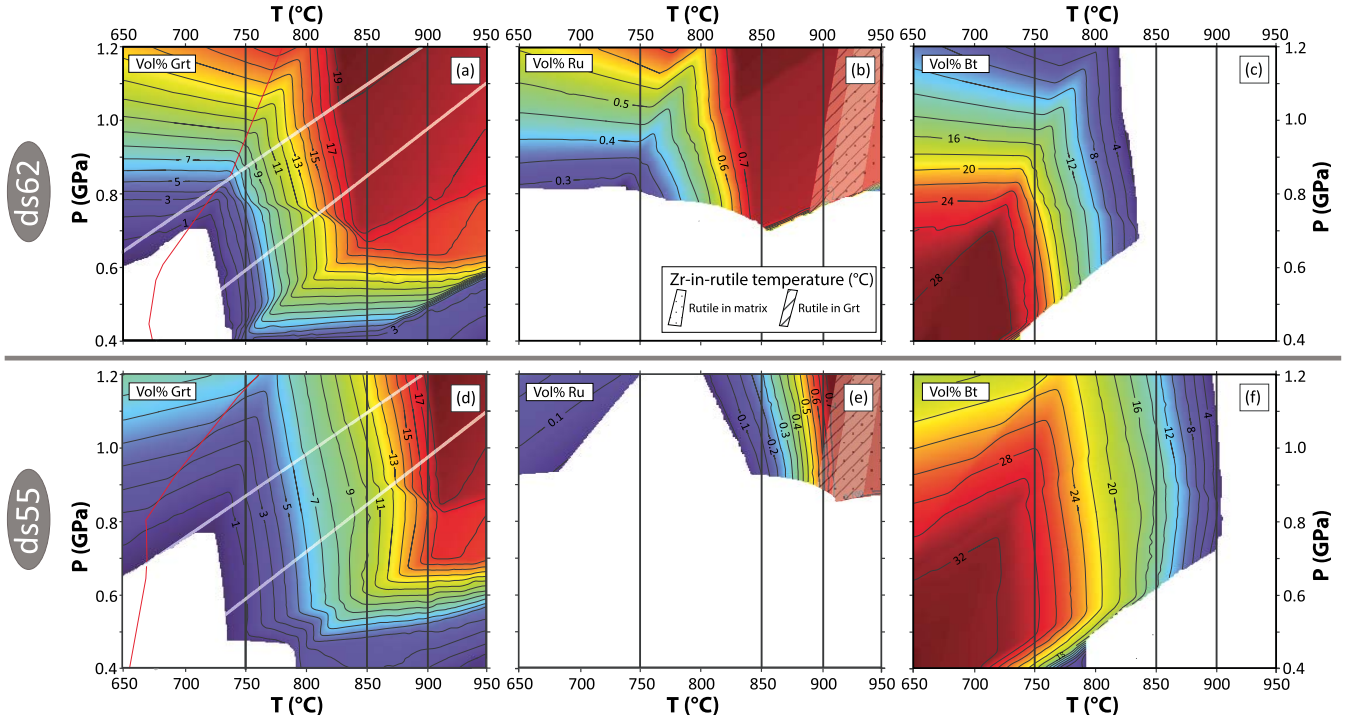

Fig. 5. Comparison between isomodes of garnet, rutile and biotite from the work of Carvalho *et al.* (2023a). Isopleths are based on P–T pseudosections derived from the two datasets ds62 and ds55 and calculated for an upper-amphibolite metapelite from Ivrea-Verbano Zone. Red curve represents the solidus, the white lines delimit the metamorphic field gradient in Val Strona (from Redler *et al.*, 2012) and Zr-in-rutile temperature are compiled from the literature.

the related *a*–*x* models (White *et al.*, 2014), one could conclude that most suprasolidus garnet in metapelite should grow between 750 and 850°C, at pressure typical of orogenic metamorphism (Fig. 5a; Yakymchuk *et al.*, 2017; Johnson *et al.*, 2021). However, using the biotite model of Tajčmanová *et al.* (2009) along with the related thermodynamic dataset ds55 (Holland & Powell, 2003), about 50% of garnet is predicted to form between 850 and 900°C, because this model stabilizes biotite at higher temperature (Fig. 5b). As the benchmark tests of Gervais & Trapy (2021) show that the biotite model of Tajčmanová *et al.* (2009) better reproduces suprasolidus equilibria of experimental metapelites, we consider its results more reliable in terms of the temperatures it provides.

Additional complexity on the stabilization of biotite at T > 900°C is given by the possible role of fluorine (Peterson *et al.*, 1991; Sun *et al.*, 2022), which cannot yet be accounted for in *a*-*x* thermodynamic models. For instance, residual biotite in pelitic granulites from the archetypal crustal section of the Ivrea-Verbano Zone (IVZ, NW Italy) contains up to 2.10 wt % F, higher than the fluorine content of biotite in melting experiments of metapelites at 975°C (Patiño-Douce & Johnston, 1991). Garnet in IVZ pelitic granulites contains primary melt and fluid inclusions along with rutile grains, recording Zr-in-rutile temperatures >900°C (Carvalho *et al.*, 2023b) and NI in these rocks were successfully rehomogenized at 900°C (Carvalho *et al.*, 2019). Therefore, all the textural and petrological constraints indicate that suprasolidus garnet in IVZ granulites formed along a prograde path at temperature > 850–900°C. The only way to reduce the mismatch between these natural occurrences and model predictions is to adopt the biotite model proposed by Tajčmanová *et al.* (2009) (Fig. 5), with the important assumption that the temperatures obtained for garnet formation are minimum values, because fluorine was not considered in phase equilibrium modelling.

Subsolidus versus suprasolidus garnet

Figure 4a poses an additional issue. In most metapelitic rocks, garnet begins to form at subsolidus conditions and, after crossing the solidus, garnet growth may continue over a prolonged temperature interval (Fig. 4a). Therefore, the suprasolidus garnet formed by incongruent melting reactions should commonly appear as overgrowths on previously formed metamorphic (i.e. subsolidus) grains. In addition, in the case of garnet growth over a prolonged temperature interval at suprasolidus conditions, MI should record the outwards entrapment of melt produced at increasing temperature (and sometimes also pressure) conditions. However, MI are generally observed throughout garnet crystals (Cesare *et al.*, 2009; Ferrero *et al.*, 2012; Borghini *et al.*, 2018; Carvalho *et al.*, 2019) or form isolated clusters in garnet core (Acosta-Vigil *et al.*, 2010; Bartoli *et al.*, 2013a, 2013b, 2013c; Ferrero *et al.*, 2014, 2015, 2023; Parisatto *et al.*, 2018), without evidence of a subsolidus core. Only Carosi *et al.* (2015) and Bartoli *et al.* (2019) reported NI systematically distributed in an intermediate annulus between core and rim in garnet from the Greater Himalayan Sequence (Nepal). Similarly, only Acosta-Vigil *et al.* (2016) documented different melt composition (coexisting with different mineral inclusions) across a single garnet grain, suggesting that growth of this garnet occurred during a protracted prograde story. On the other hand, only Stepanov *et al.* (2016) reported the presence of two compositionally different melts in two texturally distinct garnet populations (melanosome vs. leucosome) in a single rock from the Kokchetav Massif.

The majority of MI-bearing garnets in granulitic rocks, instead, do not show evidence of a core formed under sub- and/or supra-solidus amphibolite-facies conditions. An example is represented by pelitic granulites from the IVZ, where the coupling of melt and mineral inclusions occurrences (Carvalho *et al.*, 2019, 2020, 2023a) and chemical zoning of low diffusivity elements such as P and Lu

(Connop et al., 2024; Bartoli et al., 2024b) indicate that garnet grew solely under granulite-facies conditions. However, garnet is also a common phase in IVZ amphibolite-facies metapelites, considered the lower grade counterparts of the granulites.

The oddity of having MI hosted in cores of garnet for which phase equilibrium modelling would predict a subsolidus origin has been pointed out by Beyer & Chakraborty (2021). These authors proposed a process of diffusion coupled with dissolution-precipitation of new garnet crystals, which should entirely cancel the subsolidus garnet and form completely new crystals elsewhere in the rock. Alternatively, dissolution could take place randomly and irregularly as observed in experiments (Putnis, 2002) and in accessory minerals (Daczko et al., 2024 and references therein). Since the concentric zones defining euhedral crystal shapes prevail in phosphorus distribution maps of IVZ granulitic garnet (Bartoli et al., 2024b), this mineral should have completely dissolved and recrystallized. Experimental re-homogenization of MI and the application of Zr-in-rutile thermometry to rutile grains in garnet interior (Carvalho et al., 2023a) indicate that this process occurred under-granulite facies conditions. An alternative explanation could be that the growth of garnet was highly overstepped (Spear, 2017) in a way such that garnet growth occurs completely at suprasolidus conditions. However, 200–300°C of overstepping would be necessary to explain formation of new garnet grains and, in turn, entrapment of MI at 800–900°C, a much greater value than commonly documented in subsolidus samples (≤50°C; see compilation in Nagurney et al., 2021). Even though there are no studies on the possible effect of overstepping on the formation of granulitic garnet, such a large degree of overstepping (200–300°C) is difficult to reconcile with high-temperature conditions, which favours nucleation at equilibrium. We therefore reject the overstepping hypothesis and state that complete recrystallization of subsolidus garnet is more plausible. However, this is a matter for further studies.

A thorough understanding of garnet behaviour during high-grade metamorphism must be based on detailed and reliable 3D characterization of garnet chemistry and distribution of MI. So far, with the exception of Parisatto et al. (2018), microstructural studies on the distribution of MI within garnet have relied on partially incomplete information provided by 2D sections of minerals in thin sections. It is desirable that more research by 3D X-ray microtomography—now becoming almost a routine tool in microstructural analysis—is undertaken on MI-bearing garnets, in order to complement the microchemical information provided by major and trace elements mapping.

WORKING WITH MELT INCLUSIONS: ANALYTICAL METHODS AND APPROACHES

MI can be preliminarily identified in regular 30-μm thin sections using an optical microscope. However, due to their small size (often <20 μm, rarely ~100 μm) further analytical techniques with higher spatial resolution are essential to confirm their presence, e.g. Raman spectroscopy, imaging and energy dispersive spectroscopy (EDS) and analysis of well-polished sections using scanning electron microscope (SEM). Geochemical analyses of melt compositions are mainly done through electron microprobe (EPMA), laser ablation inductively coupled–plasma mass-spectroscopy (LA-ICPMS) and NanoSIMS. In cases where MI have crystallized during cooling (i.e. when NI are present), re-homogenization experiments are required (see details below). In some cases, more cutting-edge analytical techniques have been used, such as FIB-SEM serial slicing (Cesare et al., 2015; Carvalho et al., 2023a) and time-of-flight secondary ion mass spectrometry (ToF-SIMS), transmission electron microscopy (TEM) and atom probe tomography (Tacchetto et al., 2021). Ferrero et al. (2011) applied the TEM on fluid inclusions coexisting with glassy MI.

The microstructural research on MI is fundamental for a correct interpretation of information and data obtained from inclusions. Microstructures of MI have been described in detail by Ferrero et al. (2012) and reviewed by Cesare et al. (2015). Here, we only briefly resume some fundamental aspects or highlight new developments.

Optical microscopy

A common practice in the investigation of melt and fluid inclusions is to use doubly polished thick sections. However, a preliminary examination with an optical microscope can and should be done using regular 30-μm thin sections. In this way, the clearer visualization within the crystals guarantees an easier identification of inclusions and consequently allows to better select the most suitable samples for further analyses. Well-prepared thin sections and good high-magnification (20× to 50×) lenses allow fast and easy reconnaissance of MI or multiphase inclusions in transparent hosts.

MI can occur as glass, partially crystallized and/or fully crystallized inclusions, thus the variable degree of crystallization of the inclusions will result in distinctive optical features. Glassy MI are transparent under plane polarized light and isotropic under cross-polarized light, and many of them contain shrinkage bubbles, which help at lot in their identification; even though not all glassy inclusions contain visible bubbles. In contrast, NI (i.e. fully crystallized inclusions) are polycrystalline and consequently are slightly darker under plane polarized light and display multiple birefringent crystallites under cross-polarized light (Cesare et al., 2009; Ferrero et al., 2012). Partially crystallized inclusions cannot be identified using optical microscopy only, and further investigation is required using Raman spectroscopy or SEM.

Recent detailed studies of MI in metamorphic rocks have revealed the common coeval presence of NI and MFI in the same clusters, and there are >15 case studies where this situation has been observed so far (Table 1; see also Carvalho et al., 2020 and Nicoli & Ferrero, 2021a). Also in this case, distinction of the two inclusion types is not possible by petrography alone and requires confirmation by Raman spectroscopy and/or SEM analyses. Like NI, MFI are polycrystalline, but the solid phases in the latter are not feldspars, quartz and micas, but carbonates and OH-bearing phyllosilicates (e.g. pyrophyllite, kaolinite), and the inclusions also contain a considerable proportion of residual C-bearing fluid. Consequently, MFI are usually even darker than NI under plane polarized light and have much higher birefringence under crosspolarized light, because of the presence of carbonates. Some case studies, also show that MSI are slightly smaller in size (Tacchetto et al., 2019). Optical microscopy also shows that MI, as well as MFI, generally display a negative crystal shape, apparent in polygonal outlines (Figs 3 and 6).

SEM

Backscattered-mode imaging with an SEM combined with EDS analyses is the most common, and likely the easiest, method used to identify MI within metamorphic minerals. Consequently, most of the literature in Table 1 used this technique to report their presence. SEM investigation is specifically needed to identify inclusions in very small minerals (e.g. zircon and monazite) or opaque and semi-opaque minerals (e.g. ilmenite and rutile), for which optical microscopy would not suffice.

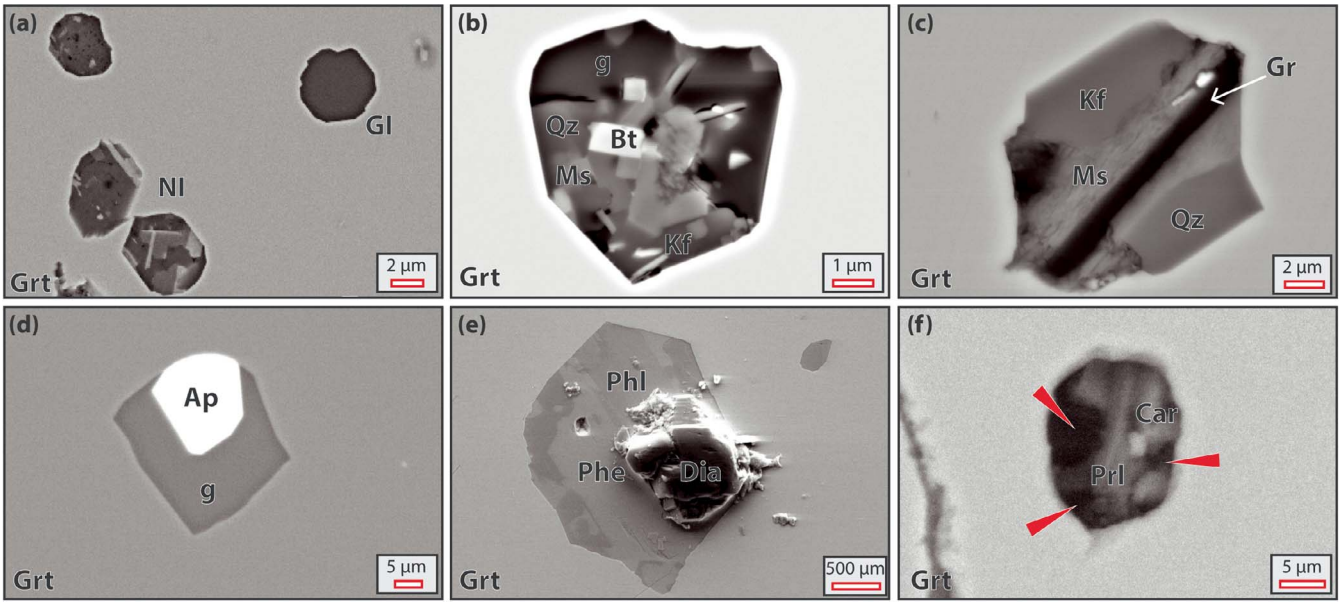

Fig. 6. BSE images of MI in garnet. (a) Cluster of primary inclusions showing the coexistence of glassy and NI inclusions in diatexites from Ronda (Spain); see Bartoli *et al.* (2013a,b,c, 2014, 2016) and Tacchetto *et al.* (2021). (b) NI containing residual silicate glass in metatexite from Ronda. (c) (d) Glassy inclusion with trapped apatite in UHT granulite from Rundvågshetta (Antarctica). (e) Diamond-bearing MI from Erzgebirge, Germany (photo courtesy by B. Stöckhert; see Stöckhert *et al.*, 2001 for further details) (f) Exposed multiphase fluid inclusion exhibiting a large empty cavity accompanied by carbonate and pyrophyllite.

Using SEM, well-polished samples can be thoroughly investigated and the microstructure of MI, the presence of residual glass or small phases (feldspars, quartz and micas) can be quickly identified (Fig. 6a–c) by single point analyses or compositional maps. Although glassy inclusions may also be identified, caution is advised on the intensive use of EDS on them, as it may cause alkali- and volatile-loss, making subsequent EPMA analyses unreliable. Furthermore, only EDS could cause confusion between glass and some new peculiar phases such as phase 430 (S. Ferrero personal communication; see more details about these phases on the Raman spectroscopy section). Ideally, EPMA analyses should be prioritized when glassy inclusions are identified using the optical microscope.

Microstructurally, NI can be quite heterogeneous. Some inclusions may contain euhedral to subhedral grains, typical of melt crystallization, but others show the presence of feldspar + quartz, feldspar + biotite intergrowths and skeletal crystals. Nucleation of daughter minerals (i.e. minerals crystallizing from the melt) occurs due to supersaturation upon cooling (Roedder, 1984) and starts by short-range segregation of elements (e.g. Al, Fe, K and Na) through the glass towards the rims/edges of the inclusion, resulting in the crystallization of micas and feldspars (Tacchetto *et al.*, 2021). Indeed, most common daughter phases in NI comprise plagioclase, quartz, K-feldspar (or their polymorphs; Ferrero *et al.*, 2016), biotite (which may exhibit high Mg contents as a result of re-equilibration with host garnet during cooling; Gianola *et al.*, 2021) and less commonly muscovite (Fig. 6b and c). Chlorite is also described in some case studies where high H_2O was measured in the melt, and it can be formed under subsolidus conditions (i.e. transformation of biotite) during cooling as supported by thermodynamic modelling (Bartoli *et al.*, 2019). Other daughter minerals previously found in crystallized MI are osumilite (Borghini *et al.*, 2018; 2019), anthophyllite (Ferrero *et al.*, 2021), pargasite (Gianola *et al.*, 2021; Ferrero *et al.*, 2021) and carbonates (Carvalho *et al.*, 2019; Borghini *et al.*, 2023). The variety of phases in the inclusion will depend on the bulk composition of the trapped melt.

Nanoporosity (i.e. cavities or voids formed once the minerals precipitated from the melt in the inclusion) can also be observed on exposed inclusions during SEM imaging. However, care should be taken to determine if porosity represents a natural feature or results from sample damage during polishing. Additional Raman spectroscopy investigation or FIB-SEM serial slicing of unexposed inclusions may provide further insights into revealing fluid-filled pores within the inclusions (Bartoli *et al.*, 2013a; Ferrero *et al.*, 2015; Carvalho *et al.*, 2023a; see details below).

Accidentally trapped phases, i.e. minerals that did not crystallize from the anatectic melt but were already present and have been trapped during the growth of the host mineral (‘*solid inclusions*’ as in Roedder, 1984), are frequently found both in glassy and crystallized MI (Fig. 6c–e; see also Cesare *et al.*, 1997; Cesare & Maineri, 1999; Acosta-Vigil *et al.*, 2007). The presence of these small accessory phases in the matrix of a rock can favour the entrapment of the melt during the growth of the host mineral. Small solids create imperfections and embayments on the surface of growing crystal facets, which can be preferentially wetted by melt/fluid and can eventually be closed leaving a melt + solid inclusion (Hollister & Crawford, 1981; Roedder, 1984). Some features that help to identify their ‘accidentally trapped’ character and rule out crystallization from the melt are the large size of these minerals relative to the inclusion, their contact relationships with the host (e.g. accidentally trapped minerals can be partially enclosed by the host mineral) and their behaviour during rehomogenization experiments (e.g. they remain unmelted in successfully rehomogenized NI; Ferrero *et al.*, 2012). The most common trapped minerals are accessory phases like zircon (Darling, 2013; Arab *et al.*, 2021), apatite (Fig. 6d) and rutile (Ferri *et al.*, 2020; Carvalho *et al.*, 2023a, 2023b). Some studies report aluminosilicate (Acosta-Vigil *et al.*, 2016; Barich *et al.*, 2014, Tacchetto *et al.*, 2019), spinel (Ferrero *et al.*, 2012), graphite (Cesare & Maineri, 1999; Carvalho *et al.*, 2019; Fig. 6c), epidote (Ferrero *et al.*, 2018) and diamond (B. Stöckhert pers. comm., Fig. 6e) as well. The presence of specific minerals or diagnostic assemblages trapped within NI can

be used to constrain the conditions of entrapment. For instance, the pair sapphirine + quartz in rocks from Rundvågshetta, Antarctica (Carvalho *et al.*, 2023b) and high-Al orthopyroxene in rocks from Rauer Islands (Liu *et al.*, 2023a) indicated entrapment at UHT conditions, whereas solid inclusions of diamond in NI (Stöckhert *et al.*, 2009) attest for entrapment of melt at UHP. The Zr-in-rutile thermometer coupled with phase equilibria modelling elucidated the HT to near-UHT conditions of entrapment for melt and fluid inclusions in Ivrea-Verbano Zone (Carvalho *et al.*, 2023a). Sometimes, the nature of mineral inclusions coexisting with MI in the same cluster, despite not being present as trapped phase, can also help constraining trapping P–T conditions. This is the case of microdiamond inclusions in MI-bearing garnet from the Scandinavian Caledonides (Klonowska *et al.*, 2017; Janák *et al.*, 2024) and of pseudomorphs after coesite in rocks from Saidenbach (Borghini *et al.*, 2023).

As mentioned above, MFI may coexist with MI and their successful identification provide indisputable evidence of fluid–melt immiscibility at suprasolidus conditions (Cesare *et al.*, 2007; Ferrero *et al.*, 2011, 2016a, 2018; Tacchetto *et al.*, 2019; Carvalho *et al.*, 2019, 2020, 2023a; Herms *et al.*, 2023; Janak *et al.*, 2024). In contrast to NI, the MFI in the SEM exhibit considerably larger cavities, formerly occupied by a fluid, accompanied by carbonates and OH-bearing minerals (Fig. 6f). Due to the larger size of the cavity and to the presence of a substantial residual porosity, the step-daughter minerals have incomplete and therefore weaker adhesion to walls. Consequently, MFI are more easily mechanically emptied during sample preparation.

Raman spectroscopy

Since the mid 1970's until today, Raman spectroscopy remains a fundamental tool commonly applied in the study of melt and fluid inclusions (Delhaye & Dhamelincourt, 1975; Rosasco & Roedder, 1979) as it consists in a nondestructive technique that allows: (1) to characterize solids, liquids and gaseous components within inclusions (Frezzotti *et al.*, 2012; Bodnar & Frezzotti, 2020 and references therein) and (2) to determine the volatile contents of silicate glasses (see details below). The method is based on the molecular and bonding properties of materials (Bodnar & Frezzotti, 2020) to obtain a spectrum, and the spectral features like peak position can be considered to identify the phases using a proper database (Frezzotti *et al.*, 2012; *RRUFF Project website* at https://rruff.info/ and the *Handbook of Raman Spectra for geology* at http://www.geologie-lyon.fr/Raman/; all these sources contain an integrated database of Raman spectra). The considerably small spatial and spectral resolution (~1 μm and 1 cm^{-1}, respectively) and the fast acquisition of spectra favour an easy identification of different components within the inclusions. More time consuming, but also very efficient is to obtain 2D (Fig. 7) or 3D maps of inclusions by collecting regularly spaced spectra (e.g. using 0.5 or 1 μm steps) covering horizontally (X-Y) and vertically (Z) the inclusion. These maps allow reconstruction and identification of the relative areas (2D) or volumes (3D) of the different phases (see Aradi *et al.*, 2023). Further details on the application of Raman spectroscopy and on the method itself can be found in comprehensive reviews to which the reader is referred to (Frezzotti *et al.*, 2012; Bodnar & Frezzotti, 2020).

The systematic use of Raman spectroscopy revealed some interesting peculiarities that seem to be typical (but not exclusive) of MI in metamorphic rocks. Ferrero *et al.* (2016b) identified the presence of the polymorphs kumdykolite (orthorhombic polymorph of $NaAlSi_3O_8$; Hwang *et al.*, 2009), kokchetavite (hexagonal polymorph of K-feldspar; Hwang *et al.*, 2004), cristobalite and in some cases tridymite within NI. However, according to the previous literature, kumdykolite and kokchetavite had been only reported in UHP rocks (Hwang *et al.*, 2004, 2009). Because the rocks studied by Ferrero *et al.* (2016b) did not experience such extreme pressure conditions, they interpreted all these polymorphs as crystallizing products of the melt within the NI. An important observation was that the polymorphs only occur in inclusions without decrepitation cracks. Hence, those authors proposed that the occurrence of polymorphs in NI represent 'direct mineral criteria to identify former MI with preserved original compositions' including volatile contents. Indeed, decrepitation likely induces the polymorphs to transform into more thermodynamically stable albite and K-feldspar. After this seminal work, numerous localities of various P–T conditions ($P > 0.5$ GPa and $T > 800$°C) have been reported to contain these uncommon minerals within crystallized MI (Borghini *et al.*, 2018, 2020, 2024; Ferrero *et al.*, 2018, 2021a; Carvalho *et al.*, 2019; Gianola *et al.*, 2021; Wannhoff *et al.*, 2022; Liu *et al.*, 2023a). Schneider & Balen (2024) also identified kokchetavite and kumdykolite in crystallized MI in zircon from A-type granites, showing that the presence of polymorphs is not exclusive of MI in metamorphic rocks.

Other polymorphs that have more recently been found in NI are dmisteinbergite (rare trigonal form of $CaAl_2Si_2O_8$; Wannhoff *et al.*, 2022) and the so-called 'phase 430' (Gianola *et al.*, 2021; Ferrero *et al.*, 2021a, 2024; Liu *et al.*, 2023a; Borghini *et al.*, 2024) and 'phase 412' or 'Pfaffenbergite' (Borghini *et al.*, 2024; Ferrero *et al.*, 2024). According to Borghini *et al.* (2024), both 'phase 430' and 'phase 412' contain a small amount of F (<0.11 wt %) in their crystalline structure.

Raman spectroscopy can also provide estimates of the H_2O contents dissolved in glassy inclusions. This technique is fast, accurate and especially useful in the case of small inclusions (~3 μm). Widely applied in anatectic MI, the classic method proposed by Thomas (2000) to measure the H_2O contents of MI considers the intensity of the asymmetric OH stretching vibration band between 2800 and 3980 cm^{-1} in the melt and in standards of known composition measured at the same conditions (e.g. 4 mW laser power, an acquisition time of 50 s and 5 accumulations). Considering the data obtained for the known standards, a correlation curve can be generated, allowing to recover the H_2O contents of the unknown samples (<10% relative error). Thomas *et al.* (2006) tested and extended this approach for MI below the surface, within the host mineral. Other approaches, which consider compositional effects on H_2O contents and propose correction methods, are also available (Zajacz *et al.*, 2005; Severs *et al.*, 2007; Behrens *et al.*, 2006; Schiavi *et al.*, 2018 and many others).

The CO_2 contents in glasses ranging from 0.2 to 16 wt % can also be measured using Raman spectroscopy (Morizet *et al.*, 2013, 2017). This method, not yet applied to anatectic MI, utilizes the combination of the area of the spectrum corresponding to carbonate v1 peaks and the aluminosilicate spectral features in the high-frequency region between 700–1200 cm^{-1}. Again, in this case, it is necessary to compare data of standards of known CO_2 contents analyzed at the same conditions as the unknown samples.

Raman spectroscopy is used to determine not only the volatiles dissolved into the glass, but also those present within NI and glassy MI. For instance, Bartoli *et al.* (2013b) showed the presence of liquid H_2O in nanopores of unexposed inclusions, Ferrero *et al.* (2015) showed the presence of OH-bearing residual glass, and other works also report the presence of CH_4 and CO_2 as residual fluid in MI (Carvalho *et al.*, 2019; Borghini *et al.*, 2024).

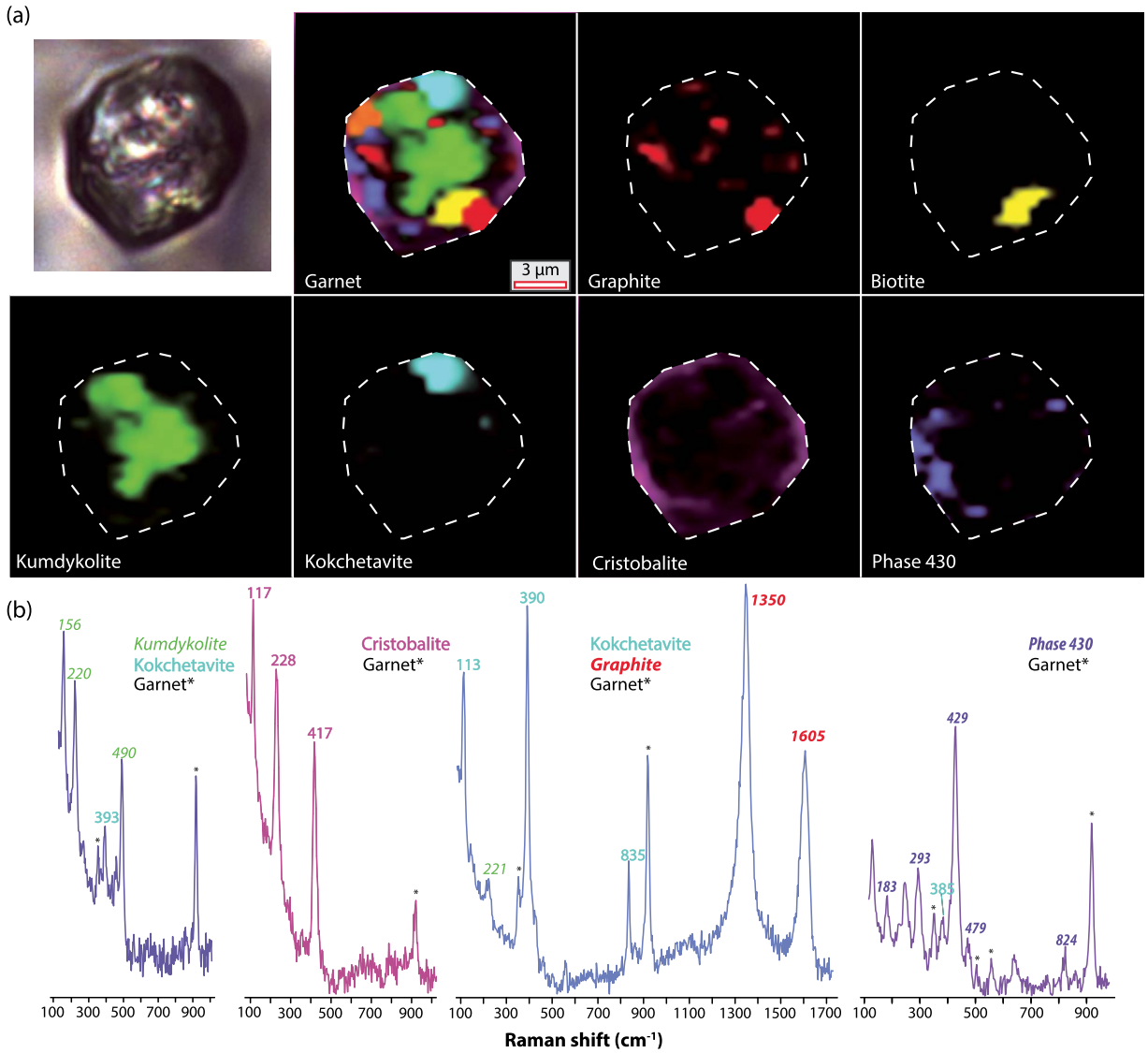

Fig. 7. (a) Two-dimensional Raman maps of a NI below the garnet surface of a metapelitic granulite from Black Point, Sleaford Complex (Australia). (b) Raman spectra of phases in the inclusion in (a).

Shrinkage bubbles in glassy and remelted inclusions also indicate the presence of CO_2 and N_2 (Bartoli *et al.*, 2013b; Gianola *et al.*, 2021; Carvalho *et al.*, 2023b). All these volatiles were likely previously dissolved in the melt but exsolved after cooling, filling up nanoporosities and shrinkage bubbles. Raman spectroscopy is used for the characterization of immiscible fluids potentially trapped with melt in MI (Cesare *et al.*, 2007).

Optimal conditions for micro-Raman spectroscopy analyses of MI using a Nd:YAG laser ($\lambda = 532$ nm) are ~2–3 mW of laser power on sample, grating of 300 lines mm^{-1}, considering multiwindow option between 100 and 4000 cm^{-1} to monitor solid, liquid and gaseous components. Acquisition time can vary, but a minimum 15 s and 3 accumulations are advised for clearer spectra. When working with small bubbles and volatiles, grating of 600 lines mm^{-1} and narrower window options may be preferred to monitor more restricted areas in the spectrum. A useful tip before Raman spectroscopy of MI is to identify inclusions with trapped accessory minerals before trace element analysis. This approach helps to avoid the analysis of inclusions that would provide extremely high contents of trace elements and would not be representative of the anatectic melt itself.

Rehomogenization of melt inclusions

An essential practice in MI studies is to perform rehomogenization experiments to determine the geochemical composition of the inclusions. Since inclusions may be partially or completely crystallized during the slow cooling of regional metamorphic rocks, experimental remelting is adopted in order to reverse the process of crystallization of daughter and step-daughter crystals, but also to completely dissolve the volatiles exsolved after cooling and stored in shrinkage bubbles and nanoporosities. Successful and complete rehomogenization is also strong evidence that NI are former MI (see below). Once the experimental remelting is completed, cooling rates of ~40–50°C/s quench the liquid into glass to prevent chemical changes, recrystallization and volatile loss. Subsequently, the major and volatile element composition of the melt (analyses of trace elements do not require rehomogenization; see details below) can be obtained by analyzing the homogenized glass with a range of techniques (e.g. EPMA, NanoSIMS and SIMS).

Rehomogenization experiments can be done at ambient pressures using a heating stage (Roedder, 1979; Sobolev *et al.*, 1980; Esposito *et al.*, 2012) or 1-atm furnaces (Sinton *et al.*, 1993), and

these approaches are commonly adopted in MI studies of igneous rocks (see Rosa-Koga *et al.*, 2021 for a recent review). However, MI in high-grade metamorphic rocks are trapped at elevated pressures (0.3–4.5 GPa) and, when heated, undergo internal pressurization at or above the trapping values. Consequently, experiments at ambient pressure or at pressures lower than that of entrapment imply a high chance of decrepitation and failure (see Fig. 9 in Bartoli *et al.*, 2013a for the conceptual model on MI evolution during laboratory heating). The main features of failed rehomogenization experiments are irregular walls of the MI, decrepitation cracks filled with melt around the inclusion, the persistence of unmelted phases, the presence of new crystals not observed before the experiments (e.g. iron oxides, orthopyroxene, new garnet of discernibly different composition on inclusion walls), and the occurrence of multiple bubbles within the glass (Bartoli *et al.*, 2013a; Cesare *et al.*, 2015; Ferrero *et al.*, 2019).

Ferrero *et al.* (2012) were the first to perform ambient pressure experiments on doubly polished garnet wafers using a LINKAM TS1500 heating stage and variable heating rates. They obtained some nicely homogenous inclusions. However, many inclusions after experiments showed decrepitation tails, and multiple shrinkage bubbles in the glass, indicating that the experimental confining pressure should have been greater.

To avoid problems related to the internal overpressuring and consequent decrepitation and volatile loss of inclusions during rehomogenization, adapting a previous approach by Malaspina *et al.* (2006), Bartoli *et al.* (2013a) proposed the use of a piston cylinder apparatus. This approach allows the heating of MI under confining pressure equal or greater than the entrapment values established or inferred for the studied sample. Experiments with slightly higher pressures are usually preferred to minimize decrepitation. Regarding the temperature, an important aspect is not to exceed the temperatures of entrapment, as overheating may also induce decrepitation, volatile loss and melt–host interaction (see Fig. 9 in Bartoli *et al.*, 2013a). The experimental method consists of loading MI-bearing host crystals separated by matrix powder into Au or Pt capsules of ca. 3 mm in diameter and 3–4 mm in length. Depending on the number of MI in the sample, a diverse approach is advised, and experiments can be done using single crystals, doubly polished wafers (200–300 μm thick) or even drilled cores of host minerals (cf. Fig. 10 in Cesare *et al.*, 2015). An essential advantage of doubly polished wafers and drilled cores is that portions of the host containing abundant inclusions can be selected for mechanical removal, guaranteeing a higher probability of recovery and precise microstructural control. A matrix powder is used to isolate the crystals from each other and from the capsule walls, and several options have been reported in the literature: powder of SiO_2 (Bartoli *et al.*, 2013a), mixture of SiO_2 and $Al(OH)_3$ (Malaspina *et al.*, 2006; Stepanov *et al.*, 2016), oxalic acid dihydrate ($H_2C_2O_4{*}2H_2O$; Stepanov *et al.*, 2016), $CaCO_3$ (Ferri *et al.*, 2020) or graphite (Gianola *et al.*, 2021). When powdered SiO_2 and Si–Al mixture is used as a matrix medium, the capsules can be directly mounted into epoxy resin and then polished to expose the inclusions to the surface for further analysis. In contrast, when using graphite, the capsules must be dissolved into aqua regia to recover the host crystals (Gianola *et al.*, 2021). In the case of $CaCO_3$, the capsules are opened and immersed in diluted HCl to dissolve the carbonate and recover the host crystals (Ferri *et al.*, 2020). In the last two cases, garnet crystals were mounted separately in epoxy resin afterward; this procedure may be useful also when the host mineral is zircon, and it is necessary to work separately on each single zircon grain after re-homogenization experiments. Caution is advised for the use of SiO_2 and $Al(OH)_3$ mixture as matrix powder because $Al(OH)_3$ releases water upon heating, destabilizing garnet (Stepanov *et al.*, 2016). To evaluate the effects of H_2O gain and loss, Bartoli *et al.* (2013a) compared experiments at both dry and wet runs (i.e. by adding doubly distilled water in some capsules) and observed negligible H_2O loss or gain in the MI rehomogenized at 700°C and 0.5 GPa.

Malaspina *et al.* (2006) and Stepanov *et al.* (2016) performed experimental rehomogenization of inclusions in UHP rocks using piston cylinder at 900°C and 3.5 GPa. More recently, Acosta-Vigil *et al.* (2024) also investigated the entrapment conditions of carbonate-bearing multiphase solid inclusions through piston cylinder experiments at 4.0–4.5 GPa, 1000–1225°C and 30 min to 24 h of duration. Nanogranitoids in UHP rocks have been successfully rehomogenized by Borghini *et al.* (2023) and Slupski (2023) with a 1000-ton Walker-type multianvil module at pressure conditions of 4.5 GPa and temperatures >850°C.

Something to be aware of when performing experimental remelting is the presence of interstitial melt, which may form by the melting of matrix biotite + quartz + feldspar sometimes introduced with the garnet in the experimental assemblies. Stepanov *et al.* (2016) and Gianola *et al.* (2021) observed the formation of matrix melt around, and within fractures of, garnet. Since the geochemical analyses revealed that such melt was substantially different in composition than the melt within the inclusions, both authors excluded the possibility of contamination. Nonetheless, care should be taken to clean carefully garnet grains (mechanically or chemically) from the surrounding rock matrix, in order avoid introduction of additional phases into the experimental capsule.

A considerable disadvantage of using a piston-cylinder apparatus is that MI cannot be monitored during rehomogenization. Hence, more experiments are necessary to get a reasonable number of inclusions with homogeneous glass, with a trial-and-error approach to identify the best conditions for each case study. An alternative and likely viable technique that can circumvent such inconveniency is to use a hydrothermal diamond anvil cell (HDAC), which allows to observe with an optical microscope the behaviour of inclusions undergoing rehomogenization at the desired P–T conditions (Basset *et al.*, 1993). Li *et al.* (2016) and, more recently, Li *et al.* (2020, 2022) proposed a new and more efficient HDAC system and established good practices for a successful approach. Up to date, this technique has not yet been applied to MI in high-grade metamorphic rocks.

Studies of MI in igneous rocks show that experimental homogenization can be affected by key factors such as the heating rate, inclusion size, volatile contents and time duration because reaction kinetics play a role on melting behaviour (Sobolev & Danyushevsky, 1994; Audétat & Lowestern, 2014; Bodnar & Student, 2006). This is particularly relevant in vary small inclusions like most NI. The behaviour of inclusions using different heating rates, inclusion sizes and volatile content has not been specifically investigated in the case of MI in metamorphic rocks. Regarding time, a duration of 24 hours was preferred by most authors in the available literature (50% of the works used such duration). However, each case study has its own experimental strategy. For instance, Ferri *et al.* (2020) performed longer experiments (46–68 h) at lower temperatures (<780°C) and obtained nicely rehomogenized inclusions, whereas Herms *et al.* (2023) report considerable melt–host interaction when durations are >48 h. Several works also report that short experiments (30 min up to 5 h) provided better results in near-UHT to UHT rocks, as melt–host interaction is minimized (e.g. 30 min to 4 h, Stepanov *et al.*, 2016; Ferrero *et al.*, 2021; 30 min, Acosta-Vigile *et al.*, 2024; 5 h, Carvalho *et al.*, 2019;

1 to 10 h Gianola *et al.*, 2021 and 1 to 6 h, Liu *et al.*, 2023a). Further research on time-resolved experiments is still necessary to obtain better constraints on the effects of the run duration on rates of homogenization and problems related to melt–host interaction.

As shown above, there are diverse methods that can and should be applied, but a crucial finding is that after rehomogenization, crystallized inclusions exhibit similar geochemical features as the preserved glassy inclusions occurring in the same samples (Bartoli *et al.*, 2013a; Ferrero *et al.*, 2019, 2023). Therefore, in cases where glassy MI are not present, re-homogenization of NI is fundamental. Only when a considerable number of glassy inclusions is preserved, rehomogenization experiments are not required (Acosta-Vigil *et al.*, 2007; Cesare *et al.*, 2007; Ferrero *et al.*, 2014; Bartoli *et al.*, 2016a; Gianola *et al.*, 2023; Carvalho *et al.*, 2023b).

Geochemical analyses of melt inclusions

Glassy and rehomogenized MI can be analyzed to recover the major, trace and volatile contents of anatectic melts.

Although several analytical methods are currently available (see below), it is paramount to ensure that the obtained compositions are representative of the melt that was present at the time of entrapment. One syn-entrapment process that can affect the melt composition is the formation of diffusive boundary layers at the interface between the growing crystal and the melt (Baker, 2008). This possibility has been carefully explored for anatectic MI from granulitic xenoliths of El Hoyazo, Spain (Acosta-Vigil *et al.*, 2010, 2012). By characterizing the MI composition in several coexisting plagioclase and garnet grains, these authors concluded that, with respect to incompatible elements, MI reflect the composition of the pre-entrapment melt. Conversely, compatible elements are likely to be influenced by the formation of layers around growing crystals. Although such a study is still lacking for migmatitic/granulitic terranes, the MI dataset described and discussed below consists of inclusions trapped in garnet, for which analyses of compatible elements (HREE, Y) are difficult to impossible due to the small size of the MI (see below).

In MI in igneous rocks, it is widely known that postentrapment crystallization (PEC) can modify the composition of the melt mainly as result of decrepitation and/or crystallization of minor amounts of host mineral along the inclusion walls (Roedder, 1984; Audétat & Lowestern, 2014). In metamorphic rocks, MI can also be affected by the same processes, but both can be identified microstructurally (see discussion in Cesare *et al.*, 2015). Specifically, in the case of MI in garnet, which are mostly trapped during heating, crystallization of the host along the inclusion walls is unlikely, as this mineral does not crystallize during decompression (The reader is referred to the Introduction section where the relationships between internal and external P–T conditions are described.) Moreover, garnet is not easily crystallized in granitic systems. Acosta-Vigil *et al.* (2012) looked at the compositional zoning around inclusions by doing profiles across MI and host minerals, but did not observe diffusional exchanges. A more recent nanoscale investigation by Tacchetto *et al.* (2021) using ToF-SIMS did not reveal any variations in Mg, Al, Fe and Ca in garnet at the interface with MI, that would occur in case of host–melt interaction during cooling. These observations confirm that measured compositions of MI in garnet, if successfully rehomogenized, should be pristine.

Whether any melt/host interaction occurred during cooling, experimental remelting should revert it (Cesare *et al.*, 2015; see details on experimental re-homogenization above). However, in the cases where interaction is induced or maintained during the experiments, for instance when overheating has occurred, or when garnet growth has been identified, a geochemical correction can be applied. This kind of correction was done by Stepanov *et al.* (2016) using FeO as correction factor based on the experimental work of Hermann & Spandler (2008). Stepanov *et al.* (2016) observed that re-homogenized inclusions from Kokchetav had 10–25% garnet component. Considering these estimates, the authors successfully corrected the melt compositions.

The electron microprobe is regularly used to obtain major element composition of the melts, as well as their B, F and Cl contents (Acosta-Vigil *et al.*, 2007; Cesare *et al.*, 2007; Di Martino *et al.*, 2011; Ferrero *et al.*, 2012, 2024; Acosta-Vigil *et al.*, 2016; Gianola *et al.*, 2021; Liu *et al.*, 2023a; Borghini *et al.*, 2024). Alkali migration is a common problem when analyzing hydrous silicate melts (Morgan & London, 1996, 2005); therefore, particular caution is necessary during analyses. Strategies that can be used are to prioritize the acquisition of Na and K during analysis, to use a defocused beam, and correction factors for the affected elements Na, K, Si and Al (Morgan & London, 2005). In the case of very small inclusions, however, a defocused beam cannot be used.

To constrain the trace element signature of anatectic melts, LA-ICP-MS can be used in both NI and glassy MI. An advantage of this technique, when compared to the electron microprobe or NanoSIMS, is that rehomogenization of the inclusions is not required. However, these analyses may be challenging due to the size of the inclusions (mostly <20 μm across), as in most cases the spot size of the laser is larger than the inclusions, and consequently some host garnet is ablated together with the inclusion. Despite this difficulty, the signal of the host garnet can be removed (i.e. separated from the signal of the melt) through specific data treatment using different methods (Halter *et al.*, 2002). It can be removed by using a fixed known concentration of a chosen element in the melt, using a representative distribution coefficient between the host and the inclusion, or even considering the volume ratios between the inclusion and total ablated volume. An error in the order of ±10% relative is expected if the bulk of the inclusion represent more than 20% of the ablated mass. With this approach, the concentration of elements strongly compatible with the host mineral should not be considered for the melt, as after data treatment, they often result below detection limits. This implies disregarding mainly the HREE and Y values in the MI when the host is garnet.

When the inclusions are large enough for the beam (i.e. >10 × 10 μm; Bartoli *et al.*, 2013a), volatiles such as H_2O, CO_2, Cl, F, B and S can be obtained using SIMS. However, because most anatectic MI are rather small (<10 μm), NanoSIMS is usually preferred (Bartoli *et al.*, 2014; Ferrero *et al.*, 2024 and references therein), whereas SIMS analysis would require mass balance calculations to take into account the decrease of the volatile signal when inclusion and host are contemporaneously sputtered (see procedure in Bartoli *et al.*, 2013a).

The reliability of chemical data from MI can be questioned, particularly regarding the volatile content, that may have been modified by diffusion of volatile species (e.g. H) in and out of the hosts after entrapment, as discussed by Acosta-Vigil *et al.* (2024) with reference to experiments by Reynes *et al.* (2018). It should be kept in mind that diffusional processes require chemical gradients in order to proceed, and that in natural systems like migmatites and granulites, the gradients established after entrapment should drive both H loss (lower external aH_2O) and gain (higher external aH_2O) in MI. The available data (discussed below), showing relatively narrow H_2O contents within each sample, as well as a general negative correlation between H_2O content and

inferred T of entrapment (also observed in experimental works – Johannes & Holtz, 1996), suggest that MI behave as closed systems also with respect to volatiles, and that the garnet host generally represents an impermeable barrier around the inclusion. In this sense, it is important to note the main differences between MI trapped in lava phenocrysts and in peritectic minerals of suprasolidus metamorphic rocks. In the former case, volatile pressure gradients are continuously established between the melt within inclusions and the external degassing magma. On the contrary, large and systematic gradients of fluid activity are not expected during the postcrystallization evolution of a peritectic host. An additional key difference between the two modes of occurrence is the temperature, where the higher temperature of igneous/volcanic systems favours diffusional processes. The reader is referred to Bartoli *et al.* (2014) and Bartoli & Cesare (2020) for a more complete discussion where also the equation of mass transport by diffusion is considered.

DEVIL'S ADVOCATE: COULD THESE INCLUSIONS BE FORMED BY MELTING OF FORMER SOLID INCLUSIONS? NO.

The common thread behind our works and this review is that MI and NI result from entrapment of melt droplets by a growing mineral. An alternative origin for MI was proposed by Vernon (2007) for the interpretation of the glassy inclusions hosted in the crustal xenoliths of El Hoyazo (Spain). According to his view, mineral aggregates originally trapped in subsolidus phases may undergo melting once rocks reach hotter temperatures, resulting in the formation of melt droplets dispersed all through the grains. Vernon's model was challenged by Cesare *et al.* (2008) through microstructural, mass-balance and thermodynamic arguments, which are here summarized. (1) In the case of congruent melting, all the aggregates of mineral inclusions present in a single garnet grain must contain the same minerals in exactly the right proportions to melt completely (together with some amounts of garnet) to produce homogeneous melt droplets dispersed throughout the host mineral (as observed at El Hoyazo). This is the only way to obtain relatively homogeneous compositions for MI trapped in the same host mineral, as documented in different case studies (Cesare *et al.*, 2015). (2) In the case of incongruent melting, the partial (!) melting of mineral inclusions would produce some amounts of solids (peritectic phases) along with melt. At that time, the research on MI in high-grade rocks was mostly focused on residual metasedimentary enclaves, where melt droplets in mineral hosts appear as glassy inclusions, without any solid minerals (Acosta-Vigil *et al.*, 2007; Cesare *et al.*, 2007). Therefore, their pure glassy nature was the main argument against an origin from incongruent melting of mineral aggregates (see Cesare, 2008).

Here, we provide further arguments against the hypothesis of melting of pre-existing solid phases as viable process for the origin of MI and NI in anatectic rocks, taking advantage of phase equilibrium modelling and by studying the evolution of mineral inclusions in garnet during heating along a prograde path (Fig. 8). We used garnet as mineral host, assuming eight different scenarios from pure mica to polycrystalline aggregates with 40:30:30 proportions of quartz, plagioclase and mica. The amount of host garnet in the model is 10%. Phase equilibria were calculated with the software Perple_X (Connolly, 2009). The model assumes mineral inclusion entrapment at subsolidus of 650°C and 7 kbar, whereas phase equilibria were calculated at 800 and 900°C, respectively, assuming an inclusion-garnet proportion of 90:10 (Fig. 8).

Some key observations demonstrate that the mineral inclusions melting model are 'geologically unreasonable', as stated by Cesare *et al.* (2008). (1) The complete melting to form a homogeneous melt inclusion requires extremely high temperatures (>1200°C), whereas the product of the mineral inclusions melting is generally dominated by peritectic solid phases (see pie diagrams in Fig. 8). (2) The solid products of incongruent melting of muscovite-bearing aggregates must contain corundum or sillimanite. Whereas the first mineral has never been reported in the tens of nanogranitoids occurrences documented so far (Table 1), crystals of aluminosilicates were solely reported in crystallized MI from Jubrique, Spain (Barich *et al.*, 2014; Acosta-Vigil *et al.*, 2016), Athabasca (Tacchetto *et al.*, 2019) and Usagaran (Herms *et al.*, 2023). At Jubrique, an aluminosilicate was always present after experimental remelting of these polycrystalline inclusions by piston cylinder, often showing an overgrowth of staurolite resulting from aluminosilicate–melt interaction (Acosta-Vigil *et al.*, 2016). This experimental outcome indicates that the aluminosilicate phase was originally not in equilibrium with the trapped melt, reinforcing other lines of evidence that aluminosilicates in these MI are trapped minerals (i.e. accidental minerals trapped with the melt during garnet growth; see discussion in Barich *et al.*, 2014). Much lower amounts of melt are predicted to form when biotite (rather than muscovite) is part of the inclusion assemblage (Fig. 8). In scenarios with an inclusion solely made of biotite or with inclusions containing biotite-plagioclase and biotite-quartz pairs in the 50:50 proportion, undetectable amounts of liquid and peritectic spinel and K-feldspar are predicted to form. Only in the case of a former polycrystalline aggregate of biotite, quartz and plagioclase, the newly formed inclusion at 900°C contains a granitoid phase assemblage mostly composed of quartz, plagioclase and K-feldspar, along with some amounts of orthopyroxene and ilmenite and the products of melt crystallization (mostly quartz and feldspars). However, the experimental remelting of these inclusions would never obtain a completely re-homogenized inclusion, i.e. inclusions totally composed of glass (i.e. melt), as instead documented in many nanogranitoids occurrences (Kerala Khondalite Belt, Cesare *et al.*, 2009; Ferrero *et al.*, 2012; La Galite, Ferrero *et al.*, 2014; Ronda Migmatites, Bartoli *et al.*, 2016b; Gruf Complex, Gianola *et al.*, 2021; Rundvågshetta, Carvalho *et al.*, 2023b; Saidenbach, Borghini *et al.*, 2023).

Further microstructural considerations on size, 3D distribution and mode of occurrence of MI also point against the process proposed by Vernon (2007). While we can confidently rule it out in all the case studies referred to in this review, we cannot exclude that solid inclusions in garnet or other hosts may melt when heated, as long as they respect the thermal and mass balance constraints posed by the above thermodynamic modelling example, i.e. producing melt and peritectic phases in compatible amounts. Processes such as those described by Perchuk *et al.* (2008) and envisaged by Faryad *et al.* (2018) and Faryad & Cuthberth (2020) for the origin of multiphase inclusions by melting of solid zoisite and 'hydrous phase' inclusions, respectively, cannot produce the MI and NI in migmatites and granulites object of this review. An example of partial melting of former mineral inclusions in garnet resulting in a polycrystalline aggregate is given in Liu *et al.* (2020). Notably, these authors also identified true MI and discussed the evident differences between them in terms of processes, textures and geochemistry.

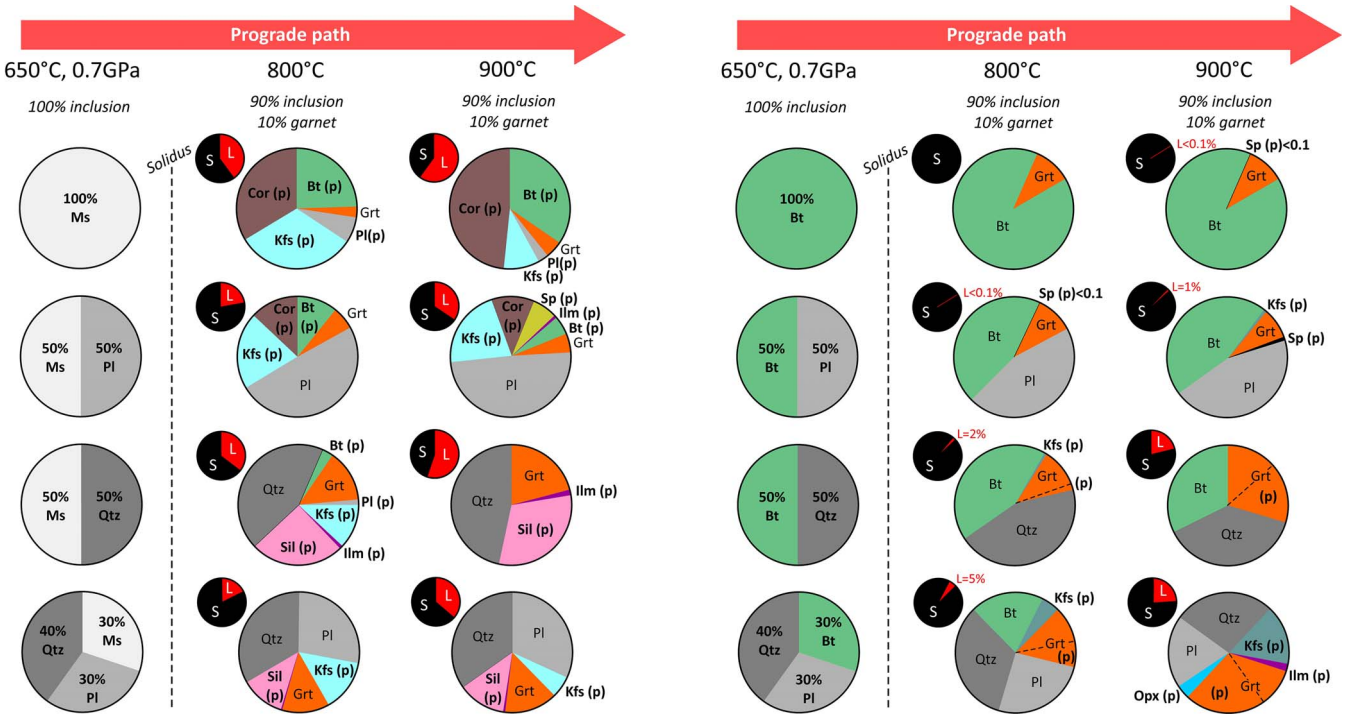

Fig. 8. Results of phase equilibrium modelling for mineral inclusions trapped in garnet. The pie diagrams on the left reflect four different initial scenarios from pure mica (muscovite or biotite) to polycrystalline aggregates with 40:30:30 proportion of quartz, plagioclase and mica. The pie diagrams represent the solid (S) to liquid (L) ratio. The letter p identifies the peritectic products. In the case of garnet, the dashed black line separates the residual amount from the peritectic one. Calculations were performed by Perple_X software (Connolly, 2009). See Carvalho *et al.* (2023a) for the selected thermodynamic databases and a–x models.

ANATECTIC MELTS IN THEIR SOURCE

Here we compare the geochemistry (major, trace and volatile elements) of anatectic MI in garnet available to date (see Table 1). For the major element analyses, due to the variable H_2O contents of the inclusions, we have recalculated the compositions on anhydrous basis. For better clarity of several diagrams, the available database is divided by pressure conditions <1 GPa, 1–2.5 GPa and 2.5–4.5 GPa. A compilation of major, trace and volatile (H_2O and CO_2) elements of MI up to date are presented in Tables S1, S2 and S3. This dataset completes the MI database from crustal xenoliths reported in Bartoli *et al.* (2016a).

Major elements and CIPW-normative compositions

The multicationic classification (Debon & Le Fort, 1988) and CIPW-normative diagrams are used to evaluate the major element and mineralogical signatures of MI from the literature (Figs 9 and 10). Amongst the MI studied to date, the peraluminous character ($A > 0$; A = molar $[Al - (Na + K + 2\,Ca)]$) is prevalent, and only a small group of samples are metaluminous or peralkaline ($A < 0$). These peraluminous melts are expected to contain muscovite and biotite (fields I and II in Fig. 9). These observations concur with the fact that the most commonly investigated protoliths are metasedimentary (ca. 65%). Metaluminous melts were mainly the product of granite s.l. remelting in the case study of La Galite (Ferrero *et al.*, 2014). Peralkaline melts were described in MI from Orlica-Śnieżnik Dome (Ferrero *et al.*, 2015), Granulitgebirge (Borghini *et al.*, 2018), Rundvågshetta (Carvalho *et al.*, 2023b) and Saidenbach (Borghini *et al.*, 2023). The crystallization of these peralkaline melts is expected to yield pyroxene, amphibole and biotite in the mineral assemblage (fields III, IV and V in Fig. 9).

The maficity of MI (i.e. their $Fe + Mg + Ti$ contents) is predominantly low, and consequently, the majority of MI are classified as leucogranites (Fig. 9). Slightly higher maficity (corresponding to $FeO + MgO + TiO_2 > 3$ wt %) is observed only in some case studies: Kerala Khondalite (Ferrero *et al.*, 2012), Dronning Maud Land (Ferrero *et al.*, 2018), Ivrea-Verbano Zone (Carvalho *et al.*, 2019), Central Maine Terrane (Ferrero *et al.*, 2021b) and Kokchetav Massif (Stepanov *et al.*, 2016). According to experimental data (Vielzeuf & Holloway, 1988), an increase of melt maficity is expected at higher temperature conditions of anatexis, as confirmed by MI (see Fig. 8b in Ferrero *et al.*, 2021b). Caution is also advised when an increase in maficity is observed only in some analyses, as these may indicate contamination from the host garnet, either during microprobe analysis or during experimental re-homogenization. Contamination from the host garnet can be confirmed when a clear correlation for $FeO_t + MgO$ and ASI occurs (Cesare *et al.*, 2015).

When the first MI were described, only granitic compositions were found (Cesare *et al.*, 2009), and after a few years of research tonalite, trondhjemite and granodiorite compositions were described as well (see Bartoli *et al.*, 2016a). The up-to-date database reveals that MI display a wide range of granitic compositions, and according to the CIPW normative Ab-An-Or diagram (Fig. 10a–c), most of the MI are classified as granite, tonalite, trondjemite, granodiorite and only rarely quartz monzonite. Figure 10b shows that MI trapped between 1.0 and 2.5 GPa show higher Ab and An contents.

In a Ab-Qz-Or normative diagram of the haplogranite system (Fig. 10d–f) a considerable spread away from the experimentally determined eutectic and cotectic lines at different pressures is observed for all the MI of the compilation. This observation was

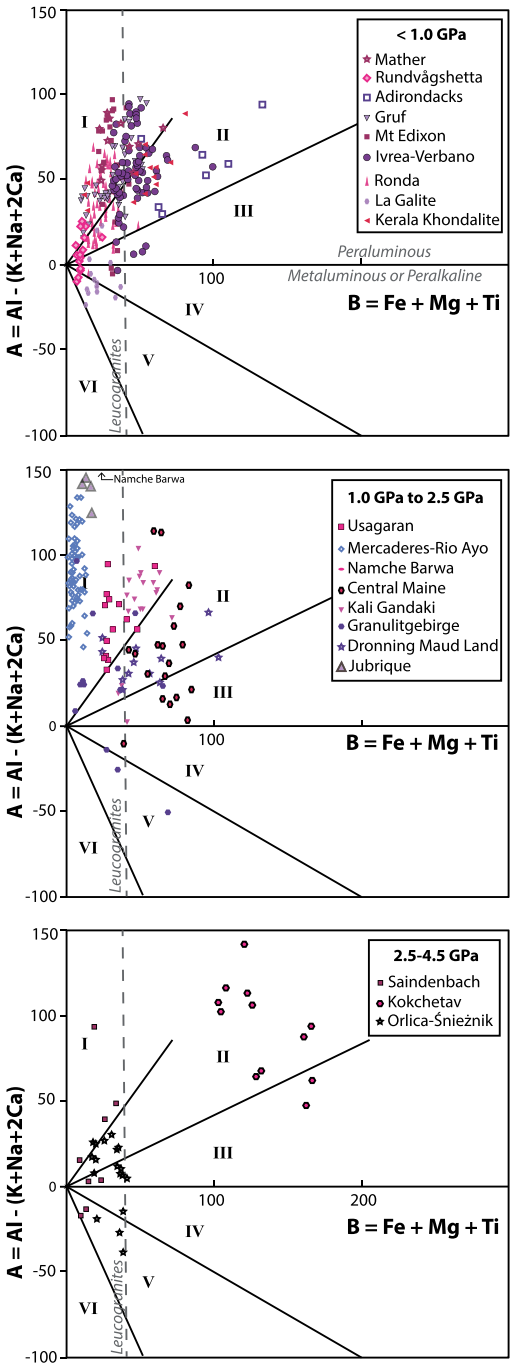

Fig. 9. Multicationic A-B diagram (Debon & Le Fort, 1988) for MI. Peraluminous index A = molar [Al − (Na + K + 2 Ca)] versus differentiation index B = molar (Fe + Mg + Ti). When A > 0 peraluminous; A < 0 metaluminous or peralkaline. Fields represent granites with different mineralogy: I = Muscovite > Biotite; II = Biotite > Muscovite; III = Biotite ± minor amphibole; IV = Biotite, amphibole ± pyroxene; V = pyroxene ± amphibole ± biotite. MI data from: Kerala Khondalite Belt, Ferrero *et al.* (2012); La Galite, Maghrebian basement, Ferrero *et al.* (2014); Ronda Migmatites, Bartoli *et al.* (2016a); Ivrea-Verbano Zone, Carvalho *et al.* (2019); Mt Edixon, Ferri *et al.* (2020); Gruf Complex, Gianola *et al.* (2021); Adirondacks, Ferrero *et al.* (2021a); Rundvågshetta, Carvalho *et al.* (2023b); Mather, Liu *et al.* (2023a); Jubrique, Acosta-Vigil *et al.* (2016); Dronning Maud Land, Ferrero *et al.* (2018); Granulitgebirge, Borghini *et al.* (2018); Kali Gandaki, Bartoli *et al.* (2019); Central Maine, Ferrero *et al.* (2021b); Namche Barwa, Liu *et al.* (2023b); Mercaderes-Rio Ayo, Gianola *et al.* (2023); Usagaran, Herms *et al.* (2023); Orlica-Śnieżnik, Ferrero *et al.* (2018); Kokchetav, Stepanov *et al.* (2016); Saidenbach, Borghini *et al.* (2023).

already done by Bartoli *et al.* (2016a) who attributed the discrepancy to the 'natural multicomponent' character of MI that, in contrast to simplified haplogranitic system, contain significant amounts of additional components (e.g. Ca, Ti, Fe, Mg, P) capable of affecting phase relationships. This is in agreement with experimental studies on the effect of additional components on phase equilibria in the haplogranite system (Johannes & Holtz, 1996; Wilke *et al.*, 2015).

Another remarkable feature of some case studies is the aligned distribution of MI compositions parallel to the Qz-Ab and Qz-Or sides, something already observed in experimental works at temperatures above 800°C. This behaviour is attributed to the contrast in diffusion rates for alkalis when compared to Si and Al in the melt (see more details in Acosta-Vigil *et al.*, 2006, 2017) and the MI showing such a trend have been interpreted to reflect melts formed by high degrees of overstepping of the melt-producing reactions (Acosta-Vigil *et al.*, 2017).

In agreement with experimental studies (Patiño-Douce & Johnston, 1991), the MI from metapelitic protoliths partially melted at $P < 1.0$ GPa show that with increasing temperature, higher Or contents, and consequently, higher K/Na ratios are attained in the melt. For instance, MI in UHT rocks from Kerala, Gruf, Rundvågshetta and Mather are particularly enriched in Or when compared to MI from La Galite, Ronda and Mt Edixon, where partial melting is estimated at 700–850°C. An exception is observed in the near-UHT MI from the Ivrea-Verbano Zone, with low Or and K_2O contents (20 mol % and 2 wt %, respectively), which were interpreted to have been produced once biotite was mostly consumed (Carvalho *et al.*, 2019). The same MI are enriched in CaO that, on the basis of experimental outcomes (Johannes, 1989), may be linked to disequilibrium melting of plagioclase (Bartoli & Carvalho, 2021). The MI from Adirondacks also have extremely low Or contents, but they originated from a mafic protolith (Ferrero *et al.*, 2021a).

Contrary to expectations, MI trapped between 1.0 and 2.5 GPa (Fig. 9e) do not display a clear increase of Ab/Qz ratios with pressure. Instead, a predominant enrichment in both Qz and Ab, together with a distribution along the Qz-Ab, occur in both mafic (Mercaderes) and metasedimentary (Kali Gandaki, Jubrique) protoliths. Important exceptions are MI from Usagaran, Dronning Maud Land and Central Maine (with >40 mol % Or), but this behaviour can be related to the decrease in a_{H2O} in the fluid, which tends to displace composition towards Or (Ebadi & Johannes, 1991). Specifically in the case of Usagaran, a CO_2 fluid coexists with the melt (Herms *et al.*, 2023) indicating $a_{H2O} < 1$. As for Central Maine, an active role of brines during anatexis was proposed by Ferrero *et al.* (2021b) due to the significant CO_2, Cl and F contents detected in the MI.

Partial melting experiments of crustal lithologies mostly conducted between the 1970s and 1990s (Vielzeuf & Holloway, 1988) and modelling of partial melting via equilibrium thermodynamics since the beginning of the twenty-first century (Holland & Powell, 2011) have been the principal tools to understand and constrain how pressure, temperature, fluid regime and bulk composition shape the chemistry of crustal melts in their source region. With the advent of anatectic MI in the petrologists' toolbox, it has been possible to validate or not some paradigms. For instance, the landmark experimental study of Patiño Douce & Harris (1998) led to assume that H_2O-present melting of the metasedimentary crust produces trondhjemites, in contrast to peraluminous granites, which, instead, are the products of fluid-absent reactions. This outcome has deeply influenced the perception of a limited extent of H_2O-present melting in nature (Clemens *et al.*, 2020). However,

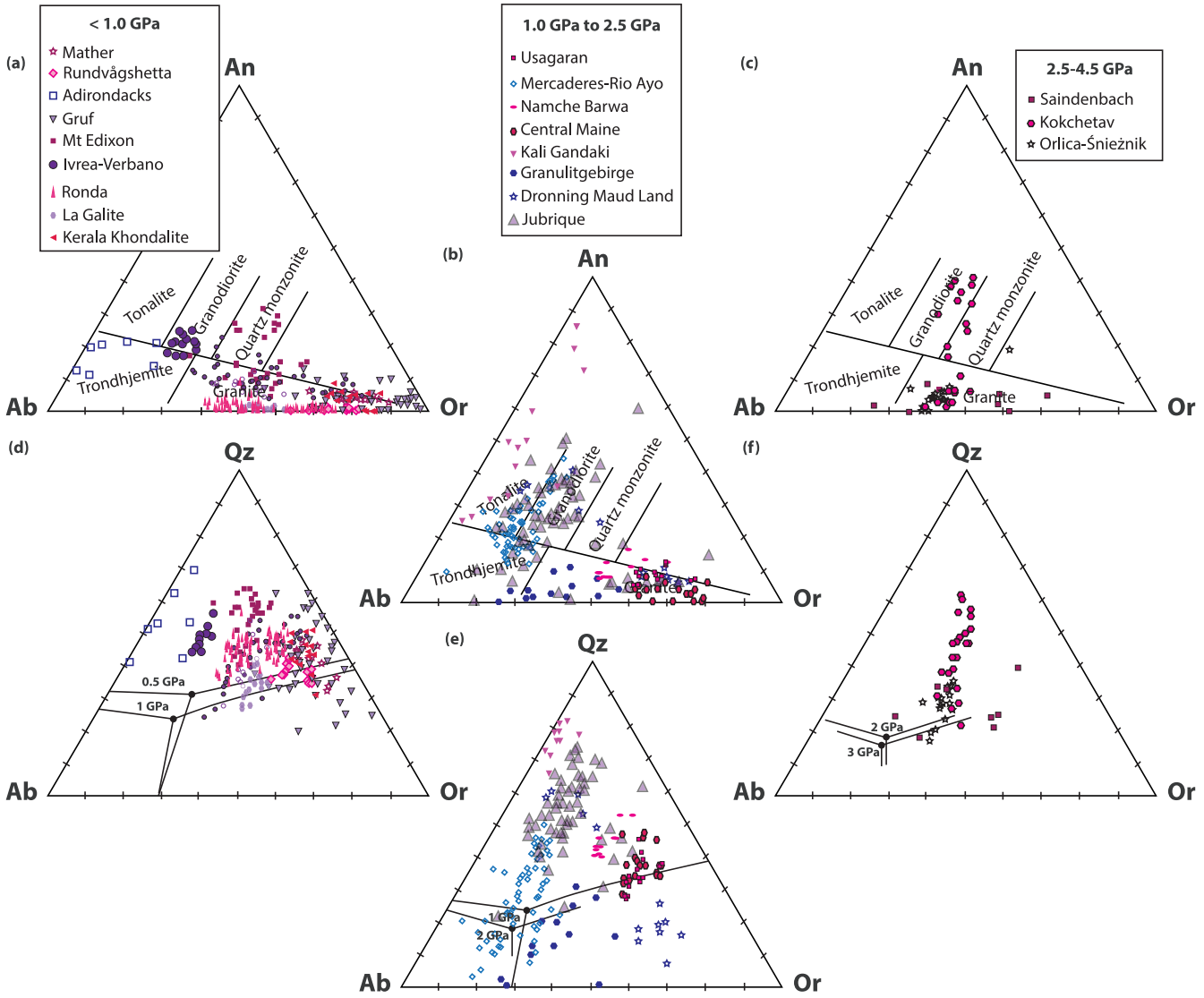

Fig. 10. CIPW–normative diagrams. (a-c) Ab (albite) – An (anorthite) – Or (orthoclase) classification diagrams with fields for granite, monzonite, granodiorite, trondhjemite and tonalite after O'Connor (1965). (d-e) Ab (albite) – Qz (quartz) – Or (orthoclase) normative diagrams. Eutectic points and cotectic lines for the haplogranite system are from Holtz *et al.* (1992), Luth *et al.* (1964) and Huang & Wyllie (1975). Source of MI data as in Fig. 8.

a comparison between experimental and calculated melts and NI allowed confirming that metastability during those experiments seriously affected melt compositions and that granite geochemistry alone cannot be used to discriminate among fluid regimes (Bartoli & Carvalho, 2021; Bartoli, 2021b).

A further application of anatectic MI is the reconstruction of a plausible subsolidus protolith composition for forward modelling. Indeed, the majority of migmatitic and granulitic rocks underwent melt loss (White & Powell, 2002) and a complete reconstruction of the prograde evolution via thermodynamic modelling requires melt reintegration (White *et al.*, 2014). In this sense, MI may provide the composition of melt to be added back to the measured bulk rock composition (more details in Bartoli, 2017, 2019).

The nanogranitoid 'alphabet soup' and the granite connection

Because anatectic MI are representative of crustal melts trapped in their source (i.e. the partially melted continental crust), it is logical to question how they compare to granites from the upper crust. The famous 'alphabet soup' classification of granites was initially proposed by Chappell & White (1974) to distinguish granites of different origins based on their geochemical and mineralogical features. In their classification, the term I-type granites were used to identify an igneous origin of the protolith and the S-type granites for a sedimentary one. When compared to the I-type, S-type granites have lower Na and Ca, are strongly peraluminous and corundum-normative. From the mineralogical point of view, they contain Al-rich silicates such as muscovite, cordierite, andalusite or sillimanite and garnet. The I-type may have slightly peraluminous (these may overlap with S-type) to metaluminous signatures. The peraluminous I-type may contain some muscovite, whereas most mafic ones are usually hornblende-bearing (Chappell, 1984). A-type (anhydrous or anorogenic) granites are another type of granite with high $FeO_{total}/(FeO_{total} + MgO)$, high Ga/Al, high abundances of alkali and high-field strength elements (HFSEs), low CaO, H_2O, Ba and Sr contents, ranging from metaluminous to slightly peraluminous, sometimes peralkaline (Loiselle & Wones, 1979; Collins *et al.*, 1982; Frost & Frost, 2011Whalen *et al.*, 1987). They can be generated by fractional crystallization of mantle-derived magmas, or by partial

melting of igneous or sedimentary protoliths (Frost & Frost, 2011; Huang *et al.*, 2011).

In Supplementary Fig. S1, a comparison is made between MI and A-, I- and S-type granites. MI show a wider spread of composition than the granites, nonetheless they overlap well in terms of SiO_2, Al_2O_3, $K_2O + Na_2O$ and to a lesser extent FeO. The largest discrepancy is observed for TiO_2, with MI displaying the lowest values. Usually, MI have lower maficity than most granites (see above), implying that several processes beyond partial melting affect anatectic magmas before they form plutons (for a recent review on most processes see Garcia-Arias, 2024 and references therein). However, other geochemical features allow to infer their connection with all the above-mentioned granite types. In the first studies, Bartoli *et al.* (2014) proposed that the MI were 'embryos of S-type granites'. This is still envisaged for case studies where the MI are strongly peraluminous (e.g. Ivrea-Verbano Zone, Mt Edixon, Gruf Complex, Mather, Usagaran, Kali Gandaki and Jubrique—Fig. 9).

Some MI can also be linked to I-type granites (La Galite, Adirondacks, Mercaderes and Dronning Maud Land). Granitic protoliths from La Galite yield MI with clear metaluminous affinity, that have the potential to contain amphibole or pyroxene in their mineral assemblage (Fig. 9a). The MI from Dronning Maud Land (Ferrero *et al.*, 2018), Adirondacks (Ferrero *et al.*, 2021a) and Mercaderes (Gianola *et al.*, 2023) were produced by mafic protoliths and represent peraluminous I-type granites. Consequently, they are muscovite and/or biotite-bearing (Fig. 9a). Importantly, MI from Adirondacks revealed an indisputable connection between partial melting of amphibolites and the generation of trondhjemitic melts (see also Fig. 10), providing significant constrains on the generation of the Archean TTG (tonalite-trondhjemite-granodiorite) series i.e. the earliest continental crust (Ferrero *et al.*, 2021a). Similarly, Fig. 10b shows that MI from Mercaderes may also have some affinities with TTGs.

Carvalho *et al.* (2023b) showed that MI in residual UHT granulites share several geochemical features with A-type granites, such as their weakly peraluminous to weakly peralkaline affinity, ferroan character, high alkali contents, high K/Na and Ga/Al and low Ca, Ba, Sr and H_2O concentrations. This evidence for the connection of MI in residual UHT granulites and A-type granites further supports works linking A-type granites with metasedimentary sources (Huang *et al.*, 2011; Zhang *et al.*, 2022).

Trace elements

The first work on the behaviour of trace elements in anatectic MI was carried out in the metasedimentary xenoliths from El Hoyazo by Acosta-Vigil *et al.* (2010, 2012), who investigated the impact of melting mechanisms on the geochemistry of anatectic MI. Subsequently, Bartoli *et al.* (2016a) compared data of MI from El Hoyazo with those from Ronda migmatites and highlighted the similarities of the two melts. When compared to the upper continental crust, these are generally enriched in elements controlled by biotite and muscovite (e.g. Cs, Rb, Li, Be and B) and depleted in elements concentrated in feldspar, zircon and monazite (Ba, Th, REE, Sr, Zr and Hf).

Since 2016, trace element data from 10 other case studies in mafic, felsic and metasedimentary protoliths were made available, and here, their main features are described and discussed. Figure 11 shows that MI from sedimentary protoliths are the richest in all trace elements, including Zn, Sc and Ni. As noted by Bartoli *et al.* (2016a), a strong effect of biotite and muscovite is evidenced in MI from metasedimentary and granitic protoliths, as they exhibit a relative enrichment in Cs, Rb, Li and B when compared to the upper continental crust (Figs 12 and 13a). In contrast, MI in mafic protoliths (Fig. 11c) display similar or slightly depleted values to those of the upper continental crust, indicating distinct reactants involved in their formation.

Elements hosted in feldspars such as Pb, Ba and Sr display variable concentrations in MI and are usually depleted relative to the upper crust. Some MI in mafic protoliths are slightly more enriched in Pb and Sr (Figs 11 and 12b), indicating the role of plagioclase in the melting reactions. Notably, Ferrero *et al.* (2021a) used the content of Sr and other trace elements of MI from Adirondacks mafic rocks to question the common approach of using trace elements of TTG to constrain the depth, and therefore, the geodynamic setting of TTG formation (Moyen, 2011).

MI are mostly depleted in Sr in metasedimentary protoliths, except for the Saidenbach case study. As evidenced by experiments, Sr is one of the most incompatible elements during high- to ultrahigh-pressure melting of metasediments, because there are no residual phases hosting significant amounts of Sr (Hermann & Rubatto, 2009). The low Ba contents of some MI (Fig. 12b) could be related to the formation peritectic K-feldspar during melting.

The behaviour of elements such as Th, U, La, Ce, Zr and Hf, mainly hosted in accessory phases varies from case to case (Figs 11 and 12c). The contents of Th, La and Ce are extremely variable in MI from metasediments compared to other protoliths, with the highest values documented in MI from Kokchetav and Saindenbach. This feature could reflect highly variable concentrations in the original protoliths. Despite being originated at similar conditions (>1000°C), contrasting behaviour is observed for Th, U, and especially for Zr and Hf in MI from mafic rocks (unusually enriched in Adirondacks; mostly depleted in Mercaderes). Ferrero *et al.* (2021a) attributed the enrichment in Zr and Hf to the presence of H_2O-rich fluids during melting, which enhanced HFSE, U and Th concentrations in the melt. The only case of MI from a granitic protolith (Orlica-Śnieżnik) shows depletion in elements hosted in accessory minerals (La, Ce, Th, U, Zr and Hf) compared to the upper crust. Another case study where the very high Th and U contents of MI were attributed to the presence of an aqueous fluid is eclogites from the Granulitgebirge (Borghini *et al.*, 2018, 2020).

In Fig. 12d and e, strongly peraluminous MI defined in the previous section are further compared to leucosomes and S-type leucogranites (20 locations worldwide, from the compilation of Acosta-Vigil *et al.*, 2012). A much wider variability occurs in MI from high-grade terranes, as already observed by Acosta-Vigil *et al.* (2012) for MI in crustal xenoliths. Nonetheless, a good match is observed mainly for MI and S-type granites for Cs and Li, whereas Sr, Ba, U and Zr show larger variations. Following Acosta-Vigil *et al.* (2012), this duality could indicate that melt equilibrated faster with micas than with feldspars and accessory minerals.

In the case of Zr, several works usually note low contents in the MI (the great majority is below 200 ppm; Fig. 12c), yielding lower saturation temperatures than expected for their interpreted entrapment conditions (Bartoli *et al.*, 2019; Ferrero *et al.*, 2019; Borghini *et al.*, 2023; Carvalho *et al.*, 2023b). This discrepancy between the expected Zr values in the melt and the predictions of solubility models have been attributed to several factors, including the disequilibrium between melt and accessory phases (Acosta-Vigil *et al.*, 2012) and the prograde zircon growth and its resistance up to UHT conditions (Carvalho *et al.*, 2023b). Caution is therefore required when converting Zr content of MIs into magmatic temperature estimates.

A similar case, where solubility equations for accessory minerals provided contrasting results with respect to anatectic MI,

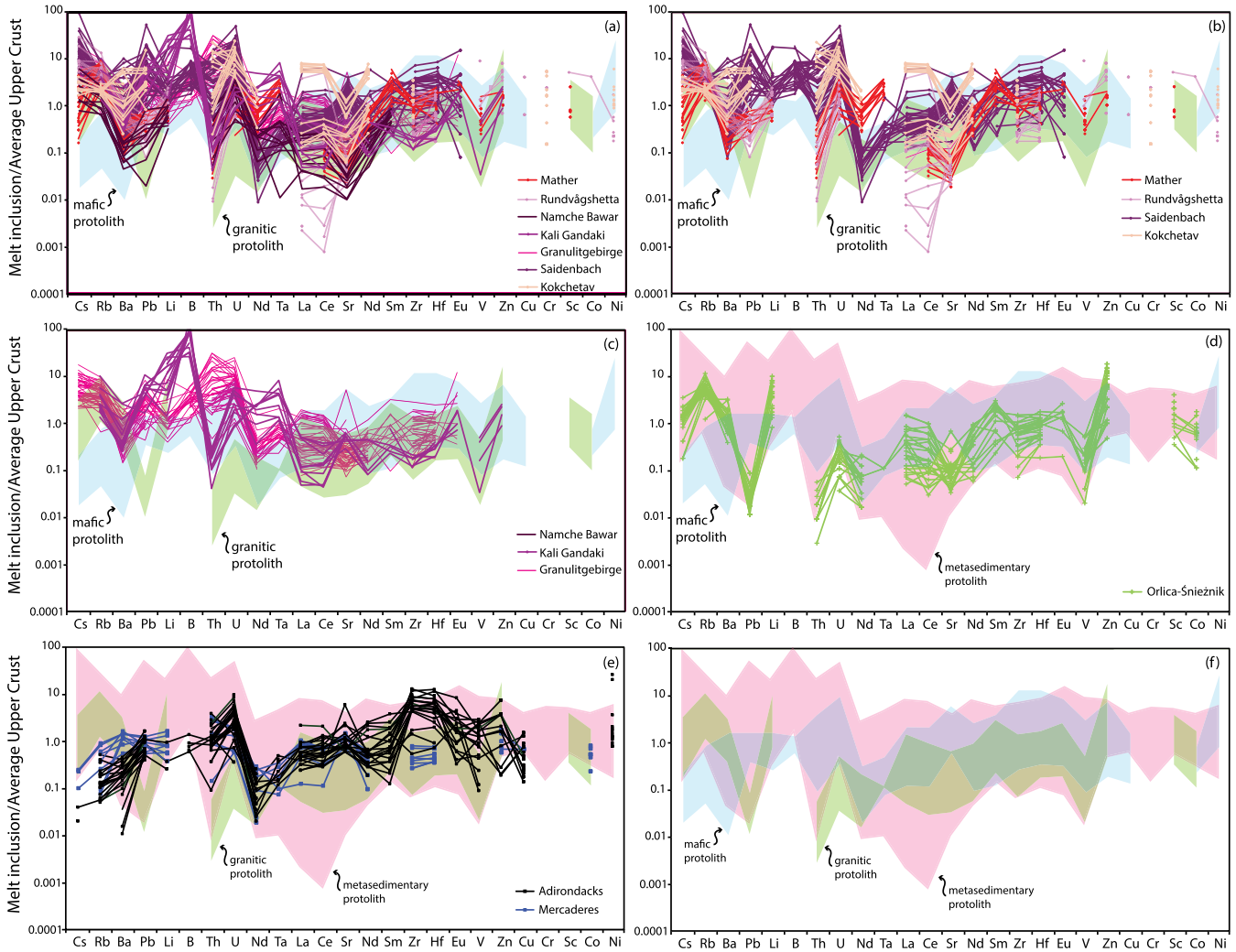

Fig. 11. Spider diagrams of anatectic MI (references as in Fig. 9) normalized to upper continental crust (Rudnick & Gao, 2003). (a) All metasedimentary protoliths (Mather, Rundvågshetta, Namche Bawar, Kali Gandaki, Granulitgebirge, Saidenbach and Kokchetav). (b) Metasedimentary protoliths of <1.0 GPa (Mather and Rundvågshetta) and 2.5–4.5 GPa (Saidenbach and Kokchetav). (c) Metasedimentary protoliths of 1.0–2.5 GPa (Namche Bawar, Kali Gandaki, Granulitgebirge). (d) Granitic protolith (Orlica-Śnieżnik). (e) Mafic protoliths (Adirondacks and Mercaderes). (f) General comparison of mafic, granitic and metasedimentary protoliths. Source of MI data as in Fig. 8.

was documented for apatite and phosphorous (Yakymchuk & Acosta-Vigil, 2019). These authors presented a well-detailed comparison from which they concluded that 'the unsuitability of the currently available solubility equations is probably the main cause for the discrepancy between the measured concentrations of phosphorus in nanogranites and those predicted from current apatite solubility expressions'.

Radiogenic heat-producing elements in anatectic melt inclusions

About one-third of the total radiogenic heat of the Earth is provided by the continental crust through radioactive decay (Huang *et al.*, 2013). The decay of ^{40}K, ^{230}Th, ^{235}U and ^{238}U generate radiogenic heat production in the crust at rates of 0.074 μWm^{-3} per wt % K_2O, 0.265 μWm^{-3} per ppm of Th and 0.072 μWm^{-3} per ppm of U (Bea, 2012). About 20% of heat is provided by K_2O, whereas U and Th provide the remaining 80%. The partitioning of the two later heat-producing elements (HPE) among different reservoirs is chiefly controlled by the stability and breakdown of accessory minerals rich in Th and U such as monazite, zircon, allanite, xenotime and apatite (Bea, 1996; Bea & Montero, 1999; Yakymchuk & Brown, 2019).

Heat production (A) can be calculated considering the following equation:

$$A\ (\mu Wm^{-3}) = \rho * (0.036\ C_{K2O} + 0.097\ C_U + 0.026\ C_{Th})$$

where ρ is the rock density ($g.cm^{-3}$) and C_{K2O}, C_U and C_{Th} are the concentrations of K_2O (wt %), U (ppm) and Th (ppm), respectively. Heat production can also be calculated at different ages when the radioactive decay in taking into account. Bulk heat production of the continental crustal is estimated at ~0.9 μWm^{-3} (Mareschal & Jaupart, 2004).

The model of crustal differentiation via anatexis and extraction of anatectic melts to shallower levels, producing a refractory lower crust and an upper crust enriched in incompatible elements (Vielzeuf *et al.*, 1990), implies in an overall decrease of heat production with depth, with the average upper and lower crustal heat production amounting ca. 1.6 and 0.2 μWm^{-3}, respectively (Rudnick & Gao, 2003). The alternative value of 0.7 μWm^{-3} has also been proposed for the lower crust by Hacker *et al.* (2011).

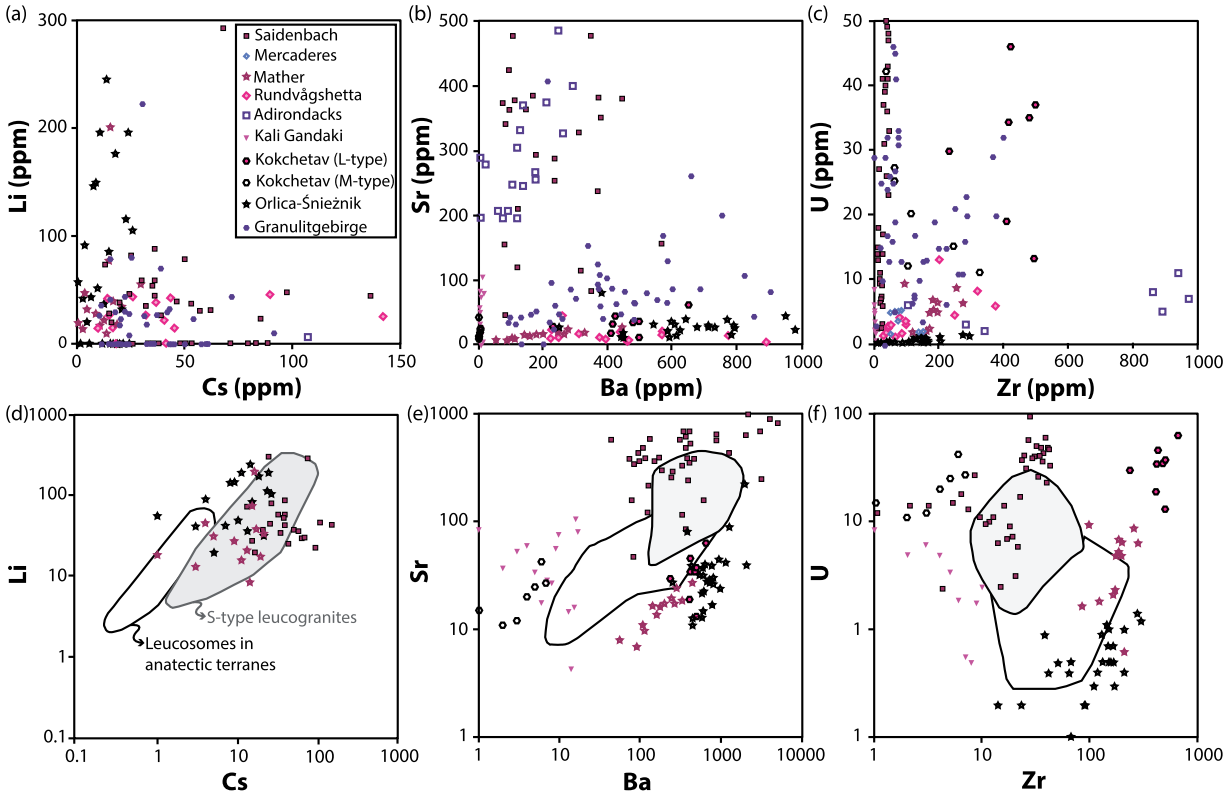

Fig. 12. (a) to (c) Binary diagrams of Li, Cs, Sr, Ba, U and Zr (ppm) in MI from the literature (as in Fig. 8). In Kokchetav, the high Zr contents have been attributed to diffusion from the host garnet and thus are not considered reliable contents of the melt (Stepanov *et al.*, 2016). (d) to (e) Binary diagrams comparing selected strongly peraluminous MI, leucosomes and S-type leucogranites (compilation from Acosta-Vigil *et al.*, 2012).

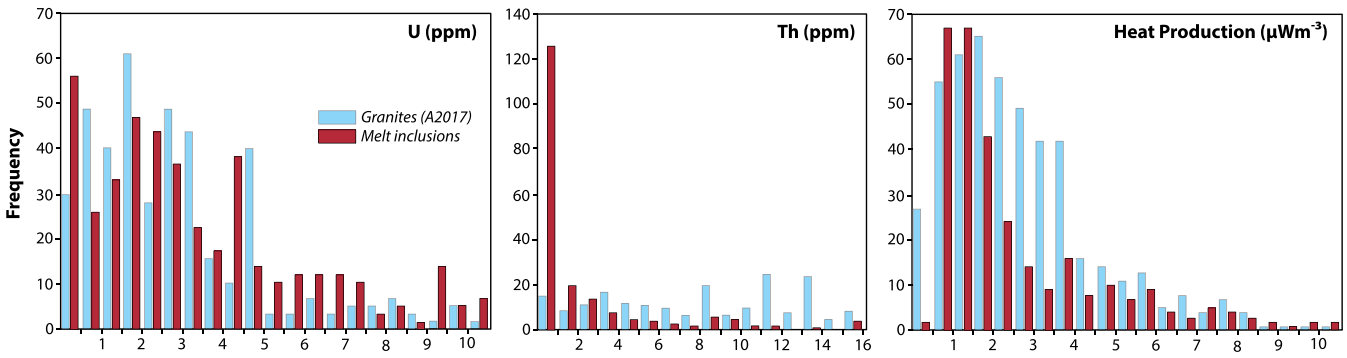

Fig. 13. Frequency diagrams of U (ppm), Th (ppm) and heat production (μWm^{-3}) comparing MI from the literature (references as in Fig. 8) and granites (database from Artemieva *et al.*, 2017). Cut-off values (10 ppm for U, 16 ppm for Th and 10 μWm^{-3}) are used to limit the comparison to the most common values and to avoid 'outliers'.

Assessment using phase equilibrium modelling also conforms with this view that melt loss leads to a depletion of HPE, U, Th and K, in the residuum because the anatectic melt will likely be saturated in those elements (Yakymchuk & Brown, 2014).

Several empirical studies on heat production of deep crustal levels now exposed at the surface display a different picture, because similar, high heat production values (varying from ~2 to 3.3 μWm^{-3}) have been measured in rocks that experienced either sub- and suprasolidus peak conditions (Alessio *et al.*, 2018). These observations concur with other works that challenge the notion of heat production decreasing at depth (Bea & Montero, 1999; Hacker *et al.*, 2011; Bea, 2012) and support the conservation of heat production even after partial melting and extraction of anatectic melt from the lower continental crust. However, these studies did not take into account the possible role of UHT metamorphism for the mobility of HPE. For instance, Ewing *et al.* (2014) documented an evident decrease in the bulk rock content of U and Th in UHT pelitic granulites (the so-called septa) from the Ivrea-Verbano Zone with respect to their HT counterparts. Similarly, Stepanov *et al.* (2014) reported a similar strong depletion in U and Th in UHT-UHP metasediments from the Kokchetav complex in Kazakhstan.

Anatectic MI may provide further insights relevant to this debate. Liu *et al.* (2023a) were the first to calculate the heat production (in μWm^{-3}) of anatectic MI. Here, we expand this approach considering all the case studies where K_2O, Th and U were analyzed. Together with calculations of heat production (considering K, Th and U), the focus is also given to the concentrations of Th and U in MI, as these elements are the highest producers of heat. From 13 case studies, 10 are of metasedimentary origin and only 3 of mafic origin (Figs 13 and 14).

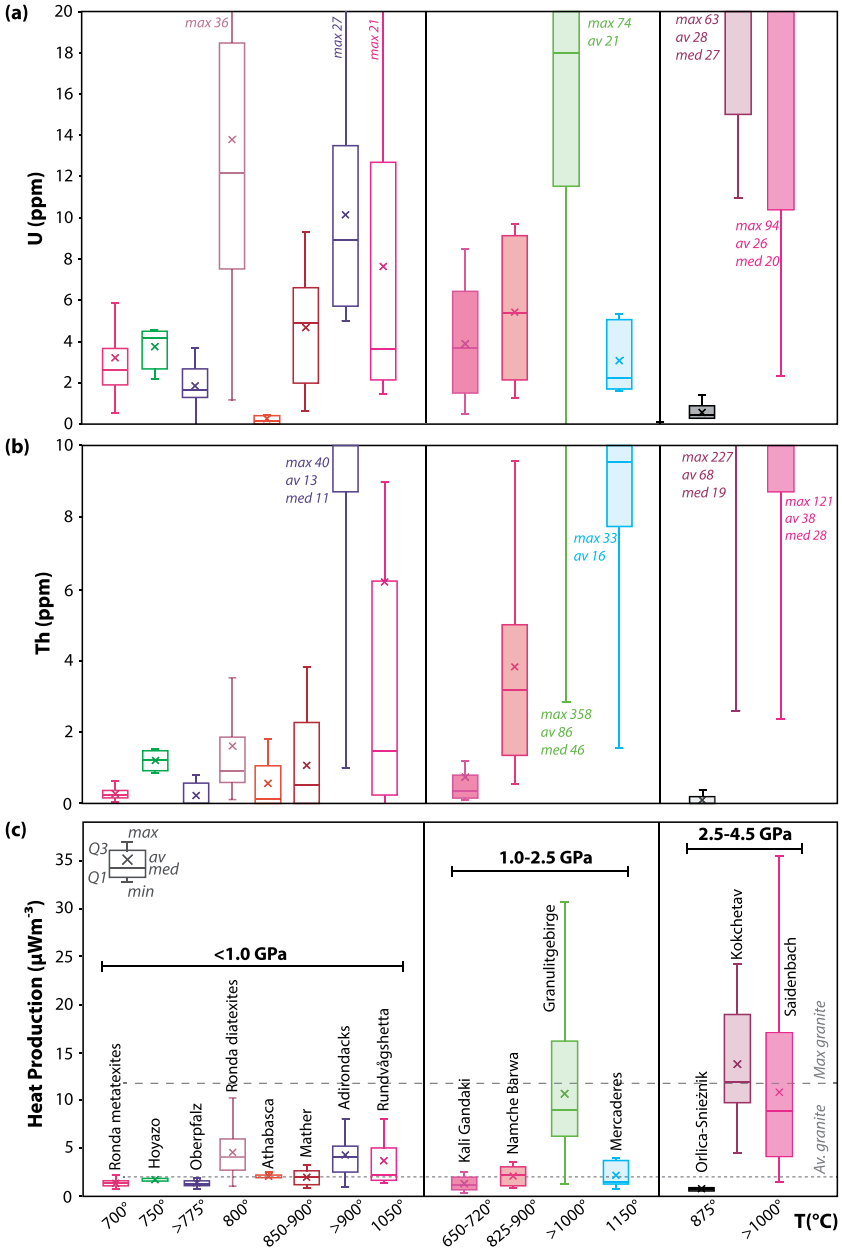

Fig. 14. Whisker plot diagrams for (a) U (ppm), (b) Th (ppm) and (c) heat production (μWm^{-3}) of MI from the literature (metasedimentary protoliths: Hoyazo, Acosta Vigil *et al.*, 2010; Orlica-Śnieżnik, Ferrero *et al.*, 2019; for Oberpfalz, Kokchetav, Kali Gandaki, Rundvågshetta, Mather, Namche Barwa and Saidenbach see references in Fig. 8). Ronda Migmatites and Athabasca are unpublished data; mafic protolith: Adirondacks and Mercaderes, references in Fig. 8. Average granite and maximum granite heat production (Artemieva *et al.*, 2017) are also presented in (c).

Due to their high K, Th and U contents, granites are among the crustal rocks with the highest heat productions (Jaupart & Mareschal, 2003; Villa *et al.*, 2010). In Fig. 13, the data of MI ($n = 320$) are compared with the granite database (GRANITE2017, $n = 500$) from Artemieva *et al.* (2017). This comparison clearly shows that the behaviour of MI and granites is similar. An asymmetric distribution with a peak shift toward lower values is observed for U, Th and, consequently, for heat production as well. The greatest discrepancy is observed for Th, displaying very low values in most MI (~45% of MI have <2 ppm). Total averages are somewhat comparable: 14.8 ppm Th in granites versus 10.6 ppm in MI, 3.9 ppm U in granites versus 8.9 ppm in MI and 2.7 μWm^{-3} in granites versus 2.0 μWm^{-3} in MI (disregarding Kokchetav and Saidenbach that are extremely enriched).

Figure 14 shows the complete MI datasets in terms of U and Th contents, as well as radiogenic heat production. Firstly, a general trend shows increasing values of U and Th in melts produced at progressively higher temperature, for $P < 1.0$ GPa (Fig. 14a and b). One exception is represented by Ronda diatexites, for which a specific role of protolith composition and/or a different behaviour of zircon cannot be ruled out (see below). Temperature and Th content are also positively correlated for the 1.0–1.5 GPa case studies (Fig. 14b). Secondly, U reaches higher concentrations in the melt than Th. Not surprisingly, the heat production (Fig. 14c) follows the similar general behaviour of Th and U with higher values observed in the higher temperature terranes, but most averages are lower or equal than the global average granite (~2 μWm^{-3}) from Artemieva *et al.* (2017). The highest values, >15 μWm^{-3}, are observed in HP to UHP case studies (Granulitgebirge,

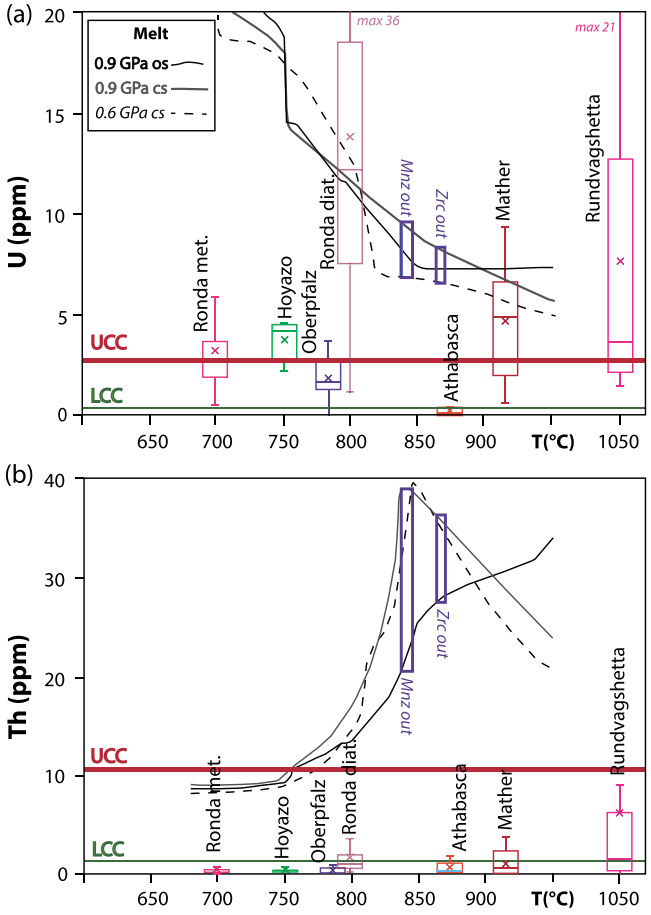

Fig. 15. (a) U and (b) Th concentrations (ppm) in MI (as in Fig. 13) and in model melts calculated for open and closed systems (from Yakymchuk *et al.*, 2018). Monazite out and zircon out intervals are from 0.6 to 0.9 GPa at closed system (Yakymchuk *et al.*, 2018).

Kokchetav and Saidenbach), and exceed those measured in most rock types (Hasterok *et al.*, 2018). On the contrary, in the near-UHP Orlica-Śnieżnik case study, values are particularly low (0.7 μWm^{-3}), but slightly higher than slab-derived melts from the Dabie orogen (not shown) with values 0.15 μWm^{-3} in average (Gao *et al.*, 2013).

A key aspect is that the U and Th contents of MI and their positive correlation with increasing temperatures at $P < 1$ GPa markedly differ from model predictions (Fig. 15). Phase equilibrium modelling is often coupled with solubility equations for accessory minerals to investigate the fate of these phases and of some key elements such as Th and U (Yakymchuk *et al.*, 2018; Yakymchuk & Brown, 2019). The comparison reported in Fig. 14 shows that the predicted U and Th contents of melt at 700 to 800°C may be up to ten times higher those observed in natural melts. The match is better for U at >850°C, whereas Th is always much higher in modelled melts. Moreover, the concentrations of U in modelled melt decrease up temperature, as opposed to MI (Fig. 15). A good match is instead observed for U in Ronda diatexites, but not for Th.

Among the several limitations of this modelling approach (discussed in Yakymchuk *et al.*, 2018), two aspects are in our opinion of upmost importance for natural systems. Firstly, the models considered in our comparison predict accessory mineral dissolution upon heating and do not account for the prograde growth of accessory minerals, in contrast to the evidence from high-grade terranes (Spear & Pyle, 2010). In particular, monazite volume proportion estimates in natural occurrences may increase through the granulite facies up to ~900°, diminishing drastically at UHT conditions (Williams *et al.*, 2022). This evolution finds support from our MI dataset, where a major increase in the Th content occurs at >900°C (Fig. 14b). Secondly, most accessory minerals in metapelites are sheltered in rock-forming minerals preventing them from being completely dissolved in melt during prograde melting (Watt & Harley, 1993). The impact of this latter process diminishes with increasing peak temperature due to consumption of reactants. This can be observed in Fig. 14a where the U content of calculated melts approaches that of MI at >900°C. At lower temperature, solely MI from Ronda diatexites matches model predictions, despite some internal variability (Fig. 15a). This could possibly be explained by the more psammitic composition of these rocks, where MI formed when most of the biotite was already consumed at 820°C and most accessory minerals were in contact with melt (Bartoli *et al.*, 2016a).

Summarizing, the comparison between MI and granites suggests that differentiation processes occurring during the ascent of crustal melts from their source to shallower crustal levels do not largely affect their HPE contents. Therefore, their impoverishment or enrichment in crustal melts should occur within the source terrain during melt generation. From the MI point of view, only the UHT metamorphism and the formation of UHT anatectic melts may mobilize sufficient amounts of HPE, resulting in the formation of an HPE-depleted residual lower crust. Therefore, the approach of Alessio *et al.* (2018) should be extended to UHT terranes for a more complete view of the mobility and crustal inventory of HPE. Another important message from MI is that phase equilibrium modelling of accessory minerals in anatectic rocks has several important limitations for natural systems (see also Yakymchuk & Acosta-Vigil (2019) for the phosphorous case) and more empirical studies on MI and on the fate of accessory minerals during anatexis are needed. A topic deserving some attention and further investigations is the important discrepancy between the Th contents of granites and those of MI.

Volatiles, fluid regimes and carbon mobility during anatexis

One of the most significant advantages of studying MI in metamorphic rocks is the opportunity to recover the volatile contents of anatectic magmas in their source region, before fluid exsolution upon decompression and crystallization, and to reconstruct the fluid regime of the deep levels of the continental crust. Thus far, efforts have been concentrated on measuring H_2O, CO_2, F and Cl contents using mainly EPMA, Raman spectroscopy, and due to the small size of most targets, NanoSIMS. Other volatiles such as CH_4 and N_2 have been detected by Raman spectroscopy, but not yet quantified in anatectic melts.

Concerning the fluid regime, fluid inclusions have been the main evidence for the presence of fluids (C-O-H fluids, and, to a lesser extent, brines) in the lower continental crust (Newton *et al.*, 1980; Hollister & Crawford, 1981; Touret, 1985; Harlov *et al.*, 2005; Touret & Huizenga, 2012). However, depending on the primary or secondary nature of fluid inclusions, it may be rather difficult to argue that a free fluid phase was present during the prograde path or at metamorphic peak conditions and anatexis (Carvalho *et al.*, 2020). The picture is clearer when primary fluid inclusions coexist with MI in the same clusters, as these are microstructural evidence for primary fluid–melt immiscibility (Roedder, 1984). Case studies clearly demonstrating fluid–melt immiscibility during anatexis of the deep crust were

initially revealed by this microstructural evidence within minerals of migmatites and granulites. Immiscibility is supposed to occur during partial melting in the presence of fluid species that have reached saturation with the anatectic melt (Cesare *et al.*, 2007). The first occurrences recording this process were described in xenoliths from the Pamir (Asia) and El Hoyazo (Spain). Granulitic xenoliths of the Pamir (Chupin *et al.*, 2006; Madyukov *et al.*, 2011) were reported to contain glassy MI and CO_2-bearing fluid inclusions in garnet, clinopyroxene and scapolite. In graphite-bearing xenoliths from El Hoyazo, glassy MI and COH-fluid inclusions occur in plagioclase, garnet and cordierite (Cesare *et al.*, 2007; Ferrero *et al.*, 2011). More recently, many other occurrences were reported where primary melt and fluid inclusions coexist in the same clusters within garnet (see Table 1): La Galite (Tunisia), Jubrique (Betic Cordillera), Athabasca granulite (Canada), Ivrea-Verbano Zone (Italy), Ktis and Stuckestein (Bohemian Massif), Gruf Complex (Central Alps), Caledonides, Mt. Edixon (Antarctica), Limpopo belt, Kangerlussuaq basement (Southeast Greenland) and Usagaran belt (Tanzania). In most of these occurrences, the melt is crystallized and the fluid has reacted to various degrees with the host, producing a range of step-daughter minerals, as interpreted in Carvalho *et al.* (2020) by means of thermodynamic modelling. These studies strongly suggest that anatexis under fluid-saturated conditions (either carbonic, aqueous or brines) may be a rather common phenomenon.

Granitic magmas have H_2O, but how much? Water content of granitic magmas depends on source composition and H_2O availability, melting reactions, P–T conditions of partial melting and the degree of fractionation (Clemens, 1984). The solubilities of H_2O and CO_2 in synthetic granitic compositions have been constrained by experimental petrology (Ebadi & Johannes, 1991; Holtz & Johannes, 1994). Bartoli *et al.* (2014) were the first to successfully measure H_2O contents of natural MI in migmatites from Ronda (Spain) using NanoSIMS, and that work paved the way for many other afterwards (Jubrique, Acosta-Vigil *et al.*, 2016; Ivrea-Verbano Zone, Carvalho *et al.*, 2019; Mt Edixon, Ferri *et al.*, 2020; Central Maine, Ferrero *et al.*, 2021b; Gruf Complex, Gianola *et al.*, 2021; Saidenbach, Borghini *et al.*, 2023; Orlica-Śnieżnik, Granulitgebirge and La Galite, Ferrero *et al.*, 2023). An up-to-date compilation of H_2O contents of MI in high-grade rocks is presented in Fig. 16a and b and Table S3 (see also recent review by Ferrero *et al.*, 2023). Current data reveal that in most case studies MI are H_2O-undersaturated at the estimated P–T conditions of formation. Each single case study may show a range of H_2O contents in MI, which can be explained as result of 'mosaic' equilibrium in terms of H_2O activity, where heterogeneities at microscale affect and buffer the H_2O contents of the melt (Bartoli *et al.*, 2014). Despite the internal variations in each occurrence, H_2O values in the melt decrease with T in agreement with experimental work. However, MI in granulite facies rocks from Ivrea-Verbano Zone (Carvalho *et al.*, 2019) and Gruf Complex (Gianola *et al.*, 2021) display slightly higher values (maximum 8.2 and 8.7 wt %, respectively) than previously estimated by experiments at $T > 850°C$ (see below).

Comparing the available database of NI and glassy inclusions (GI), Tacchetto *et al.* (2021) showed that the former inclusions were often more hydrous than the latter. They thus concluded that the low H_2O content may represent a further impediment to crystallization, along with the very small volume of these cavities (Cesare *et al.*, 2009), favouring the coexistence of glassy MI and NI. From the dataset compiled by these authors, H_2O contents $\geqq$ 5–6 wt % are likely to enhance the crystallization of MI, and therefore, they proposed that analyzing only GI may lead to underestimate the maximum H_2O contents in anatectic melts. The migmatites from Ronda were the first occurrence where the contrast in H_2O was observed (average NI 6.5 *versus* average GI 2.7 wt %; Bartoli *et al.*, 2015). Recently, the same feature was also reported in the MI from Saindenbach (Borghini *et al.*, 2023), La Galite and Granulitgebirge (Ferrero *et al.*, 2023), which display much lower H_2O values than other NI case studies (see Fig. 16a and b). Therefore, it can be concluded that, ideally, both NI and GI should be analyzed in order to have a complete picture.

Carvalho *et al.* (2019) were the first to measure CO_2 in anatectic MI in graphite-bearing metapelites of the Ivrea-Verbano Zone using NanoSIMS. The CO_2 contents of MI increase with metamorphic grade, reaching up to 2500 ppm in the granulite facies samples. Here, MI coexist with COH–fluid inclusions in the same clusters in garnet, suggesting fluid–melt immiscibility during anatexis. Because the Ivrea-Verbano Zone is considered a natural laboratory for the anatectic processes, Carvalho *et al.* (2019) proposed that in addition to fluid-present (Clemens & Droop, 1998) and dehydration melting (Thompson, 1982), COH fluid-present melting of the deep continental crust may also represent an essential key process in the origin of anatectic granitoids.

The MI from Mt. Edixon (Ferri *et al.*, 2020) and Gruf Complex (Gianola *et al.*, 2021), formed in a situation of fluid–melt immiscibility at similar pressure conditions as the melts from Ivrea-Verbano Zone, and have comparable CO_2 contents (up to 2000 and 1730 ppm, respectively). Conversely, in MI from Central Maine (Ferrero *et al.*, 2021) and Saidenbach (Borghini *et al.*, 2023), formed at HP to UHP conditions, CO_2 values are much higher (0.81–2.89 wt %, respectively). Specifically in the case of Saidenbach, an important observation was that from 5 to 40% of CO_2 in the MI was exsolved in the shrinkage bubble, so that a reintegration method was applied to recover the bulk CO_2 composition of the melt (Borghini *et al.*, 2023). Partitioning of 40 to 90% of the melt CO_2 within the inclusion bubble is common also in igneous MI (Moore *et al.*, 2015). Therefore, caution is advised in the study of bubble-bearing MI, and measurements of volatiles in both glass and bubbles must be considered to determine the total volatile budget of the melt.

Carvalho *et al.* (2023a) noticed that the NI from graphitic anatectic metapelites saturated in (immiscible with) a COH fluid generally display lower CO_2 contents than those predicted by experimentally determined CO_2 solubilities at the same *P* conditions (see Fig. 16c and d). This occurs because most of CO_2 solubility data available for rhyolitic compositions (Fogel & Rutherford, 1990; Blank *et al.*, 1993; Tamic *et al.*, 2001; Duncan & Dasgupta, 2014; Muth *et al.*, 2020) were determined at more oxidizing conditions than those occurring in many migmatites, which are graphite bearing. CO_2 solubilities determined under (highly) oxidizing conditions are likely maxima, with little possibility of extrapolation to the more reducing graphitic protoliths, in which the measured CO_2 contents of melts is lower. Through the observations of Carvalho *et al.* (2023a), it is clear that the available CO_2 solubility experiments for rhyolitic composition cannot be considered synthetic analogues of natural granulitic systems, which often display coexisting H_2O–CO_2–CH_4 ternary fluids, H_2O- and CO_2-bearing anatectic melts and graphite-bearing residues. Therefore, caution is also required when applying the CO_2 solubility models based on such experiments (Liu *et al.*, 2005; Papale *et al.*, 2006) to anatectic systems. As highlighted in Carvalho *et al.* (2023a), targeted experimental studies are needed before any precise estimates on carbon budget and fluxes in the partially melted graphitic continental crust can be made.

Borghini *et al.* (2023) measured up to 2.5 wt % CO_2 in MI from the UHP eclogites of the Saidenbach Reservoir (Bohemian Massif) (Fig. 16c and d) and used this case to argue that continental

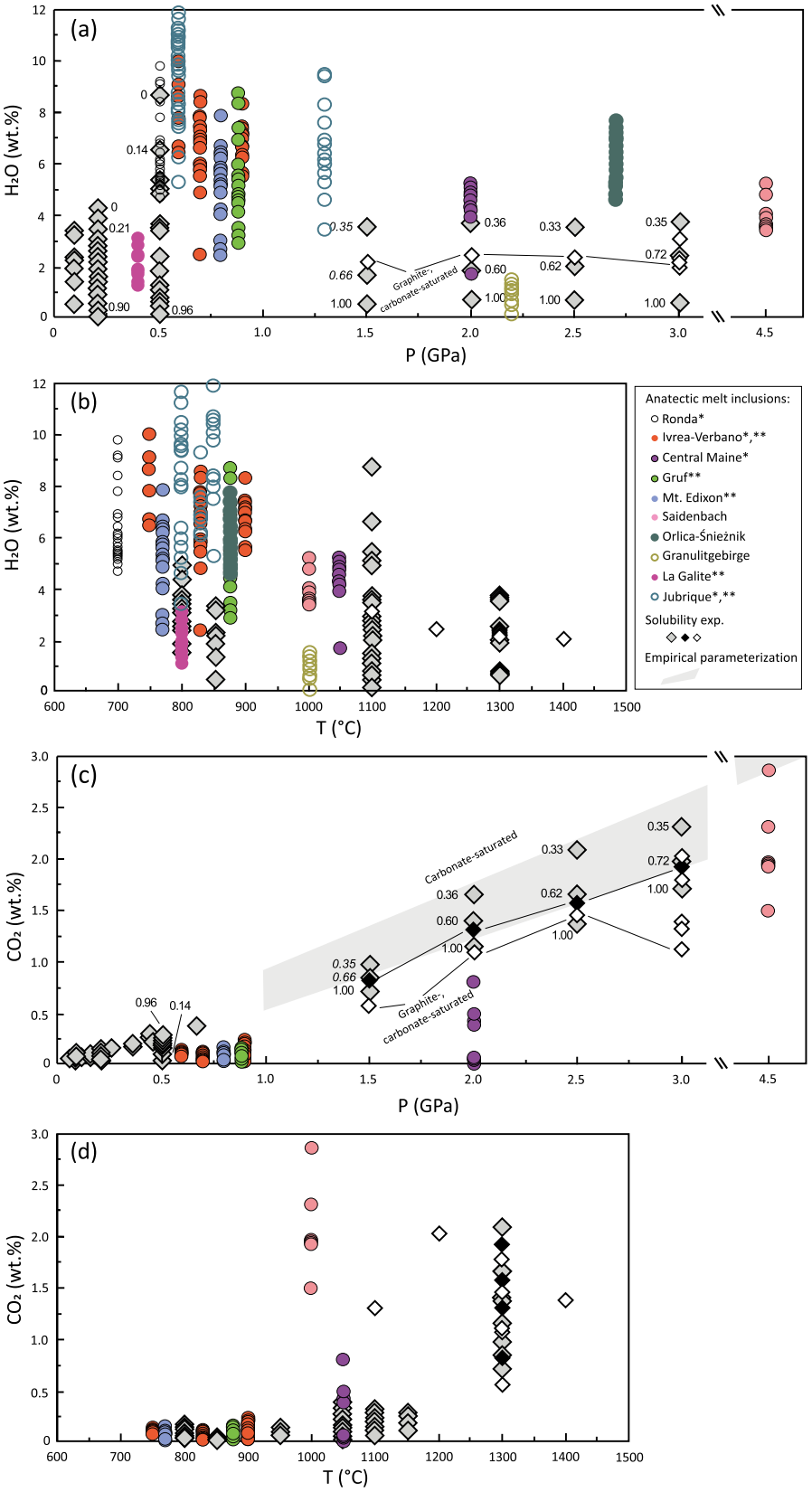

Fig. 16. Comparison between H_2O and CO_2 solubility data available for rhyolitic composition from the literature and anatectic MI (redrawn from Carvalho *et al.*, 2023a). Experimental data are from Fogel & Rutheford (1990), Blank *et al.* (1993) and Tamic *et al.* (2001) at <1 GPa, from Duncan & Dasgupta (2014, 2017) at ≥1.5 GPa. Italic values reflect the fraction of CO_2 in the fluid phase for experiments at 0.5 GPa (Tamic *et al.*, 2001) and at 1.5–2.0 GPa (Duncan & Dasgupta, 2014). MI data from Ronda (Bartoli *et al.*, 2014), Jubrique (Acosta-Vigil *et al.*, 2016), Ivrea-Verbano Zone (Carvalho *et al.*, 2019), Mt Edixon (Ferri *et al.*, 2020), Central Maine (Ferrero *et al.*, 2021), Gruf Complex (Gianola *et al.*, 2021), Saidenbach (Borghini *et al.*, 2023), Orlica-Śnieżnik, Granulitgebirge and La Galite (Ferrero *et al.*, 2023). NI from the Central Maine Terrane have two additional datapoints with CO_2 of ≈2.9 wt % and from Jubrique have four additional datapoints with ≈13 and ≈14 wt % H_2O (not shown).

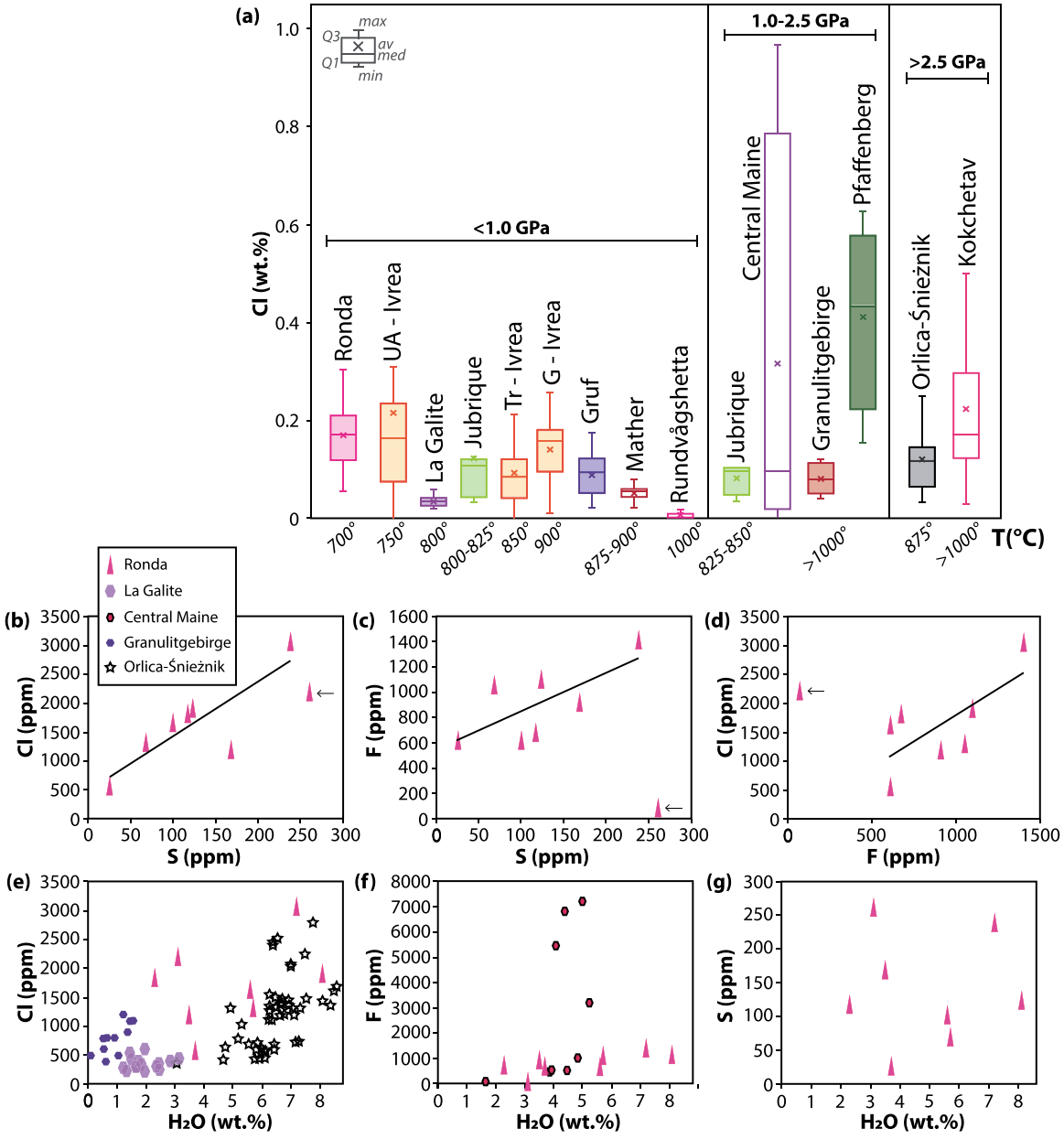

Fig. 17. (a) Whisker plot diagrams for Cl (wt %) of MI from the literature (granitic protoliths: La Galite and Orlica-Śnieżnik, Ferrero *et al.*, 2023; metasedimentary protoliths: Jubrique, Kokchetav, Ivrea-Verbano Zone, Gruf Complex, Mather and Rundvågshetta references as in Fig. 8; Pfaffenberg, Borghini *et al.*, 2024; Granulitgebirge, Ferrero *et al.*, 2023). Case studies where COH-fluid–melt immiscibility occurs are represented by filled boxes. Most of the analyses of Cl were obtained by electron microprobe, except Orlica-Śnieżnik and La Galite, which were determined by NanoSIMS. (b-d) Cl, S and F (ppm) contents of NI in Ronda Migmatites (Bartoli *et al.*, 2013a). (e-g) Cl, S, F (ppm) and H_2O (wt %) contents of NI from the literature.

subduction may redistribute a substantial volume of carbon in the lithosphere. In particular, they related these UHP melts to the postcollisional ultrapotassic magmatism in the Variscides.

The presence of Cl in glass of NI was first detected by Ferrero *et al.* (2012; see their Fig. 7). The first report of halogens (F and Cl) in anatectic MI started with Bartoli *et al.* (2013a) by SIMS measurements, followed by a systematic evaluation by Ferrero *et al.* (2021b) and Borghini *et al.* (2024). In high-pressure metasediments from the Central Maine Terrane (Ferrero *et al.*, 2021b), F contents were measured by NanoSIMS, revealing considerably high values (up to 0.72 wt %). High values of F (up to 0.24 wt %) in MI from the Pfaffenberg eclogites are also inferred indirectly based on apatite composition (Borghini *et al.*, 2024). Measured Cl values are also high in both case studies (0.32 and 0.41 wt % Cl, respectively; see also Fig. 17a).

Fluorine (up to 0.14 wt %) and Cl (up to 0.30 wt %) were measured by SIMS in experimentally rehomogenized MI from Ronda metatexites (Bartoli *et al.*, 2013a). In similar MI, which underwent overheating during experiments, F reached higher values (up to 0.65 wt %). So far, sulphur was analyzed only in these MI, with a maximum value of ≈200 ppm (Bartoli *et al.*, 2013a). In these MI, F, Cl and S are positively correlated (Fig. 17b–d). Also, the H_2O content seems to increase with increasing F, whereas no correlations are observed with S and Cl (Fig. 17e–g). Ferrero *et al.* (2023) investigated the correlation of Cl and H_2O in MI from three case studies and found an increase of Cl solubility in the melt with

pressure, as previously proposed by Webster *et al.* (2015). Ronda datapoints, instead, are relatively scattered (Fig. 17e).

In Fig. 17a, a compilation of Cl data of MI available in the literature allows for a more comprehensive assessment. The effect of pressure is confirmed for granitic protoliths as an increase in Cl (0.03 to 0.12 wt % in average) and is observed from La Galite (0.4 GPa) to Orlica-Śnieżnik (2.7 GPa). Some case studies of metasedimentary rocks could indicate an effect of pressure as well—Central Maine, Pfaffenberg and Kokchetav exhibit higher values and averages than metasedimentary rocks <1.3 GPa (i.e. Ivrea, Jubrique, Gruf, Mather and Rundvågshetta). There are however some exceptions such as Granulitgebirge, which could be related to source composition, as, pointed out by Borghini *et al.* (2024).

The high concentration of halogens in the Central Maine Terrane and the Pfaffenberg was interpreted as result of the possible contribution from brines or from a halogen-bearing phase (e.g. phengite) during anatexis (see discussion by Ferrero *et al.*, 2021a and Borghini *et al.*, 2024). When dealing with halogen contents of melt, in order to fully evaluate the extent of brine-assisted melting during crustal differentiation, the study of MI could be coupled with the oxygen isotope characterization of MI-bearing garnet (Higashino *et al.*, 2019).

Nitrogen was detected in shrinkage bubbles of GI of UHT granulites (Gruf Complex—Gianola *et al.*, 2021; Rundvågshetta, Carvalho *et al.*, 2023b) and in NI of HP eclogites (Pfaffenberg, Borghini *et al.*, 2024). Therefore, it is possible that this volatile is dissolved in the anatectic melt as well, even though it has never been analyzed so far. The N_2 component, now present together with CO_2 in the shrinkage bubble, most likely derives from traces of NH_4^+ that can be present in the structure of biotite replacing K^+ (Moin *et al.*, 1994; Cesare *et al.*, 2007) and be released during its breakdown melting.

LIMITATIONS OF MELT INCLUSION STUDIES

MI can provide unique petrological and geochemical information on suprasolidus deep crustal processes because they are the best-preserved remnants of (anatectic) melts produced in, or percolated through, high-grade metamorphic rocks. Nonetheless, MI studies have some limitations that need to be kept in mind when considering their reliability. Except for the doubts on the origin of inclusions, which should be adequately dispelled by earlier literature and in the previous chapters (Fig. 8), some main limitations still stand. They involve in general (a) the reliability and significance of chemical data obtained with MI, and in particular, (b) the possible postentrapment compositional modifications of MI and (c) the representativeness of MI composition of the bulk melt in a migmatite. The reader is referred to Cesare *et al.* (2015) for a detailed discussion of these problems.

Among postentrapment modifications of MI, a particular role is played by the 'recrystallization' of the host phase, whether dynamic, i.e. stress-related, or due to chemical reactions, in particular dissolution–precipitation. Considering garnet as the main host, extensive dynamic recrystallization is observed only in mylonites from high-strain zones (Massey *et al.*, 2011) where crystals undergo microfracturing, grain boundary sliding, grain rotation and impingement, and pressure dissolution. Under these circumstances, also considering the small scale (tens of μm) at which these phenomena occur, any MI present in the garnet would have been erased. Much more likely is the modest strain that most garnets exhibit during the retrograde history after high-grade metamorphism. This strain is often accompanied by microfracturing of the garnet, resulting in the formation of offshoots or tails pf melt emanating from the MI (Ferrero *et al.*, 2012). This process may depressurize the inclusion and open it to chemical exchange with the matrix outside garnet. The study of these MI should be avoided (Cesare *et al.*, 2015).

The garnet host may undergo recrystallization by chemical reactions consuming (part of) it and forming another garnet with a different composition. Such a process, better defined as dissolution–reprecipitation and observed experimentally in other phases (Putnis, 2002), has been proposed for garnet at both sub- (Faryad *et al.*, 2019) and suprasolidus (Beyer & Chakraborty, 2021) conditions. If an MI-bearing garnet undergoes dissolution–reprecipitation, the MI contained in the dissolved part would be erased. If the process takes place at suprasolidus conditions and in the presence of melt (melt-assisted dissolution–precipitation), new MI could form in the newly formed garnet (see discussion above on the behaviour of garnet).

Another limitation of MI studies is the petrographic resemblance of MI to multiphase fluid inclusions. Revealing the widespread occurrence of fluid/melt immiscibility during anatexis, the works of Ferrero *et al.* (2014, 2016), Tacchetto *et al.* (2019) and Carvalho *et al.* (2019, 2020, 2023) have also shown how similar former fluid and former MI may look, once they have crystallized respectively step-daughter and daughter minerals. It follows that techniques other than optical microscopy (e.g. Raman spectroscopy) are required to assess the fluid vs. melt nature of the inclusion, and their relative abundances within a host.

The 'Roedder's Rules' discussed by Bodnar & Student (2006) that state that when MI are experimentally rehomogenized in a narrow temperature interval, completely and without interaction with the host, and if the analyzed glass composition is fairly homogeneous, then they can be considered good recorders of the chemical composition of melt at the time and conditions of entrapment. Therefore, the reliability and significance of information gained from MI depends on correct and successful experimental rehomogenization, which is a very time-consuming process currently performed at the piston cylinder via a trial-and-error approach that must be fine-tuned for each different sample. This is the reason why the studies where MI remelting is performed and homogenization achieved are still limited. This problem is eminently technical and could be solved in two ways. On one hand developing or refining analytical methods that allow bulk chemical analyses of crystallized inclusions without remelting, via reintegration and signal processing methods such as those used with LA-ICP-MS analyses of fluid inclusions (Halter *et al.*, 2002), which are still of limited utility for anatectic MI. In this respect, synchrotron-based μXRF and μXRD techniques (Omori *et al.*, 2023) might in the near future allow fast data acquisition at the desired spatial resolution and represents a promising analytical strategy to reconstruct melt compositions. On the other hand, finding an alternative experimental strategy that could replace the piston-cylinder experiments, allowing real-time visual observation of the remelting of inclusions under controlled pressure and temperature conditions is desirable. The diamond anvil cell (Li *et al.*, 2022) or similar equipment could be the way forward to achieve this, but at present, the limitations of sample size and optical resolution have not yet been resolved.

FUTURE PERSPECTIVES

As shown in this review, a lot of progress has been made on the study of MI in high-grade metamorphic rocks. Despite all the advances, there is still much space for new research in general.

Some main fields that in our opinion should be developed in the future are listed below.

- Much more information is still needed on MI from mafic and granitic protoliths. In particular, MI in mafic protoliths can provide a wealth of information on the generation of the early continental crust. Moreover, they have greater potential to sample anatectic melts produced at high-pressure and high-temperature conditions.
- Computed X-ray microtomography should be potentially used for the reconstruction of the precise textural position of inclusions within the hosts before sectioning them for further studies. So far, only the work of Parisatto *et al.* (2018) investigated this aspect, but it could be used more routinely. If applied to a number of high-grade metamorphic terranes, this microstructural characterization will help understanding the behaviour of garnet in suprasolidus rocks. In turn, easier access to synchrotron-based nanotomographic facilities will allow at a much greater spatial resolution for the 3D reconstruction of solid/fluid phases in individual NI and fluid inclusions as well.
- Further research on time resolved experiments is necessary to obtain better constraints on the effects the experiment duration on rates of re-homogenization and problems related to melt–host interaction.
- A host certainly deserving more attention is zircon. Indeed, zircon behaviour in anatectic rocks is a contentious subject (Yakymchuk, 2023). The geochemical signature of MI in zircon (e.g. Li, Cs, B, Sr contents, Rb/Cs and Rb/Li ratios, etc . . .) may constrain if zircon formed during muscovite/biotite melting or not. New findings in this sense will deeply impact petrochronology in high-grade terrains.
- Despite the growing dataset of trace element contents in MI, studies devoted to understanding the extent of equilibrium/disequilibrium during crustal melting are mostly restricted to crustal xenoliths (Acosta-Vigil *et al.*, 2010, 2012). A greater effort in extending this type of studies to regional high-grade terranes is desirable.
- Case studies where fluid–melt immiscibility occurs should also be more thoroughly explored as they have crucial information on the trace element partitioning between fluids and melts in the deep crust.
- MI can also potentially provide new insights on the behaviour and mobility of critical metals during anatexis.

SUPPLEMENTARY DATA

Supplementary data are available at *Journal of Petrology* online.

ACKNOWLEDGEMENTS

We would like to thank Joerg Hermann for the invitation to write this *Perspectives in Petrology* and for his careful editorial handling. Constructive and insightful comments from Chris Yakymchuk, Leo Kriegsman and Silvio Ferrero are highly appreciated as they improved the quality of this manuscript. Our sincere gratitude also goes to all colleagues that have contributed with images of MI (as specified in the text). Martin Hand is thanked for providing samples from the Sleaford Complex (Australia). We are grateful to Lisa Santello for helping with the 2D Raman maps. B.B.C. dedicates this manuscript to Gaia.

DATA AVAILABILITY

No new data were generated or analyzed in support of this research.

FUNDING

We acknowledge funding from MUR-PRIN 2022FMFKHZ and the 'The Geosciences for Sustainable Development' project (Budget Ministero dell'Università e della Ricerca – Dipartimenti di Eccellenza 2023-2027MUR–Dipartimenti di Eccellenza 2023–2027, grant C93C23002690001). B.B.C. acknowledges funding from the Università deglid Studi di Padova (Welcome Kit) and the Programma Nazionale di Ricerca in Antartide (PNRA2018_00103). Open access funding was provided by Università degli Studi di Padova within the CRUI-CARE Agreement.

REFERENCES

Acosta-Vigil, A., London, D. & Morgan, G. B. (2006). Experiments on the kinetics of partial melting of a leucogranite at 200 MPa H 2 O and 690–800 C: compositional variability of melts during the onset of H 2 O-saturated crustal anatexis. *Contributions to Mineralogy and Petrology* **151**, 539–557. https://doi.org/10.1007/s00410-006-0081-8.

Acosta-Vigil, A., Cesare, B., London, D. & Morgan VI, G. B. (2007). Microstructures and composition of melt inclusions in a crustal anatectic environment, represented by metapelitic enclaves within El Hoyazo dacites, SE Spain. *Chemical Geology* **237**(3–4), 450–465. https://doi.org/10.1016/j.chemgeo.2006.07.014.

Acosta-Vigil, A., Buick, I., Hermann, J., Cesare, B., Rubatto, D., London, D. & Morgan, G. B. (2010). Mechanisms of crustal anatexis: a geochemical study of partially melted metapelitic enclaves and host dacite, SE Spain. *Journal of Petrology* **51**(4), 785–821. https://doi.org/10.1093/petrology/egp095.

Acosta-Vigil, A., Buick, I., Cesare, B., London, D. & Morgan, G. B. (2012). The extent of equilibration between melt and residuum during regional anatexis and its implications for differentiation of the continental crust: a study of partially melted metapelitic enclaves. *Journal of Petrology* **53**(7), 1319–1356. https://doi.org/10.1093/petrology/egs018.

Acosta-Vigil, A., Rubatto, D., Bartoli, O., Cesare, B., Meli, S., Pedrera, A. & Tajčmanová, L. (2014). Age of anatexis in the crustal footwall of the Ronda peridotites, S Spain. *Lithos* **210-211**, 147–167. https://doi.org/10.1016/j.lithos.2014.08.018.

Acosta-Vigil, A., Barich, A., Bartoli, O., Garrido, C. J., Cesare, B., Remusat, L., Poli, S. & Raepsaet, C. (2016). The composition of nanogranitoids in migmatites overlying the Ronda peridotites (Betic cordillera, S Spain): the anatectic history of a polymetamorphic basement. *Contributions to Mineralogy and Petrology* **171**, 1–31. https://doi.org/10.1007/s00410-016-1230-3.

Acosta-Vigil, A., London, D., Morgan VI, G. B., Cesare, B., Buick, I., Hermann, J. & Bartoli, O. (2017). Primary crustal melt compositions: insights into the controls, mechanisms and timing of generation from kinetics experiments and melt inclusions. *Lithos* **286-287**, 454–479. https://doi.org/10.1016/j.lithos.2017.05.020.

Acosta-Vigil, A., Kotková, J., Čopjaková, R., Wirth, R. & Hermann, J. (2024). Experimental constraints on the nature of multiphase solid inclusions and their bearing on mantle wedge metasomatism, bohemian massif. *Contributions to Mineralogy and Petrology* **179**(7), 71. https://doi.org/10.1007/s00410-024-02132-1.

Alessio, K. L., Hand, M., Kelsey, D. E., Williams, M. A., Morrissey, L. J. & Barovich, K. (2018). Conservation of deep crustal heat production. *Geology* **46**(4), 335–338. https://doi.org/10.1130/G39970.1.

Álvarez-Valero, A. M. & Kriegsman, L. M. (2008). Partial crustal melting beneath the Betic cordillera (SE Spain): the case study of mar Menor volcanic suite. *Lithos* **101**(3–4), 379–396. https://doi.org/10.1016/j.lithos.2007.08.016.

Álvarez-Valero, A. M. & Kriegsman, L. M. (2010). Chemical, petrological and mass balance con-straints on the textural evolution of pelitic enclaves. *Lithos* **116**, 300–309.

Álvarez-Valero, A. M., Cesare, B. & Kriegsman, L. M. (2005). Formation of elliptical garnet in a metapelitic enclave by melt-assisted dissolution and reprecipitation. *Journal of Metamorphic Geology* **23**(2), 65–74. https://doi.org/10.1111/j.1525-1314.2005.00562.x.

Álvarez-Valero, A. M., Cesare, B. & Kriegsman, L. M. (2007). Formation of spinel–cordierite–feldspar–glass coronas after garnet in metapelitic xenoliths: reaction modelling andgeodynamic implications. *Journal of Metamorphic Geology* **25**, 305–320.

Álvarez-Valero, A. M., Jagoutz, O., Stanley, J., Manthei, C., El Maz, A., Moukadiri, A. & Piasecki, A. (2014). Crustal attenuation as a tracer for the emplacement of the Beni Bousera ultramafic massif (Betico-Rifean belt). *Bulletin* **126**(11–12), 1614–1624. https://doi.org/10.1130/B31040.1.

Arab, A., Godard, G., Ouzegane, K., Acosta-Vigil, A., Kiénast, J. R., Román-Alpiste, M. J. & Drareni, A. (2021). Partial melting and PT evolution of eclogite-facies metapelitic migmatites from the Egere terrane (central Hoggar, South Algeria). *American Mineralogist* **106**(8), 1209–1224. https://doi.org/10.2138/am-2021-7342.

Aradi, L. E., Spránitz, T., Myovela, J. L., Guzmics, T., Patkó, L. & Berkesi, M. (2023). 3D Raman mapping combined with FIB-SEM on multiphase fluid inclusions: a tool to unravel complex phase assemblages. *Journal of Raman Spectroscopy* **54**(11), 1341–1352. https://doi.org/10.1002/jrs.6564.

Artemieva, I. M., Thybo, H., Jakobsen, K., Sørensen, N. K. & Nielsen, L. S. (2017). Heat production in granitic rocks: global analysis based on a new data compilation GRANITE2017. *Earth-Science Reviews* **172**, 1–26. https://doi.org/10.1016/j.earscirev.2017.07.003.

Audétat, A. & Lowenstern, J. B. (2014) Mel inclusions. In: Holland H. D. & Turekian K. K. (eds) *Treatise on Geochemistry*, Second edn. Oxford: Elsevier, pp.143–173.

Auzanneau, E., Vielzeuf, D. & Schmidt, M. W. (2006). Experimental evidence of decompression melting during exhumation of subducted continental crust. *Contributions to Mineralogy and Petrology* **152**(2), 125–148. https://doi.org/10.1007/s00410-006-0104-5.

Axler, J. A. & Ague, J. J. (2015). Oriented multiphase needles in garnet from ultrahigh-temperature granulites, Connecticut, USA. *American Mineralogist* **100**(10), 2254–2271. https://doi.org/10.2138/am-2015-5018.

Baker, D. R. (2008). The fidelity of melt inclusions as records of melt composition. *Contributions to Mineralogy and Petrology* **156**, 377–395.

Baldwin, S. L., Schönig, J., Gonzalez, J. P., Davies, H. & von Eynatten, H. (2021). Garnet sand reveals rock recycling processes in the youngest exhumed high-and ultrahigh-pressure terrane on Earth. *Proceedings of the National Academy of Sciences* **118**(3), e2017231118.

Barich, A., Acosta-Vigil, A., Garrido, C. J., Cesare, B., Tajčmanová, L. & Bartoli, O. (2014). Microstructures and petrology of melt inclusions in the anatectic sequence of Jubrique (Betic cordillera, S Spain): implications for crustal anatexis. *Lithos* **206-207**, 303–320. https://doi.org/10.1016/j.lithos.2014.08.003.

Barnes, C. J., Bukała, M., Callegari, R., Walczak, K., Kooijman, E., Kielman-Schmitt, M. & Majka, J. (2022). Zircon and monazite reveal late Cambrian/early Ordovician partial melting of the central Seve nappe complex, Scandinavian Caledonides. *Contributions to Mineralogy and Petrology* **177**(9), 92. https://doi.org/10.1007/s00410-022-01958-x.

Bartoli, O. (2017). Phase equilibria modelling of residual migmatites and granulites: an evaluation of the melt-reintegration approach. *Journal of Metamorphic Geology* **35**(8), 919–942. https://doi.org/10.1111/jmg.12261.

Bartoli, O. (2019). Reintegrating nanogranitoid inclusion composition to reconstruct the prograde history of melt-depleted rocks. *Geoscience Frontiers* **10**(2), 517–525. https://doi.org/10.1016/j.gsf.2018.02.002.

Bartoli, O. (2021a) Characterizing fluid and melt in high-grade metamorphic rocks. In: Lecumberri-Sanchez P., Steele-MacInnis M. & Kontak D. (eds) *Fluid and melt inclusions: applications to geologic processes*. Mineralogical Association of Canada.

Bartoli, O. (2021b). Granite geochemistry is not diagnostic of the role of water in the source. *Earth and Planetary Science Letters* **564**, 116927. https://doi.org/10.1016/j.epsl.2021.116927.

Bartoli, O. & Carvalho, B. B. (2021). Anatectic granites in their source region: a comparison between experiments, thermodynamic modelling and nanogranitoids. *Lithos* **402-403**, 106046. https://doi.org/10.1016/j.lithos.2021.106046.

Bartoli, O. & Cesare, B. (2020). Nanorocks: a 10-year-old story. *Rendiconti Lincei. Scienze Fisiche e Naturali* **31**, 249–257. https://doi.org/10.1007/s12210-020-00898-7.

Bartoli, O., Cesare, B., Poli, S., Acosta-Vigil, A., Esposito, R., Turina, A. & Hunter, J. (2013a). Nanogranite inclusions in migmatitic garnet: behavior during piston-cylinder remelting experiments. *Geofluids* **13**(4), 405–420. https://doi.org/10.1111/gfl.12038.

Bartoli, O., Cesare, B., Poli, S., Bodnar, R. J., Acosta-Vigil, A., Frezzotti, M. L. & Meli, S. (2013b). Recovering the composition of melt and the fluid regime at the onset of crustal anatexis and S-type granite formation. *Geology* **41**(2), 115–118. https://doi.org/10.1130/G33455.1.

Bartoli, O., Tajčmanová, L., Cesare, B. & Acosta-Vigil, A. (2013c). Phase equilibria constraints on melting of stromatic migmatites from R Onda (S. S pain): insights on the formation of peritectic garnet. *Journal of Metamorphic Geology* **31**(7), 775–789. https://doi.org/10.1111/jmg.12044.

Bartoli, O., Cesare, B., Remusat, L., Acosta-Vigil, A. & Poli, S. (2014). The H2O content of granite embryos. *Earth and Planetary Science Letters* **395**, 281–290. https://doi.org/10.1016/j.epsl.2014.03.031.

Bartoli, O., Acosta-Vigil, A. & Cesare, B. (2015). High-temperature metamorphism and crustal melting: working with melt inclusions. *Periodico di Mineralogia* **84**(3B), 591–614.

Bartoli, O., Acosta-Vigil, A., Ferrero, S. & Cesare, B. (2016a). Granitoid magmas preserved as melt inclusions in high-grade metamorphic rocks. *American Mineralogist* **101**(7), 1543–1559. https://doi.org/10.2138/am-2016-5541CCBYNCND.

Bartoli, O., Acosta-Vigil, A., Tajčmanová, L., Cesare, B. & Bodnar, R. J. (2016b). Using nanogranitoids and phase equilibria modeling to unravel anatexis in the crustal footwall of the Ronda peridotites (Betic cordillera, S Spain). *Lithos* **256-257**, 282–299. https://doi.org/10.1016/j.lithos.2016.03.016.

Bartoli, O., Acosta-Vigil, A., Cesare, B., Remusat, L., Gonzalez–Cano, A., Wälle, M. & Langone, A. (2019). Geochemistry of Eocene-early Oligocene low-temperature crustal melts from greater Himalayan sequence (Nepal): a nanogranitoid perspective. *Contributions to Mineralogy and Petrology* **174**, 1–18. https://doi.org/10.1007/s00410-019-1622-2.

Bartoli, O., Carvalho, B. B. & Farina, F. (2024a). Effectiveness of Ti-in-amphibole thermometry and performance of different

thermometers across lower continental crust up to UHT metamorphism. *Contributions to Mineralogy and Petrology* **179**(6), 65. https://doi.org/10.1007/s00410-024-02149-6.

Bartoli, O., Millonig, L. J., Carvalho, B. B., Marschall, H. R. & Gerdes, A. (2024b). The age of granulite-Facies metamorphism in the Ivrea–Verbano zone (NW Italy) determined ThroughIn SituU–Pb dating of garnet. *Journal of Petrology* **65**(8), egae083. https://doi.org/10.1093/petrology/egae083.

Bassett, W. A., Shen, A. H., Bucknum, M. & Chou, I. (1993). A new diamond anvil cell for hydrothermal studies to 2.5 GPa and from–190 to 1200° C. *Review of Scientific Instruments* **64**(8), 2340–2345. https://doi.org/10.1063/1.1143931.

Baxter, E. F., Caddick, M. J. & Ague, J. J. (2013). Garnet: common mineral, uncommonly useful. *Elements* **9**(6), 415–419. https://doi.org/10.2113/gselements.9.6.415.

Bea, F. (1996). Controls on the trace element composition of crustal melts. *Earth and Environmental Science Transactions of the Royal Society of Edinburgh* **87**(1–2), 33–41. https://doi.org/10.1017/S0263593300006453.

Bea, F. (2012). The sources of energy for crustal melting and the geochemistry of heat-producing elements. *Lithos* **153**, 278–291. https://doi.org/10.1016/j.lithos.2012.01.017.

Bea, F. & Montero, P. (1999). Behavior of accessory phases and redistribution of Zr, REE, Y, Th, and U during metamorphism and partial melting of metapelites in the lower crust: an example from the Kinzigite formation of Ivrea-Verbano, NW Italy. *Geochimica et Cosmochimica Acta* **63**(7–8), 1133–1153. https://doi.org/10.1016/S0016-7037(98)00292-0.

Behrens, H., Roux, J., Neuville, D. R. & Siemann, M. (2006). Quantification of dissolved H2O in silicate glasses using confocal microRaman spectroscopy. *Chemical Geology* **229**(1–3), 96–112. https://doi.org/10.1016/j.chemgeo.2006.01.014.

Beyer, C. & Chakraborty, S. (2021). Internal stress-induced recrystallization and diffusive transport in CaTiO3-PbTiO3 solid solutions: a new transport mechanism in geomaterials and its implications for thermobarometry, geochronology, and geospeedometry. *American Mineralogist: Journal of Earth and Planetary Materials* **106**(12), 1940–1949. https://doi.org/10.2138/am-2021-7588.

Blank, J. G., Stolper, E. M. & Carroll, M. R. (1993). Solubilities of carbon dioxide and water in rhyolitic melt at 850 C and 750 bars. *Earth and Planetary Science Letters* **119**(1–2), 27–36. https://doi.org/10.1016/0012-821X(93)90004-S.

Bodnar, R. J. (2003). Introduction to aqueous-electrolyte fluid inclusions.

Bodnar, R. J. & Frezzotti, M. L. (2020). Microscale chemistry: Raman analysis of fluid and melt inclusions. *Elements* **16**(2), 93–98. https://doi.org/10.2138/gselements.16.2.93.

Bodnar, R. J. & Student, J. J. (2006) *Melt Inclusions in Plutonic Rocks: Petrography and Microthermometry*. Mineralogical Association of Canada.

Borghini, A., Ferrero, S., Wunder, B., Laurent, O., O'Brien, P. J. & Ziemann, M. A. (2018). Granitoid melt inclusions in orogenic peridotite and the origin of garnet clinopyroxenite. *Geology* **46**(11), 1007–1010. https://doi.org/10.1130/G45316.1.

Borghini, A., Ferrero, S., O'Brien, P. J., Laurent, O., Günter, C. & Ziemann, M. A. (2020). Cryptic metasomatic agent measured in situ in Variscan mantle rocks: melt inclusions in garnet of eclogite, Granulitgebirge, Germany. *Journal of Metamorphic Geology* **38**(3), 207–234. https://doi.org/10.1111/jmg.12519.

Borghini, A., Nicoli, G., Ferrero, S., O'brien, P. J., Laurent, O., Remusat, L. & Milani, S. (2023). The role of continental subduction in mantle metasomatism and carbon recycling revealed by melt inclusions in UHP eclogites. *Science Advances* **9**(6), eabp9482. https://doi.org/10.1126/sciadv.abp9482.

Borghini, A., Ferrero, S., O'Brien, P. J., Wunder, B., Tollan, P., Majka, J. & Gresky, K. (2024). Halogen-bearing metasomatizing melt preserved in high-pressure (HP) eclogites of Pfaffenberg, bohemian massif. *European Journal of Mineralogy* **36**(2), 279–300. https://doi.org/10.5194/ejm-36-279-2024.

Callegari, R. (2018) *Study of nanogranites included in garnets from the Valpelline series (Austrlpine domain, Western Alps)*. Unpublished Master thesis.

Cao, W., Massonne, H. J. & Liang, X. (2021). Partial melting due to breakdown of phengite and amphibole in retrogressed eclogite of deep Precambrian crust: an example from the Algonquin terrane, western Grenville Province, Canada. *Precambrian Research* **352**, 105965. https://doi.org/10.1016/j.precamres.2020.105965.

Capriolo, M., Callegaro, S., Deegan, F. M., Merle, R., Jeon, H., Whitehouse, M. J., Aradi, L. E., Storm, M., Renne, P. R., Baker, D. R., Dal Corso, J., Newton, R. J., Szabó, C., Carvalho, B. B., Youbi, N. & Marzoli, A. (2024). Dynamic evolution of the transcrustal plumbing system in large igneous provinces: geochemical and microstructural insights from glomerocrysts and melt inclusions. *Journal of Petrology* **65**. https://doi.org/10.1093/petrology/egae103.

Carosi, R., Montomoli, C., Langone, A., Turina, A., Cesare, B., Iaccarino, S. & Rai, S. M. (2015). Eocene partial melting recorded in peritectic garnets from kyanite-gneiss, greater Himalayan sequence, Central Nepal. *Geological Society, London, Special Publications* **412**(1), 111–129. https://doi.org/10.1144/SP412.1.

Carvalho, B. B., Bartoli, O., Ferri, F., Cesare, B., Ferrero, S., Remusat, L. & Poli, S. (2019). Anatexis and fluid regime of the deep continental crust: new clues from melt and fluid inclusions in metapelitic migmatites from Ivrea zone (NW Italy). *Journal of Metamorphic Geology* **37**(7), 951–975. https://doi.org/10.1111/jmg.12463.

Carvalho, B. B., Bartoli, O., Cesare, B., Tacchetto, T., Gianola, O., Ferri, F. & Szabó, C. (2020). Primary CO2-bearing fluid inclusions in granulitic garnet usually do not survive. *Earth and Planetary Science Letters* **536**, 116170. https://doi.org/10.1016/j.epsl.2020.116170.

Carvalho, B. B., Bartoli, O. & Cesare, B. (2023a). C–O–H fluid-melt-rock interaction in graphitic granulites and problems of quantifying carbon budget in the lower continental crust. *Chemical Geology* **631**, 121503. https://doi.org/10.1016/j.chemgeo.2023.121503.

Carvalho, B. B., Bartoli, O., Cesare, B., Satish-Kumar, M., Petrelli, M., Kawakami, T., Hokada, T. & Gilio, M. (2023b). Revealing the link between A-type granites and hottest melts from residual metasedimentary crust. *Geology* **51**(9), 845–849. https://doi.org/10.1130/G51097.1.

Cesare, B. (2008) Crustal melting: working with enclaves. In: *Working with migmatites*, Vol. **38**. Quebec City: Mineralogical Association of Canada, pp.37–55.

Cesare, B. & Acosta-Vigil, A. (2011) Using melt inclusions for understanding crustal melting processes. In: *McGraw-Hill Yearbook of Science and Technology*, pp.355–359.

Cesare, B. & Gómez-Pugnaire, M. T. (2001). Crustal melting in the Alboran domain: constraints from xenoliths of the Neogene Volcanic Province. *Physics and Chemistry of the Earth, Part A: Solid Earth and Geodesy* **26**(4–5), 255–260. https://doi.org/10.1016/S1464-1895(01)00053-9.

Cesare, B. & Maineri, C. (1999). Fluid-present anatexis of metapelites at El Joyazo (SE Spain): constraints from Raman spectroscopy of graphite. *Contributions to Mineralogy and Petrology* **135**(1), 41–52. https://doi.org/10.1007/s004100050496.

Cesare, B., Mariani, E. S. & Venturelli, G. (1997). Crustal anatexis and melt extraction during deformation in the restitic xenoliths at El

Joyazo (SE Spain). *Mineralogical Magazine* **61**(404), 15–27. https://doi.org/10.1180/minmag.1997.061.404.03.

Cesare, B., Gomez-Pugnaire, M. T. & Rubatto, D. (2003a). Residence time of S-type anatectic magmas beneath the Neogene Volcanic Province of SE Spain: a zircon and monazite SHRIMP study. *Contributions to Mineralogy and Petrology* **146**, 28–43. https://doi.org/10.1007/s00410-003-0490-x.

Cesare, B., Marchesi, C., Hermann, J. & Gómez-Pugnaire, M. T. (2003b). Primary melt inclusions in andalusite from anatectic graphitic metapelites: implications for the position of the Al2SiO5 triple point. *Geology* **31**(7), 573–576. https://doi.org/10.1130/0091-7613(2003)031<0573:PMIIAF>2.0.CO;2.

Cesare, B., Meli, S., Nodari, L. & Russo, U. (2005). Fe 3+ reduction during biotite melting in graphitic metapelites: another origin of CO 2 in granulites. *Contributions to Mineralogy and Petrology* **149**, 129–140. https://doi.org/10.1007/s00410-004-0646-3.

Cesare, B., Maineri, C., Toaldo, A. B., Pedron, D. & Vigil, A. A. (2007). Immiscibility between carbonic fluids and granitic melts during crustal anatexis: a fluid and melt inclusion study in the enclaves of the Neogene Volcanic Province of SE Spain. *Chemical Geology* **237**(3–4), 433–449. https://doi.org/10.1016/j.chemgeo.2006.07.013.

Cesare, B., Ferrero, S., Salvioli-Mariani, E., Pedron, D. & Cavallo, A. (2009a). "Nanogranite" and glassy inclusions: the anatectic melt in migmatites and granulites. *Geology* **37**(7), 627–630. https://doi.org/10.1130/G25759A.1.

Cesare, B., Rubatto, D. & Gómez-Pugnaire, M. T. (2009b). Do extrusion ages reflect magma generation processes at depth? An example from the Neogene Volcanic Province of SE Spain. *Contributions to Mineralogy and Petrology* **157**, 267–279. https://doi.org/10.1007/s00410-008-0333-x.

Cesare, B., Acosta-Vigil, A., Ferrero, S., Bartoli, O. & Forster, M. A. (2011). Melt inclusions in migmatites and granulites. *Journal of the Virtual Explorer* **38**(2). https://doi.org/10.3809/jvirtex.2011.00268.

Cesare, B., Acosta-Vigil, A., Bartoli, O. & Ferrero, S. (2015). What can we learn from melt inclusions in migmatites and granulites? *Lithos* **239**, 186–216. https://doi.org/10.1016/j.lithos.2015.09.028.

Chappell, B. W. (1984). Source rocks of I-and S-type granites in the Lachlan Fold Belt, southeastern Australia. *Philosophical Transactions of the Royal Society of London. Series A, Mathematical and Physical Sciences* **310**(1514), 693–707.

Chappell, B. W. & White, A. J. R. (1974). Two contrasting granite types. *Pacif. Geol.* **8**, 173–174.

Chen, Y. X., Zheng, Y. F. & Hu, Z. (2013). Petrological and zircon evidence for anatexis of UHP quartzite during continental collision in the Sulu orogen. *Journal of Metamorphic Geology* **31**(4), 389–413. https://doi.org/10.1111/jmg.12026.

Chen, Y. X., Zheng, Y. F., Gao, X. Y. & Hu, Z. (2014). Multiphase solid inclusions in zoisite-bearing eclogite: evidence for partial melting of ultrahigh-pressure metamorphic rocks during continental collision. *Lithos* **200-201**, 1–21. https://doi.org/10.1016/j.lithos.2014.04.004.

Chen, R. X., Ding, B., Zheng, Y. F. & Hu, Z. (2015). Multiple episodes of anatexis in a collisional orogen: zircon evidence from migmatite in the Dabie orogen. *Lithos* **212**, 247–265. https://doi.org/10.1016/j.lithos.2014.11.004.

Chupin, V. P., Tomilenko, A. A. & Chupin, S. V. (1993). Origin of granulite complexes: results of study of melt and fluid inclusions in zircon and rock-forming minerals. *Geologiya i Geofizika (Russian Geology and Geophysics)* **34**(12), 116–131.

Chupin, S. V., Chupin, V. P., Barton, J. M. & Barton, E. S. (1998). Archean melt inclusions in zircon from quartzite and granitic orthogneiss from South Africa; magma compositions and probable sources of protoliths. *European Journal of Mineralogy* **10**(6), 1241–1252. https://doi.org/10.1127/ejm/10/6/1241.

Chupin, V. P., Kuz'min, D. V. & Madyukov, I. A. (2006) Melt inclusions in minerals of scapolite-bearing granulite (lower crustal xenoliths from diatremes of the Pamirs). In: *Doklady earth sciences, Vol. 407*. Springer Nature BV, pp.507–511.

Chupin, V. P., Kuzmin, D. V., Madyukov, I. A., Rodionov, N. V., Lutkov, V. S. & Touret, J. L. R. (2010) High-pressure magmatic inclusions in zircon and rock-forminh minerals of granulites/eclogites (xenoliths from diatremes of the Pamir). In: Sharygin V. V. (ed) *Abstracts vol. of ACROFI III & TBG XIV, Novosibirsk, 15–20 September, 2010*. RAS SB, IGM, Novosibirsk: Publishing House of SB RAS, pp.46–47.

Clemens, J. D. (1984). Water contents of silicic to intermediate magmas. *Lithos* **17**, 273–287.

Clemens, J. D. & Droop, G. T. R. (1998). Fluids, P–T paths and the fates of anatectic melts in the Earth's crust. *Lithos* **44**(1–2), 21–36. https://doi.org/10.1016/S0024-4937(98)00020-6.

Clemens, J. D. & Wall, V. J. (1984). Origin and evolution of a peraluminous silicic ignimbrite suite: the violet town Volcanics. *Contributions to Mineralogy and Petrology* **88**(4), 354–371. https://doi.org/10.1007/BF00376761.

Clemens, J. D., Stevens, G. & Farina, F. (2011). The enigmatic sources of I-type granites: the peritectic connexion. *Lithos* **126**(3–4), 174–181. https://doi.org/10.1016/j.lithos.2011.07.004.

Clemens, J. D., Stevens, G. & Bryan, S. E. (2020). Conditions during the formation of granitic magmas by crustal melting–hot or cold; drenched, damp or dry? *Earth-Science Reviews* **200**, 102982. https://doi.org/10.1016/j.earscirev.2019.102982.

Collins, W. J., Beams, S. D., White, A. J. R. & Chappell, B. W. (1982). Nature and origin of A-type granites with particular reference to southeastern Australia. *Contributions to Mineralogy and Petrology* **80**, 189–200. https://doi.org/10.1007/BF00374895.

Connolly, J. A. D. (2009). The geodynamic equation of state: what and how. *Geochemistry, Geophysics, Geosystems* **10**(10). https://doi.org/10.1029/2009GC002540.

Connop, C. H., Smye, A. J., Garber, J. M., Moser, A. C., Caddick, M. J. & Vervoort, J. D. (2024). Assembly of lower continental crust: a garnet Lu-Hf petrochronological investigation of the Ivrea-Verbano zone, Italy. *Earth and Planetary Science Letters* **634**, 118677. https://doi.org/10.1016/j.epsl.2024.118677.

Daczko, N. R., Piazolo, S., Meek, U., Stuart, C. A. & Elliott, V. (2016). Hornblendite delineates zones of mass transfer through the lower crust. *Scientific Reports* **6**(1), 31369. https://doi.org/10.1038/srep31369.

Daczko, N. R., Elliott, V., Piazolo, S. & Hao, K. (2024). Zircon coupled dissolution–precipitation replacement during melt–rock interaction modifies chemical signatures resulting in misleading ages. *Journal of Metamorphic Geology.* **42**, 1197–1214. https://doi.org/10.1111/jmg.12796.

Dalla, Brida, M. (2019) *Study of nanogranite inclusions in garnets from the Ulten zone (Austroalpine domain, Eastern Alps)*. Unpublished Master thesis.

Darling, R. S. (2013). Zircon-bearing, crystallized melt inclusions in peritectic garnet from the western a dirondack M ountains, N ew Y ork S tate, USA. *Geofluids* **13**(4), 453–459. https://doi.org/10.1111/gfl.12047.

Darling, R. S., Chou, I. M. & Bodnar, R. J. (1997). An occurrence of metastable cristobalite in high-pressure garnet granulite. *Science* **276**(5309), 91–93. https://doi.org/10.1126/science.276.5309.91.

Debon, F. & Le Fort, P. (1988). A cationic classification of common plutonic rocks and their magmatic associations: principles, method, applications. *Bulletin de Minéralogie* **111**(5), 493–510.

Delhaye, M. & Dhamelincourt, P. (1975). Raman microprobe and microscope with laser excitation. *Journal of Raman Spectroscopy* **3**(1), 33–43. https://doi.org/10.1002/jrs.1250030105.

Di Martino, C., Forni, F., Frezzotti, M. L., Palmeri, R., Webster, J. D., Ayuso, R. A. & Tranne, C. A. (2011). Formation of cordierite-bearing lavas during anatexis in the lower crust beneath Lipari Island (Aeolian arc, Italy). *Contributions to Mineralogy and Petrology* **162**, 1011–1030. https://doi.org/10.1007/s00410-011-0637-0.

Dong, J., Wei, C., Chen, J. & Zhang, J. (2020). P–T–t path of garnetites in South Altyn Tagh, West China: a complete record of the ultra-deep subduction and exhumation of continental crust. *Journal of Geophysical Research: Solid Earth* **125**(2), e2019JB018881.

Dos Santos, T. M. B., Munhá, J. M., Tassinari, C. C., Noronha, F. M., Guedes, A., Fonseca, P. E. & Dória, A. (2011). P–T-fluid evolution and graphite deposition during retrograde metamorphism in Ribeira Fold Belt, SE Brazil: oxygen fugacity, fluid inclusions and C–O–H isotopic evidence. *Journal of South American Earth Sciences* **31**(1), 93–109. https://doi.org/10.1016/j.jsames.2010.02.002.

Dubacq, B., Soret, M., Jewison, E., & Agard, P. (2019). Early subduction dynamics recorded by the metamorphic sole of the Mt. Albert ophiolitic complex (Gaspé, Quebec). *Lithos*, **334**, 161–179.

Duncan, M. S. & Dasgupta, R. (2014). CO_2 solubility and speciation in rhyolitic sediment partial melts at 1.5–3.0 GPa–implications for carbon flux in subduction zones. *Geochimica et Cosmochimica Acta* **124**, 328–347. https://doi.org/10.1016/j.gca.2013.09.026.

Duncan, M. S., & Dasgupta, R. (2017). Rise of Earth's atmospheric oxygen controlled by efficient subduction of organic carbon. *Nature Geoscience*, **10**(5), 387–392.

Ebadi, A. & Johannes, W. (1991). Beginning of melting and composition of first melts in the system Qz-ab-or-H_2O-CO_2. *Contributions to Mineralogy and Petrology* **106**, 286–295. https://doi.org/10.1007/BF00324558.

Esposito, R., Klebesz, R., Bartoli, O., Klyukin, Y., Moncada, D., Doherty, A. & Bodnar, R. (2012). Application of the Linkam TS1400XY heating stage to melt inclusion studies. *Open Geosciences* **4**(2), 208–218. https://doi.org/10.2478/s13533-011-0054-y.

Ewing, T. A., Rubatto, D. & Hermann, J. (2014). Hafnium isotopes and Zr/Hf of rutile and zircon from lower crustal metapelites (Ivrea–Verbano zone, Italy): implications for chemical differentiation of the crust. *Earth and Planetary Science Letters* **389**, 106–118. https://doi.org/10.1016/j.epsl.2013.12.029.

Faryad, S. W., Baldwin, S. L., Jedlicka, R., & Ježek, J. (2019). Two-stage garnet growth in coesite eclogite from the southeastern Papua New Guinea (U) HP terrane and its geodynamic significance. *Contributions to Mineralogy and Petrology*, **174**, 1–16.

Faryad, S. W. & Cuthbert, S. J. (2020). High-temperature overprint in (U) HPM rocks exhumed from subduction zones; a product of isothermal decompression or a consequence of slab break-off (slab rollback)? *Earth-Science Reviews* **202**, 103108. https://doi.org/10.1016/j.earscirev.2020.103108.

Faryad, S. W., Jedlicka, R., Hauzenberger, C. & Racek, M. (2018). High-pressure crystallization vs. recrystallization origin of garnet pyroxenite-eclogite within subduction related lithologies. *Mineralogy and Petrology* **112**, 603–616. https://doi.org/10.1007/s00710-018-0557-z.

Ferrando, S., Frezzotti, M. L., Dallai, L. & Compagnoni, R. (2005). Multiphase solid inclusions in UHP rocks (Su-Lu, China): remnants of supercritical silicate-rich aqueous fluids released during continental subduction. *Chemical Geology* **223**(1–3), 68–81. https://doi.org/10.1016/j.chemgeo.2005.01.029.

Ferrero, S. & Angel, R. J. (2018). Micropetrology: are inclusions grains of truth? *Journal of Petrology* **59**(9), 1671–1700. https://doi.org/10.1093/petrology/egy075.

Ferrero, S., Bodnar, R. J., Cesare, B. & Viti, C. (2011). Re-equilibration of primary fluid inclusions in peritectic garnet from metapelitic enclaves, El Hoyazo, Spain. *Lithos* **124**(1–2), 117–131. https://doi.org/10.1016/j.lithos.2010.09.004.

Ferrero, S., Bartoli, O., Cesare, B., Salvioli-Mariani, E., Acosta-Vigil, A., Cavallo, A. & Battiston, S. (2012). Microstructures of melt inclusions in anatectic metasedimentary rocks. *Journal of Metamorphic Geology* **30**(3), 303–322. https://doi.org/10.1111/j.1525-1314.2011.00968.x.

Ferrero, S., Braga, R., Berkesi, M., Cesare, B. & Laridhi Ouazaa, N. (2014). Production of metaluminous melt during fluid-present anatexis: an example from the Maghrebian basement, La Galite archipelago, Central Mediterranean. *Journal of Metamorphic Geology* **32**(2), 209–225. https://doi.org/10.1111/jmg.12068.

Ferrero, S., Wunder, B., Walczak, K., O'Brien, P. J. & Ziemann, M. A. (2015). Preserved near ultrahigh-pressure melt from continental crust subducted to mantle depths. *Geology* **43**(5), 447–450. https://doi.org/10.1130/G36534.1.

Ferrero, S., Wunder, B., Ziemann, M. A., Wälle, M. & O'Brien, P. J. (2016a). Carbonatitic and granitic melts produced under conditions of primary immiscibility during anatexis in the lower crust. *Earth and Planetary Science Letters* **454**, 121–131. https://doi.org/10.1016/j.epsl.2016.08.043.

Ferrero, S., Ziemann, M. A., Angel, R. J., O'Brien, P. J. & Wunder, B. (2016b). Kumdykolite, kokchetavite, and cristobalite crystallized in nanogranites from felsic granulites, Orlica-Snieznik dome (bohemian massif): not evidence for ultrahigh-pressure conditions. *Contributions to Mineralogy and Petrology* **171**, 1–12. https://doi.org/10.1007/s00410-015-1220-x.

Ferrero, S., Godard, G., Palmeri, R., Wunder, B. & Cesare, B. (2018). Partial melting of ultramafic granulites from Dronning Maud land, Antarctica: constraints from melt inclusions and thermodynamic modeling. *American Mineralogist* **103**(4), 610–622. https://doi.org/10.2138/am-2018-6214.

Ferrero, S., O'Brien, P. J., Borghini, A., Wunder, B., Wälle, M., Günter, C. & Ziemann, M. A. (2019). A treasure chest full of nanogranitoids: an archive to investigate crustal melting in the bohemian massif. *Geological Society, London, Special Publications* **478**(1), 13–38. https://doi.org/10.1144/SP478.19.

Ferrero, S., Wannhoff, I., Laurent, O., Yakymchuk, C., Darling, R., Wunder, B., Borghini, A. & O'Brien, P. J. (2021a). Embryos of TTGs in Gore Mountain garnet megacrysts from water-fluxed melting of the lower crust. *Earth and Planetary Science Letters* **569**, 117058. https://doi.org/10.1016/j.epsl.2021.117058.

Ferrero, S., Ague, J. J., O'Brien, P. J., Wunder, B., Remusat, L., Ziemann, M. A. & Axler, J. (2021b). High-pressure, halogen-bearing melt preserved in ultrahigh-temperature felsic granulites of the Central Maine terrane, Connecticut (USA). *American Mineralogist* **106**(8), 1225–1236. https://doi.org/10.2138/am-2021-7690.

Ferrero, S., Borghini, A., Remusat, L., Nicoli, G., Wunder, B. & Braga, R. (2023). H_2O and Cl in deep crustal melts: the message of melt inclusions in metamorphic rocks. *European Journal of Mineralogy* **35**(6), 1031–1049. https://doi.org/10.5194/ejm-35-1031-2023.

Ferrero, S., Lorenzon, S., Borriello, R., Borghini, A., Wirth, R., Schreiber, A., Fuchs, R., O'Brien, P. J., Grew, E. S. & Mugnaioli, E. (2024) Pfaffenbergite, $KNa_3(Al_4Si_{12})O_{32}$, a polymorph of sodic feldspar isostructural with kokchetavite and wodegongijieite, found in crystallized melt inclusions in metamorphic garnet. *American Mineralogist* **2025**. https://doi.org/10.2138/am-2025-9750.

Ferri, F., Cesare, B., Bartoli, O., Ferrero, S., Palmeri, R., Remusat, L. & Poli, S. (2020). Melt inclusions at MT. Edixon (Antarctica): chemistry, petrology and implications for the evolution of the

Lanterman range. *Lithos* **374**, 105685. https://doi.org/10.1016/j.lithos.2020.105685.

Fogel, R. A. & Rutherford, M. J. (1990). The solubility of carbon dioxide in rhyolitic melts; a quantitative FTIR study. *American Mineralogist* **75**(11–12), 1311–1326.

Forshaw, J. B. & Pattison, D. R. (2023). Major-element geochemistry of pelites. *Geology* **51**(1), 39–43. https://doi.org/10.1130/G50542.1.

Frezzotti, M. L. (2001). Silicate-melt inclusions in magmatic rocks: applications to petrology. *Lithos* **55**(1–4), 273–299. https://doi.org/10.1016/S0024-4937(00)00048-7.

Frezzotti, M. L. & Ferrando, S. (2007). Multiphase solid inclusions in ultra-high pressure metamorphic rocks: a petrographic approach. *Periodico di Mineralogia* **76**, 113–125.

Frezzotti, M. L. & Ferrando, S. (2015). The chemical behavior of fluids released during deep subduction based on fluid inclusions. *American Mineralogist* **100**(2–3), 352–377. https://doi.org/10.2138/am-2015-4933.

Frezzotti, M. L., Peccerillo, A., Zanon, V. & Nikogosian, I. (2004). Silica-rich melts in quartz xenoliths from Vulcano Island and their bearing on processes of crustal anatexis and crust–magma interaction beneath the Aeolian arc, southern Italy. *Journal of Petrology* **45**(1), 3–26. https://doi.org/10.1093/petrology/egg080.

Frezzotti, M. L., Tecce, F. & Casagli, A. (2012). Raman spectroscopy for fluid inclusion analysis. *Journal of Geochemical Exploration* **112**, 1–20. https://doi.org/10.1016/j.gexplo.2011.09.009.

Frost, C. D. & Frost, B. R. (2011). On ferroan (A-type) granitoids: their compositional variability and modes of origin. *Journal of Petrology* **52**(1), 39–53. https://doi.org/10.1093/petrology/egq070.

Fu, B., Touret, J. L., Zheng, Y. F. & Jahn, B. M. (2003). Fluid inclusions in granulites, granulitized eclogites and garnet clinopyroxenites from the Dabie–Sulu terranes, eastern China. *Lithos* **70**(3–4), 293–319. https://doi.org/10.1016/S0024-4937(03)00103-8.

Ganzhorn, A. C., Labrousse, L., Prouteau, G., Leroy, C., Vrijmoed, J. C., Andersen, T. B. & Arbaret, L. (2014). Structural, petrological and chemical analysis of syn-kinematic migmatites: insights from the Western gneiss region, Norway. *Journal of Metamorphic Geology* **32**(6), 647–673. https://doi.org/10.1111/jmg.12084.

Gao, X. Y., Zheng, Y. F., Chen, Y. X. & Hu, Z. (2013). Trace element composition of continentally subducted slab-derived melt: insight from multiphase solid inclusions in ultrahigh-pressure eclogite in the D abie orogen. *Journal of Metamorphic Geology* **31**(4), 453–468. https://doi.org/10.1111/jmg.12029.

Gao, X. Y., Zheng, Y. F., Chen, Y. X. & Hu, Z. (2014). Composite carbonate and silicate multiphase solid inclusions in metamorphic garnet from ultrahigh-P eclogite in the Dabie orogen. *Journal of Metamorphic Geology* **32**(9), 961–980. https://doi.org/10.1111/jmg.12102.

Gao, X. Y., Chen, Y. X. & Zhang, Q. Q. (2017). Multiphase solid inclusions in ultrahigh-pressure metamorphic rocks: a snapshot of anatectic melts during continental collision. *Journal of Asian Earth Sciences* **145**, 192–204. https://doi.org/10.1016/j.jseaes.2017.03.036.

García-Arias, M. (2024). Restite entrainment in S-type granites: a systematic review. *Lithos* **490-491**, 107850. https://doi.org/10.1016/j.lithos.2024.107850.

Garcia-Arias, M. & Stevens, G. (2017). Phase equilibrium modelling of granite magma petrogenesis: A. An evaluation of the magma compositions produced by crystal entrainment in the source. *Lithos* **277**, 131–153. https://doi.org/10.1016/j.lithos.2016.09.028.

Georgieva, M., Mogessie, A. & Cherneva, Z. (2005). Mineral needles and melt inclusions in garnet from the Chepelare area, central Rhodope, Bulgaria. *P Mitt. Цsterr. Miner. Ges.* **150**, 40.

Gervais, F. & Trapy, P. H. (2021). Testing solution models for phase equilibrium (forward) modeling of partial melting experiments. *Contributions to Mineralogy and Petrology* **176**, 4. https://doi.org/10.1007/s00410-020-01762-5.

Gianola, O., Bartoli, O., Ferri, F., Galli, A., Ferrero, S., Capizzi, L. S. & Cesare, B. (2021). Anatectic melt inclusions in ultra high temperature granulites. *Journal of Metamorphic Geology* **39**(3), 321–342. https://doi.org/10.1111/jmg.12567.

Gianola, O., Costa, B., Ferri, F., Gilio, M., Petrelli, M., Murri, M. & Cesare, B. (2023). Melt inclusions in Arclogitic xenoliths constrain the genesis of the lower continental arc crust beneath the northern volcanic zone, Colombia. *Journal of Petrology* **64**(6), egad038. https://doi.org/10.1093/petrology/egad038.

Goncalves, P., Raimondo, T., Paquette, J. L., de Souza, S. & de Oliveira, J. (2021). Garnet as a monitor for melt–rock interaction: textural, mineralogical, and compositional evidence of partial melting and melt-driven metasomatism. *Journal of Metamorphic Geology* **39**(5), 617–648. https://doi.org/10.1111/jmg.12592.

Green, E. C. R., White, R. W., Diener, J. F. A., Powell, R., Holland, T. J. B. & Palin, R. M. (2016). Activity–composition relations for the calculation of partial melting equilibria in metabasic rocks. *Journal of Metamorphic Geology* **34**(9), 845–869. https://doi.org/10.1111/jmg.12211.

Groppo, C., Rolfo, F. & Indares, A. (2012). Partial melting in the higher Himalayan Crystallines of eastern Nepal: the effect of decompression and implications for the 'channel Flow'model. *Journal of Petrology* **53**(5), 1057–1088. https://doi.org/10.1093/petrology/egs009.

Hacker, B. R., Kelemen, P. B. & Behn, M. D. (2011). Differentiation of the continental crust by relamination. *Earth and Planetary Science Letters* **307**(3–4), 501–516. https://doi.org/10.1016/j.epsl.2011.05.024.

Halter, W. E., Pettke, T., Heinrich, C. A. & Rothen-Rutishauser, B. (2002). Major to trace element analysis of melt inclusions by laser-ablation ICP-MS: methods of quantification. *Chemical Geology* **183**(1–4), 63–86. https://doi.org/10.1016/S0009-2541(01)00372-2.

Harley, S. L., & Nandakumar, V. (2014). Accessory mineral behaviour in granulite migmatites: a case study from the Kerala Khondalite Belt, India. *Journal of Petrology*, **55**(10), 1965–2002.

Harlov, D. E., Wirth, R. & Förster, H. J. (2005). An experimental study of dissolution–reprecipitation in fluorapatite: fluid infiltration and the formation of monazite. *Contributions to Mineralogy and Petrology* **150**, 268–286. https://doi.org/10.1007/s00410-005-0017-8.

Hartel, T. H. D., Pattison, D. R. M., Helmers, H. & Maaskant, P. (1990) *Primary Granitoid-Composition Inclusions in Garnet From Granulite Facies Metapelite: Direct Evidence for the Presence of a Melt*. Geological Association of Canada.

Hasterok, D., Gard, M. & Webb, J. (2018). On the radiogenic heat production of metamorphic, igneous, and sedimentary rocks. *Geoscience Frontiers* **9**(6), 1777–1794. https://doi.org/10.1016/j.gsf.2017.10.012.

He, Q., Zhang, S. B., Zheng, Y. F. & Chen, R. X. (2022). Peritectic minerals record partial melting of the deeply subducted continental crust in the Sulu orogen. *Journal of Metamorphic Geology* **40**(1), 87–120. https://doi.org/10.1111/jmg.12620.

Hermann, J. & Rubatto, D. (2009). Accessory phase control on the trace element signature of sediment melts in subduction zones. *Chemical Geology* **265**(3–4), 512–526. https://doi.org/10.1016/j.chemgeo.2009.05.018.

Hermann, J. & Spandler, C. J. (2008). Sediment melts at sub-arc depths: an experimental study. *Journal of Petrology* **49**(4), 717–740. https://doi.org/10.1093/petrology/egm073.

Hermann, J., Spandler, C., Hack, A. & Korsakov, A. V. (2006). Aqueous fluids and hydrous melts in high-pressure and ultra-high pressure rocks: implications for element transfer in subduction zones. *Lithos* **92**(3–4), 399–417. https://doi.org/10.1016/j.lithos.2006.03.055.

Hermann, J., Zheng, Y. F. & Rubatto, D. (2013). Deep fluids in subducted continental crust. *Elements* **9**(4), 281–287. https://doi.org/10.2113/gselements.9.4.281.

Herms, P., Raase, P., Giehl, C., Aradi, L. E., Fußwinkel, T., Rohrbach, A. & Möller, A. (2023). High-pressure melting in metapelites of a 2 Ga old subducted oceanic crust (Usagaran belt, Tanzania): implications from melt inclusions, fluid inclusions and thermodynamic modelling. *Contributions to Mineralogy and Petrology* **178**(11), 84. https://doi.org/10.1007/s00410-023-02063-3.

Higashino, F. & Kawakami, T. (2022). Ultrahigh–temperature metamorphism and melt inclusions from the Sør Rondane Mountains, East Antarctica. *Journal of Mineralogical and Petrological Sciences* **117**(1), 220325. https://doi.org/10.2465/jmps.220325.

Higashino, F., Kawakami, T., Tsuchiya, N., Satish-Kumar, M., Ishikawa, M., Grantham, G. & Hirata, T. (2019). Brine infiltration in the middle to lower crust in a collision zone: mass transfer and microtexture development through wet grain–boundary diffusion. *Journal of Petrology* **60**(2), 329–358. https://doi.org/10.1093/petrology/egy116.

Hirayama, E., Tsunogae, T., Malaviarachchi, S. P., Takamura, Y., Dharmapriya, P. L. & Tsutsumi, Y. (2020). Prolonged Neoproterozoic high-grade metamorphism of the Wanni complex, Sri Lanka: new insights from petrology, phase equilibria modelling, and zircon U–Pb geochronology of partially melted cordierite gneiss from Walpita. *Geological Journal* **55**(9), 6147–6168. https://doi.org/10.1002/gj.3792.

Hiroi, Y., Yanagi, A., Kato, M., Kobayashi, T., Prame, B., Hokada, T. & Shiraishi, K. (2014). Supercooled melt inclusions in lower-crustal granulites as a consequence of rapid exhumation by channel flow. *Gondwana Research* **25**, 226–234. https://doi.org/10.1016/j.gr.2013.04.001.

Hiroi, Y., Hokada, T., Kato, M., Yanagi, A., Adachi, T., Osanai, Y. & Shiraishi, K. (2019). Felsite–nanogranite inclusions and three Al2SiO5 polymorphs in the same garnet in ultrahigh–temperature granulites from Rundvågshetta, Lützow–holm complex, East Antarctica. *Journal of Mineralogical and Petrological Sciences* **114**(2), 60–78. https://doi.org/10.2465/jmps.181118.

Hiroi, Y., Hokada, T., Adachi, T., Shiraishi, K., Motoyoshi, Y. & Grew, E. S. (2023). Nanogranitoid inclusions with grandidierite in mafic granulite from Austhovde, Lützow-holm complex, East Antarctica. *Journal of Mineralogical and Petrological Sciences* **118**, 221209. https://doi.org/10.2465/jmps.221209.

Holland, T. & Powell, R. (2003). Activity–composition relations for phases in petrological calculations: an asymmetric multicomponent formulation. *Contributions to Mineralogy and Petrology* **145**, 492–501. https://doi.org/10.1007/s00410-003-0464-z.

Holland, T. J. B. & Powell, R. (2011). An improved and extended internally consistent thermodynamic dataset for phases of petrological interest, involving a new equation of state for solids. *Journal of Metamorphic Geology* **29**, 333–383. https://doi.org/10.1111/j.1525-1314.2010.00923.x.

Hollister, L. S. & Crawford, M. L. (eds) (1981) Fluid Inclusions: Applications to Petrology. In: *Mineralogical Association of Canada, Ontario, Short Course Handbook, v.6*, 304 pp.

Holness, M. B., Cesare, B. & Sawyer, E. W. (2011). Melted rocks under the microscope: microstructures and their interpretation. *Elements* **7**(4), 247–252. https://doi.org/10.2113/gselements.7.4.247.

Holtz, F., Pichavant, M., Barbey, P. & Johannes, W. (1992). Effects of H2O on liquidus phase relations in the haplogranite system at 2 and 5 kbar. *American Mineralogist* **77**(11–12), 1223–1241.

Holtz, F., & Johannes, W. (1994). Maximum and minimum water contents of granitic melts: implications for chemical and physical properties of ascending magmas. *Lithos*, **32**(1-2), 149–159.

Huang, W. L. & Wyllie, P. J. (1975). Melting reactions in the system NaAlSi3O8-KAlSi3O8-SiO2 to 35 kilobars, dry and with excess water. *The Journal of Geology* **83**(6), 737–748. https://doi.org/10.1086/628165.

Huang, H. Q., Li, X. H., Li, W. X. & Li, Z. X. (2011). Formation of high δ18O fayalite-bearing A-type granite by high-temperature melting of granulitic metasedimentary rocks, southern China. *Geology* **39**(10), 903–906. https://doi.org/10.1130/G32080.1.

Huang, Y., Chubakov, V., Mantovani, F., Rudnick, R. L. & McDonough, W. F. (2013). A reference earth model for the heat-producing elements and associated geoneutrino flux. *Geochemistry, Geophysics, Geosystems* **14**(6), 2003–2029. https://doi.org/10.1002/ggge.20129.

Hwang, S. L., Shen, P., Chu, H. T., Yui, T. F. & Lin, C. C. (2001). Genesis of microdiamonds from melt and associated multiphase inclusions in garnet of ultrahigh-pressure gneiss from Erzgebirge, Germany. *Earth and Planetary Science Letters* **188**(1–2), 9–15. https://doi.org/10.1016/S0012-821X(01)00314-4.

Hwang, S. L., Shen, P., Chu, H. T., Yui, T. F., Liou, J. G., Sobolev, N. V., Zhang, R.-Y., Shatsky, V. S. & Zayachkovsky, A. A. (2004). Kokchetavite: a new potassium-feldspar polymorph from the Kokchetav ultrahigh-pressure terrane. *Contributions to Mineralogy and Petrology* **148**, 380–389. https://doi.org/10.1007/s00410-004-0610-2.

Hwang, S. L., Shen, P., Chu, H. T., Yui, T. F., Liou, J. G. & Sobolev, N. V. (2009). Kumdykolite, an orthorhombic polymorph of albite, from the Kokchetav ultrahigh-pressure massif, Kazakhstan. *European Journal of Mineralogy* **21**(6), 1325–1334. https://doi.org/10.1127/0935-1221/2009/0021-1970.

Iaccarino, S., Montomoli, C., Carosi, R., Massonne, H. J. & Visonà, D. (2017). Geology and tectono-metamorphic evolution of the Himalayan metamorphic core: insights from the Mugu Karnali transect, Western Nepal (central Himalaya). *Journal of Metamorphic Geology* **35**(3), 301–325. https://doi.org/10.1111/jmg.12233.

Janák, M., Borghini, A., Klonowska, I., Yoshida, K., Dujnič, V., Kurylo, S., Froitzheim, N., Petrík, I. & Majka, J. (2024). Metamorphism and partial melting at UHP conditions revealed by microdiamonds and melt inclusions in metapelitic gneiss from Heia, Arctic Caledonides, Norway. *Journal of Petrology* **65**. https://doi.org/10.1093/petrology/egae114.

Jaupart, C., & Mareschal, J.-C. (2003). Constraints on crustal heat production from heat owdata. In: Rudnick, R.L. (Ed.), The Crust, Vol. 3 *Treatise on Geochemistry (Eds. H.D.Holland and K.K. Turekian)*. Elsevier-Pergamon, Oxford, pp. 65–84.

Ji, M., Gao, X. Y., & Zheng, Y. F. (2023). The petrogenetic relationship between migmatite and granite in the Himalayan orogen: Petrological and geochemical constraints. *Lithos*, **444**, 107110.

Johannes, W. (1989). Melting of plagioclase-quartz assemblages at 2 kbar water pressure. *Contributions to Mineralogy and Petrology*, **103**(3), 270–276.

Johannes, W., & Holtz, F. (1996). The haplogranite system Qz-Ab-Or. In *Petrogenesis and Experimental Petrology of Granitic Rocks*, vol 22. Berlin, Heidelberg: Springer, p. 18–57.

Johnson, T., Yakymchuk, C. & Brown, M. (2021). Crustal melting and suprasolidus phase equilibria: from first principles to the state-of-the-art. *Earth-Science Reviews* **221**, 103778. https://doi.org/10.1016/j.earscirev.2021.103778.

Kang, D., Zhang, Z., Palin, R. M., Tian, Z. & Dong, X. (2020). Prolonged partial melting of garnet amphibolite from the eastern Himalayan syntaxis: implications for the tectonic evolution of large hot orogens. *Journal of Geophysical Research: Solid Earth* **125**(6), e2019JB019119. https://doi.org/10.1029/2019JB019119.

Kawakami, T., Yamaguchi, I., Miyake, A., Shibata, T., Maki, K., Yokoyama, T. D. & Hirata, T. (2013). Behavior of zircon in the upper-amphibolite to granulite facies schist/migmatite transition, Ryoke metamorphic belt, SW Japan: constraints from the melt inclusions in zircon. *Contributions to Mineralogy and Petrology* **165**, 575–591. https://doi.org/10.1007/s00410-012-0824-7.

Kendrick, J. & Yakymchuk, C. (2020). Garnet fractionation, progressive melt loss and bulk composition variations in anatectic metabasites: complications for interpreting the geodynamic significance of TTGs. *Geoscience Frontiers* **11**(3), 745–763. https://doi.org/10.1016/j.gsf.2019.12.001.

Khanal, G. P., Wang, J. M., Wu, F. Y., Wang, J. G. & Yang, L. (2020). In-sequence buoyancy extrusion of the Himalayan metamorphic core, Central Nepal: constraints from monazite petrochronology and thermobarometry. *Journal of Asian Earth Sciences* **199**, 104406. https://doi.org/10.1016/j.jseaes.2020.104406.

Klonowska, I., Janák, M., Majka, J., Petrik, I., Froitzheim, N., Gee, D. G. & Sasinková, V. (2017). Microdiamond on Åreskutan confirms regional UHP metamorphism in the Seve nappe complex of the Scandinavian Caledonides. *Journal of Metamorphic Geology* **35**(5), 541–564. https://doi.org/10.1111/jmg.12244.

Korhonen, F. J., Brown, M., Clark, C. & Bhattacharya, S. (2013). Osumilite–melt interactions in ultrahigh temperature granulites: phase equilibria modelling and implications for theP–T–tevolution of the eastern Ghats Province,India. *Journal of Metamorphic Geology* **31**(8), 881–907. https://doi.org/10.1111/jmg.12049.

Korsakov, A. V. & Hermann, J. (2006). Silicate and carbonate melt inclusions associated with diamonds in deeply subducted carbonate rocks. *Earth and Planetary Science Letters* **241**(1–2), 104–118. https://doi.org/10.1016/j.epsl.2005.10.037.

Kotková, J., Škoda, R. & Machovič, V. (2014). Kumdykolite from the ultrahigh-pressure granulite of the bohemian massif. *American Mineralogist* **99**(8–9), 1798–1801. https://doi.org/10.2138/am.2014.4889.

Lang, H. M. & Gilotti, J. A. (2007). Partial melting of metapelites at ultrahigh-pressure conditions, Greenland Caledonides. *Journal of Metamorphic Geology* **25**(2), 129–147. https://doi.org/10.1111/j.1525-1314.2006.00687.x.

Li, H. Y., Chen, R. X., Zheng, Y. F., & Hu, Z. (2016). The crust-mantle interaction in continental subduction channels: Zircon evidence from orogenic peridotite in the Sulu orogen. *Journal of Geophysical Research: Solid Earth*, **121**(2), 687–712.

Li, W. C., Chen, R. X., Zheng, Y. F., Tang, H. & Hu, Z. (2016a). Two episodes of partial melting in ultrahigh-pressure migmatites from deeply subducted continental crust in the Sulu orogen, China. *Bulletin* **128**(9–10), 1521–1542. https://doi.org/10.1130/B31366.1.

Li, J., Bassett, W. A., Chou, I., Ding, X., Li, S. & Wang, X. (2016b). An improved hydrothermal diamond anvil cell. *Review of Scientific Instruments* **87**(5). https://doi.org/10.1063/1.4947506.

Li, J., Chou, I., Bassett, W. A. & Wang, X. (2020). A new type of hydrothermal diamond-anvil cell with cooling system. *Review of Scientific Instruments* **91**(5), 053104. https://doi.org/10.1063/1.5143596.

Li, B., Massonne, H. J., Hartmann, L. A., Zhang, J. & Luo, T. (2021). Kyanite-garnet granulite from the Andrelândia nappe system, Brasília belt, registers two late Neoproterozoic metamorphic cycles. *Precambrian Research* **355**, 106086. https://doi.org/10.1016/j.precamres.2020.106086.

Li, S., Li, J. & Chou, I. M. (2022). Experimental melt inclusion homogenization in a hydrothermal diamond-anvil cell: comparison with homogenization at one atmosphere. *American Mineralogist* **107**(1), 65–73. https://doi.org/10.2138/am-2021-7781.

Liu, Y., Zhang, Y. & Behrens, H. (2005). Solubility of H2O in rhyolitic melts at low pressures and a new empirical model for mixed H2O–CO2 solubility in rhyolitic melts. *Journal of Volcanology and Geothermal Research* **143**, 219–235. https://doi.org/10.1016/j.jvolgeores.2004.09.019.

Liu, Q., Hermann, J. & Zhang, J. (2013). Polyphase inclusions in the Shuanghe UHP eclogites formed by subsolidus transformation and incipient melting during exhumation of deeply subducted crust. *Lithos* **177**, 91–109. https://doi.org/10.1016/j.lithos.2013.06.010.

Liu, P., Wu, Y., Liu, Q., Zhang, J., Zhang, L. & Jin, Z. (2014). Partial melting of UHP calc-gneiss from the Dabie Mountains. *Lithos* **192-195**, 86–101. https://doi.org/10.1016/j.lithos.2014.01.012.

Liu, P. H., Liu, F. L., Tian, Z. H., Cai, J., Ji, L. & Wang, F. (2019). Petrological and geochronological evidence for Paleoproterozoic granulite-facies metamorphism of the south Liaohe Group in the Jiao-Liao-Ji belt, North China craton. *Precambrian Research* **327**, 121–143. https://doi.org/10.1016/j.precamres.2019.03.002.

Liu, Q., Hermann, J., Zheng, S. & Zhang, J. (2020). Evidence for UHP anatexis in the Shuanghe UHP paragneiss from inclusions in clinozoisite, garnet, and zircon. *Journal of Metamorphic Geology* **38**(2), 129–155. https://doi.org/10.1111/jmg.12515.

Liu, S., Zhang, G., Zhang, L., Wang, S., Upreti, B. N., Adhikari, D. P. & Wang, J. (2022). Diverse anatexis in the Main central thrust zone, eastern Nepal: implications for melt evolution and exhumation process of the Himalaya. *Journal of Petrology* **63**(3), egac003. https://doi.org/10.1093/petrology/egac003.

Liu, S., Zhang, G., Zhang, L. & Webb, A. A. G. (2023). Omphacite melting and the destruction of early high-pressure rock records. *Journal of Geophysical Research: Solid Earth* **128**(11), e2023JB027395. https://doi.org/10.1029/2023JB027395.

Liu, Z., Carvalho, B. B., Li, W., Tong, L., Bartoli, O., Chen, L. & Wu, H. (2023a). Into the high to ultrahigh temperature melting of Earth's crust: investigation of melt and fluid inclusions within Mg-rich Metapelitic Granulites from the Mather peninsula, East Antarctica. *Journal of Petrology* **64**(7), egad051. https://doi.org/10.1093/petrology/egad051.

Liu, Q., Liu, P., Li, X. & Zhang, J. (2023b). The origin and compositions of melt inclusions in an Al2SiO5-free paragneiss from the Namche Barwa complex in the eastern Himalayan Syntaxis. *Journal of Metamorphic Geology* **41**(7), 879–898. https://doi.org/10.1111/jmg.12721.

Liu, Z., Chen, L., Carvalho, B. B. & Li, C. (2024). Post–peak petrochronology and C–O–H fluid influx in the lower crust: a case study of garnet–orthopyroxene granulites from the Rauer Islands, East Antarctica. *Lithos* **482-483**, 107722. https://doi.org/10.1016/j.lithos.2024.107722.

Loiselle, M. C. & Wones, D. R. (1979). Characteristics and origin of anorogenic granites. *Geological Society of America Abstracts with Programs* **11**, 468.

Lowenstern, J. B. (1995) Applications of silicate melt inclusions to the study of magmatic volatiles. In: Thompson J. F. H. (ed) *Magmas, Fluids and Ore Deposits*, Vol. **23**. Mineralogical Association of Canada Short Course, pp.71–99.

Luth, W. C., Jahns, R. H. & Tuttle, O. F. (1964). The granite system at pressures of 4 to 10 kilobars. *Journal of Geophysical Research* **69**(4), 759–773. https://doi.org/10.1029/JZ069i004p00759.

Madyukov, I. A., Chupin, V. P. & Kuzmin, D. V. (2011). Genesis of scapolite from granulites (lower-crustal xenoliths from the Pamir diatremes): results of study of melt inclusions. *Russian Geology and Geophysics* **52**(11), 1319–1333. https://doi.org/10.1016/j.rgg.2011.10.005.

Maffeis, A., Ferrando, S., Connolly, J. A., Groppo, C., Frezzotti, M. L. & Castelli, D. (2021). Thermodynamic analysis of HP-UHP fluid inclusions: the solute load and chemistry of metamorphic fluids. *Geochimica et Cosmochimica Acta* **315**, 207–229. https://doi.org/10.1016/j.gca.2021.08.044.

Malaspina, N., Hermann, J., Scambelluri, M. & Compagnoni, R. (2006). Polyphase inclusions in garnet–orthopyroxenite (Dabie Shan, China) as monitors for metasomatism and fluid-related trace element transfer in subduction zone peridotite. *Earth and Planetary Science Letters* **249**(3–4), 173–187. https://doi.org/10.1016/j.epsl.2006.07.017.

March, S., Hand, M., Tamblyn, R., Carvalho, B. B. & Clark, C. (2022). A diachronous record of metamorphism in metapelites of the Western gneiss region, Norway. *Journal of Metamorphic Geology* **40**(6), 1121–1158. https://doi.org/10.1111/jmg.12660.

Mareschal, J. C. & Jaupart, C. (2004). Variations of surface heat flow and lithospheric thermal structure beneath the north American craton. *Earth and Planetary Science Letters* **223**(1–2), 65–77. https://doi.org/10.1016/j.epsl.2004.04.002.

Massey, M. A., Prior, D. J. & Moecher, D. P. (2011). Microstructure and crystallographic preferred orientation of polycrystalline microgarnet aggregates developed during progressive creep, recovery, and grain boundary sliding. *Journal of Structural Geology* **33**(4), 713–730. https://doi.org/10.1016/j.jsg.2010.12.009.

Massonne, H. J. (2014). Wealth of P–T–t information in medium-high grade metapelites: example from the Jubrique unit of the Betic cordillera, S Spain. *Lithos* **208-209**, 137–157. https://doi.org/10.1016/j.lithos.2014.08.027.

Meng, Z. Y., Gao, X. Y., Chen, R. X., Zheng, Y. F., Zhang, Q. Q., & Ji, M. (2021). Fluid-present and fluid-absent melting of muscovite in migmatites in the Himalayan orogen: Constraints from major and trace element zoning and phase equilibrium relationships. *Lithos*, **388**, 106071.

Miranda, E. A. & Klepeis, K. A. (2016). The interplay and effects of deformation and crystallized melt on the rheology of the lower continental crust, Fiordland, New Zealand. *Journal of Structural Geology* **93**, 91–105. https://doi.org/10.1016/j.jsg.2016.09.007.

Moin, B., Guillot, C. & Gibert, F. (1994). Controls of the composition of nitrogen-rich fluids originating from reaction with graphite and ammonium-bearing biotite. *Geochimica et Cosmochimica Acta* **58**(24), 5503–5523. https://doi.org/10.1016/0016-7037(94)90246-1.

Moore, L. R., Gazel, E., Tuohy, R., Lloyd, A. S., Esposito, R., Steele-MacInnis, M., Hauri, E. H., Wallace, P. J., Plank, T. & Bodnar, R. J. (2015). Bubbles matter: an assessment of the contribution of vapor bubbles to melt inclusion volatile budgets. *American Mineralogist* **100**(4), 806–823. https://doi.org/10.2138/am-2015-5036.

Morgan, G. B. & London, D. (1996). Chemistry of bone mineral, based on the hypermineralized rostrum of the beaked whale Mesoplodon densirostris. *American Mineralogist* **99**, 645–653. https://doi.org/10.2138/am-1996-9-1016.

Morgan, G. B. V. I. & London, D. (2005). Effect of current density on the electron microprobe analysis of alkali aluminosilicate glasses. *American Mineralogist* **90**(7), 1131–1138. https://doi.org/10.2138/am.2005.1769.

Morizet, Y., Brooker, R. A., Iacono-Marziano, G. & Kjarsgaard, B. A. (2013). Quantification of dissolved CO_2 in silicate glasses using micro-Raman spectroscopy. *American Mineralogist* **98**(10), 1788–1802. https://doi.org/10.2138/am.2013.4516.

Morizet, Y., Gennaro, E., Jégo, S., Zajacz, Z., Iacono-Marziano, G., Pichavant, M. & Lesne, P. (2017). A Raman calibration for the quantification of SO42− groups dissolved in silicate glasses: application to natural melt inclusions. *American Mineralogist* **102**(10), 2065–2076. https://doi.org/10.2138/am-2017-6100.

Mosca, P., Groppo, C. & Rolfo, F. (2012). Structural and metamorphic features of the Main central thrust zone and its contiguous domains in the eastern Nepalese Himalaya. *Journal of the Virtual Explorer* **41**(2). https://doi.org/10.3809/jvirtex.2011.00294.

Moyen, J. F. (2011). The composite Archaean grey gneisses: petrological significance, and evidence for a non-unique tectonic setting for Archaean crustal growth. *Lithos* **123**(1–4), 21–36.

Muth, M., Duncan, M. S. & Dasgupta, R. (2020) The Effect of Variable Na/K on the CO2 Content of Slab-Derived Rhyolitic Melts. In: *Carbon in Earth's Interior*. Wiley, pp.195–208.

Nagurney, A. B., Caddick, M. J., Dragovic, B. & Busse, K. (2021). The (chemical) potential for understanding overstepped garnet nucleation and growth. *American Mineralogist* **106**(5), 812–829. https://doi.org/10.2138/am-2021-7354.

Németh, B., Török, K., Bali, E., Zajacz, Z., Fodor, L. & Szabó, C. (2021). Melt-rock interaction in the lower crust based on silicate melt inclusions in mafic garnet granulite xenoliths, Bakony-Balaton Highland volcanic field (Hungary). *Geologica Carpathica* **72**(3), 232–252. https://doi.org/10.31577/GeolCarp.72.3.4.

Newton, R. C., Smith, J. V. & Windley, B. F. (1980). Carbonic metamorphism, granulites and crustal growth. *Nature* **288**(5786), 45–50. https://doi.org/10.1038/288045a0.

Nicoli, G. & Ferrero, S. (2021a). Nanorocks, volatiles and plate tectonics. *Geoscience Frontiers* **12**(5), 101188. https://doi.org/10.1016/j.gsf.2021.101188.

Nicoli, G., Gresky, K. & Ferrero, S. (2021). Mesoarchean melt and fluid inclusions in garnet from the Kangerlussuaq basement, Southeast Greenland. *Mineralogia* **53**(1), 1–9. https://doi.org/10.2478/mipo-2022-0001.

O'Connor, J. T. (1965). A classification for quartz-rich igneous rocks based on feldspar ratios. *US geological survey professional paper B* **525**, 79–84.

Omori, N. E., Bobitan, A. D., Vamvakeros, A., Beale, A. M. & Jacques, S. D. (2023). Recent developments in X-ray diffraction/scattering computed tomography for materials science. *Philosophical Transactions of the Royal Society A* **381**(2259), 20220350. https://doi.org/10.1098/rsta.2022.0350.

Palin, R. M., White, R. W., Green, E. C., Diener, J. F., Powell, R. & Holland, T. J. (2016). High-grade metamorphism and partial melting of basic and intermediate rocks. *Journal of Metamorphic Geology* **34**(9), 871–892. https://doi.org/10.1111/jmg.12212.

Palke, A. C., Renfro, N. D. & Berg, R. B. (2016). Origin of sapphires from a lamprophyre dike at Yogo gulch, Montana, USA: clues from their melt inclusions. *Lithos* **260**, 339–344. https://doi.org/10.1016/j.lithos.2016.06.004.

Palke, A. C., Wong, J., Verdel, C. & Ávila, J. N. (2018). A common origin for Thai/Cambodian rubies and blue and violet sapphires from Yogo gulch, Montana, USA? *American Mineralogist* **103**(3), 469–479. https://doi.org/10.2138/am-2018-6164.

Papale, P., Moretti, R. & Barbato, D. (2006). The compositional dependence of the saturation surface of H2O+ CO2 fluids in silicate melts. *Chemical Geology* **229**(1–3), 78–95. https://doi.org/10.1016/j.chemgeo.2006.01.013.

Parisatto, M., Turina, A., Cruciani, G., Mancini, L., Peruzzo, L. & Cesare, B. (2018). Three-dimensional distribution of primary melt inclusions in garnets by X-ray microtomography. *American Mineralogist* **103**(6), 911–926. https://doi.org/10.2138/am-2018-6216.

Patiño Douce, A. E. & Harris, N. (1998). Experimental constraints on Himalayan anatexis. *Journal of Petrology* **39**(4), 689–710. https://doi.org/10.1093/petroj/39.4.689.

Patiño Douce, A. E. & Johnston, A. D. (1991). Phase equilibria and melt productivity in the pelitic system: implications for the origin of peraluminous granitoids and aluminous granulites. *Contributions to Mineralogy and Petrology* **107**, 202–218. https://doi.org/10.1007/BF00310707.

Perchuk, A. L., Burchard, M., Maresch, W. V. & Schertl, H. P. (2008). Melting of hydrous and carbonate mineral inclusions in garnet host during ultrahigh pressure experiments. *Lithos* **103**(1–2), 25–45. https://doi.org/10.1016/j.lithos.2007.09.008.

Peterson, J. W., Chacko, T. & Kuehner, S. M. (1991). The effects of fluorine on the vapor-absent melting of phlogopite+ quartz: implications for deep-crustal processes. *American Mineralogist* **76**, 470–476.

Philippot, P. (1993). Fluid-melt-rock interaction in mafic eclogites and coesite-bearing metasediments: constraints on volatile recycling during subduction. *Chemical Geology* **108**(1–4), 93–112. https://doi.org/10.1016/0009-2541(93)90319-E.

Philippot, P., Chevallier, P., Chopin, C. & Dubessy, J. (1995). Fluid composition and evolution in coesite-bearing rocks (Dora-Maira massif, Western Alps): implications for element recycling during subduction. *Contributions to Mineralogy and Petrology* **121**, 29–44. https://doi.org/10.1007/s004100050088.

Pownall, J. M., Armstrong, R. A., Williams, I. S., Thirlwall, M. F., Manning, C. J., & Hall, R. (2019). Miocene UHT granulites from Seram, eastern Indonesia: a geochronological–REE study of zircon, monazite and garnet. *Geological Society, London, Special Publications*, **478**(1), 167–196.

Putnis, A. (2002). Mineral replacement reactions: from macroscopic observations to microscopic mechanisms. *Mineralogical Magazine* **66**(5), 689–708. https://doi.org/10.1180/0026461026650056.

Rapa, G., Groppo, C., Mosca, P. & Rolfo, F. (2016). Petrological constraints on the tectonic setting of the Kathmandu nappe in the Langtang–Gosainkund–Helambu regions, Central Nepal Himalaya. *Journal of Metamorphic Geology* **34**(9), 999–1023. https://doi.org/10.1111/jmg.12219.

Rapp, R. P. & Watson, E. B. (1995). Dehydration melting of metabasalt at 8–32 kbar: implications for continental growth and crust-mantle recycling. *Journal of Petrology* **36**(4), 891–931. https://doi.org/10.1093/petrology/36.4.891.

Redler, C., Johnson, T. E., White, R. W. & Kunz, B. E. (2012). Phase equilibrium constraints on a deep crustal metamorphic field gradient: metapelitic rocks from the Ivrea zone (NW Italy). *Journal of Metamorphic Geology* **30**, 235–254. https://doi.org/10.1111/j.1525-1314.2011.00965.x.

Reubi, O., Blundy, J. & Varley, N. R. (2013). Volatiles contents, degassing and crystallisation of intermediate magmas at Volcan de Colima, Mexico, inferred from melt inclusions. *Contributions to Mineralogy and Petrology* **165**, 1087–1106. https://doi.org/10.1007/s00410-013-0849-6.

Reynes, J., Jollands, M., Hermann, J. & Ireland, T. (2018). Experimental constraints on hydrogen diffusion in garnet. *Contributions to Mineralogy and Petrology* **173**, 1–23. https://doi.org/10.1007/s00410-018-1492-z.

Roberts, N. M., Hernández-Montenegro, J. D. & Palin, R. M. (2024). Garnet stability during crustal melting: implications for chemical mohometry and secular change in arc magmatism and continent formation. *Chemical Geology* **659**, 122142. https://doi.org/10.1016/j.chemgeo.2024.122142.

Roedder, E. (1979). Origin and significance of magmatic inclusions. *Bulletin de Mineralogie* **102**(5), 487–510. https://doi.org/10.3406/bulmi.1979.7299.

Roedder, E. (1984). Volume 12: fluid inclusions. *Reviews in Mineralogy* **12**, 644.

Rosasco, G. J. & Roedder, E. (1979). Application of a new Raman microprobe spectrometer to nondestructive analysis of sulfate and other ions in individual phases in fluid inclusions in minerals. *Geochimica et Cosmochimica Acta* **43**(12), 1907–1915. https://doi.org/10.1016/0016-7037(79)90004-8.

Rose-Koga, E. F., Bouvier, A. S., Gaetani, G. A., Wallace, P. J., Allison, C. M., Andrys, J. A. & Zhou, T. (2021). Silicate melt inclusions in the new millennium: a review of recommended practices for preparation, analysis, and data presentation. *Chemical Geology* **570**, 120145. https://doi.org/10.1016/j.chemgeo.2021.120145.

Rossetti, F., Lucci, F., Theye, T., Bouybaouenne, M., Gerdes, A., Opitz, J., Dini, A. & Lipp, C. (2020). Hercynian anatexis in the envelope of the Beni Bousera peridotites (Alboran domain, Morocco): implications for the tectono-metamorphic evolution of the deep crustal roots of the Mediterranean region. *Gondwana Research* **83**, 157–182. https://doi.org/10.1016/j.gr.2020.01.020.

Rudnick, R. L. & Gao, S. (2003) *Composition of the Continental Crust, Volume 4*. Elsevier Ltd., pp.1–51.

Safonov, O. G., Mityaev, A. S., Yapaskurt, V. O., Belyanin, G. A., Elburg, M., Rajesh, H. M., Golunova, M. A., Shcherbakov, V. D., Butvina, V. G., van Reenen, D. D. & Smit, A. C. (2020). Carbonate-silicate inclusions in garnet as evidence for a carbonate-bearing source for fluids in leucocratic granitoids associated with granulites of the southern marginal zone, Limpopo complex, South Africa. *Gondwana Research* **77**, 147–167. https://doi.org/10.1016/j.gr.2019.07.012.

Schiavi, F., Bolfan-Casanova, N., Withers, A. C., Médard, E., Laumonier, M., Laporte, D., Flaherty, T. & Gómez-Ulla, A. (2018). Water quantification in silicate glasses by Raman spectroscopy: correcting for the effects of confocality, density and ferric iron. *Chemical Geology* **483**, 312–331. https://doi.org/10.1016/j.chemgeo.2018.02.036.

Schneider, P. & Balen, D. (2024). Inclusions in magmatic zircon from Slavonian mountains (eastern Croatia): anatase, kumdykolite and kokchetavite and implications for the magmatic evolution. *European Journal of Mineralogy* **36**(1), 209–223. https://doi.org/10.5194/ejm-36-209-2024.

Severs, M. J., Azbej, T., Thomas, J. B., Mandeville, C. W. & Bodnar, R. J. (2007). Experimental determination of H2O loss from melt inclusions during laboratory heating: evidence from Raman spectroscopy. *Chemical Geology* **237**(3–4), 358–371. https://doi.org/10.1016/j.chemgeo.2006.07.008.

Shatsky, V., Zedgenizov, D., Ragozin, A. & Kalinina, V. (2019). Silicate melt inclusions in diamonds of eclogite paragenesis from placers on the northeastern Siberian craton. *Minerals* **9**(7), 412. https://doi.org/10.3390/min9070412.

Shrestha, S., Larson, K. P., Duesterhoeft, E., Soret, M. & Cottle, J. M. (2019). Thermodynamic modelling of phosphate minerals and its implications for the development of PTt histories: a case study in garnet-monazite bearing metapelites. *Lithos* **334-335**, 141–160. https://doi.org/10.1016/j.lithos.2019.03.021.

Shrestha, S., Larson, K. P., Martin, A. J., Guilmette, C., Smit, M. A. & Cottle, J. M. (2020). The greater Himalayan thrust belt: insight into the assembly of the exhumed Himalayan metamorphic core, Modi Khola Valley, Central Nepal. *Tectonics* **39**(9), e2020TC006252. https://doi.org/10.1029/2020TC006252.

Sinton, C. W., Christie, D. M., Coombs, V. L., Nielsen, R. L. & Fisk, M. R. (1993). Near-primary melt inclusions in anorthite phenocrysts from the Galapagos Platfrom. *Earth and Planetary Science Letters* **119**(4), 527–537. https://doi.org/10.1016/0012-821X(93)90060-M.

Słupski, P. M. (2023) *Former Melt Inclusions in Garnet From UHP Gneisses of the Seve Nappe Complex, Scandinavian Caledonides*, Unpublished PhD thesis.

Słupski, P., Ferrero, S. & Walczak, K. (2018). Former melt inclusions in garnets from granulites of the Góry Sowie block, NE bohemian massif. *Geophys. Res* .

Sobolev, A. V., Dmitriev, L. V., Barsukov, V. L., Nevsorov, V. N., & Slutskii, A. B. (1980). The formation conditions of the high-magnesium olivines from the monomineralic fraction of Luna 24 regolith. In: *Lunar and Planetary Science Conference, 11th, Houston, TX, March 17–21, 1980, Proceedings. Volume 1.(A82–22251 09–91)*. New York: Pergamon Press, p. 105–116.

Sobolev, A. V., & Danyushevsky, L. V. (1994). Petrology and geochemistry of boninites from the north termination of the Tonga Trench: constraints on the generation conditions of primary high-Ca boninite magmas. *Journal of Petrology*, **35**(5), 1183–1211.

Sorby, H. C. (1858). On the microscopical, structure of crystals, indicating the origin of minerals and rocks. *Quarterly Journal of the Geological Society* **14**(1–2), 453–500. https://doi.org/10.1144/GSL.JGS.1858.014.01-02.44.

Sorger, D., Hauzenberger, C. A., Finger, F. & Linner, M. (2020). Two generations of Variscan garnet: implications from a petrochronological study of a high-grade Avalonia-derived paragneiss from the Drosendorf unit, bohemian massif. *Gondwana Research* **85**, 124–148. https://doi.org/10.1016/j.gr.2020.04.004.

Spear, F. S. (2017). Garnet growth after overstepping. *Chemical Geology* **466**, 491–499.

Spear, F. S. & Pyle, J. M. (2010). Theoretical modeling of monazite growth in a low-Ca metapelite. *Chemical Geology* **273**(1–2), 111–119.

Spear, F. S., Kohn, M. J. & Cheney, J. T. (1999). P-T paths from anatectic pelites. *Contributions to Mineralogy and Petrology* **134**, 17–32. https://doi.org/10.1007/s004100050466.

Stepanov, A. S., Hermann, J., Korsakov, A. V. & Rubatto, D. (2014). Geochemistry of ultrahigh-pressure anatexis: fractionation of elements in the Kokchetav gneisses during melting at diamond-facies conditions. *Contributions to Mineralogy and Petrology* **167**, 1–25. https://doi.org/10.1007/s00410-014-1002-x.

Stepanov, A. S., Hermann, J., Rubatto, D., Korsakov, A. V. & Danyushevsky, L. V. (2016). Melting history of an ultrahigh-pressure paragneiss revealed by multiphase solid inclusions in garnet, Kokchetav massif, Kazakhstan. *Journal of Petrology* **57**(8), egw049–egw1554. https://doi.org/10.1093/petrology/egw049.

Stöckhert, B., Duyster, J., Trepmann, C. & Massonne, H. J. (2001). Microdiamond daughter crystals precipitated from supercritical COH+ silicate fluids included in garnet, Erzgebirge, Germany. *Geology* **29**(5), 391–394. https://doi.org/10.1130/0091-7613(2001)029<0391:MDCPFS>2.0.CO;2.

Stöckhert, B., Trepmann, C. A. & Massonne, H. J. (2009). Decrepitated UHP fluid inclusions: about diverse phase assemblages and extreme decompression rates (Erzgebirge, Germany). *Journal of Metamorphic Geology* **27**(9), 673–684. https://doi.org/10.1111/j.1525-1314.2009.00835.x.

Stuart, C. A., Piazolo, S. & Daczko, N. R. (2018). The recognition of former melt flux through high-strain zones. *Journal of Metamorphic Geology* **36**(8), 1049–1069. https://doi.org/10.1111/jmg.12427.

Sun, J., Yang, Y., Ingrin, J., Wang, Z. & Xia, Q. (2022). Impact of fluorine on the thermal stability of phlogopite. *American Mineralogist* **107**(5), 815–825. https://doi.org/10.2138/am-2022-8051.

Suzuki, K., Kawakami, T., Kogiso, T., Sakata, S., Higashino, F., Yokoi, M. & Kudo, S. (2025). Tectonic Setting and Evolution of Anatectic Melt Composition During Prograde Metamorphism up to UHT Metamorphism: Constraints From P–T–t–Melting Path From Rundvågshetta, Lützow–holm Complex, East Antarctica. *Journal of Metamorphic Geology* . https://doi.org/10.1111/jmg.12815.

Tacchetto, T., Bartoli, O., Cesare, B., Berkesi, M., Aradi, L. E., Dumond, G. & Szabó, C. (2019). Multiphase inclusions in peritectic garnet from granulites of the Athabasca granulite terrane (Canada): evidence of carbon recycling during Neoarchean crustal melting. *Chemical Geology* **508**, 197–209.

Tacchetto, T., Reddy, S. M., Bartoli, O., Rickard, W. D., Fougerouse, D., Saxey, D. W., Quadir, Z. & Clark, C. (2021). Pre-nucleation geochemical heterogeneity within glassy anatectic inclusions and the role of water in glass preservation. *Contributions to Mineralogy and Petrology* **176**(9), 70. https://doi.org/10.1007/s00410-021-01826-0.

Tajčmanová, L., Connolly, J. A. D. & Cesare, B. (2009). A thermodynamic model for titanium and ferric iron solution in biotite. *Journal of Metamorphic Geology* **27**(2), 153–165. https://doi.org/10.1111/j.1525-1314.2009.00812.x.

Tamic, N., Behrens, H. & Holtz, F. (2001). The solubility of H2O and CO2 in rhyolitic melts in equilibrium with a mixed CO2–H2O fluid phase. *Chemical Geology* **174**(1–3), 333–347. https://doi.org/10.1016/S0009-2541(00)00324-7.

Tedeschi, M., Ferrero, S., Wunder, B., Hermann, J., Borghini, A., Pettke, T., Lanari, P., Paiva-Silva, P., Rubatto, D., Van Schijndel, V., Tollan, P. & O'Brien, P. J. (2024) *Nanorocks in Zircon From a Garnet-Free Granulite: Insights From Petrography and Major and Trace Element Compositions*, Abstract Book, Granulites & Granulites Conference, Verbania (Italy).

Thomas, R. (2000). Determination of water contents of granite melt inclusions by confocal laser Raman microprobe spectroscopy. *American Mineralogist* **85**(5–6), 868–872. https://doi.org/10.2138/am-2000-5-631.

Thomas, J. B., Bodnar, R. J., Shimizu, N. & Chesner, C. A. (2003). Melt inclusions in zircon. *Reviews in Mineralogy and Geochemistry* **53**(1), 63–87. https://doi.org/10.2113/0530063.

Thomas, R., Kamenetsky, V. S. & Davidson, P. (2006). Laser Raman spectroscopic measurements of water in unexposed glass inclusions. *American Mineralogist* **91**(2–3), 467–470.

Thompson, D. T. (1982). EULDPH: A new technique for making computer-assisted depth estimates from magnetic data. *Geophysics*, **47**(1), 31–37.

Touret, J. L. (1985). Fluid regime in southern Norway: the record of fluid inclusions. *The deep proterozoic crust in the north Atlantic provinces*, 517–549. https://doi.org/10.1007/978-94-009-5450-2_30.

Touret, J. L. & Huizenga, J. M. (2012). Fluid-assisted granulite metamorphism: a continental journey. *Gondwana Research* **21**(1), 224–235. https://doi.org/10.1016/j.gr.2011.07.022.

Vernon, R. H. (2007). Problems in identifying restite in S-type granites of southeastern Australia, with speculations on sources of magma and enclaves. *The Canadian Mineralogist* **45**(1), 147–178. https://doi.org/10.2113/gscanmin.45.1.147.

Vielzeuf, D. & Holloway, J. R. (1988). Experimental determination of the fluid-absent melting relations in the pelitic system: consequences for crustal differentiation. *Contributions to Mineralogy and Petrology* **98**, 257–276. https://doi.org/10.1007/BF00375178.

Vielzeuf, D., Clemens, J. D., Pin, C. & Moinet, E. (1990) Granites, granulites, and crustal differentiation. In: *Granulites and crustal evolution*. Dordrecht: Springer Netherlands, pp.59–85.

Vila, M., Fernández, M. & Jiménez-Munt, I. (2010). Radiogenic heat production variability of some common lithological groups and its significance to lithospheric thermal modeling. *Tectonophysics* **490**(3–4), 152–164. https://doi.org/10.1016/j.tecto.2010.05.003.

Wang, J., Zhang, J., Wei, C., Rai, S., Wang, M. & Qian, J. (2015). Characterising the metamorphic discontinuity across the Main central thrust zone of eastern-Central Nepal. *Journal of Asian Earth Sciences* **101**, 83–100. https://doi.org/10.1016/j.jseaes.2015.01.027.

Wang, J. M., Wu, F. Y., Rubatto, D., Liu, S. R., Zhang, J. J., Liu, X. C. & Yang, L. (2017). Monazite behaviour during isothermal decompression in pelitic granulites: a case study from Dinggye, Tibetan Himalaya. *Contributions to Mineralogy and Petrology* **172**, 1–30. https://doi.org/10.1007/s00410-017-1400-y.

Wannhoff, I., Ferrero, S., Borghini, A., Darling, R. & O'Brien, P. J. (2022). First evidence of dmisteinbergite (CaAl2Si2O8 polymorph) in high-grade metamorphic rocks. *American Mineralogist* **107**(12), 2315–2319. https://doi.org/10.2138/am-2022-8505.

Waters, D. J. (1988). Partial melting and the formation of granulite facies assemblages in Namaqualand, South Africa. *Journal of Metamorphic Geology* **6**(4), 387–404. https://doi.org/10.1111/j.1525-1314.1988.tb00430.x.

Watt, G. R. & Harley, S. L. (1993). Accessory phase controls on the geochemistry of crustal melts and restites produced during water-undersaturated partial melting. *Contributions to Mineralogy and Petrology* **114**(4), 550–566. https://doi.org/10.1007/BF00321759.

Webster, J. D. (2006) *Melt Inclusions in Plutonic Rocks*. In: *Mineralogical Association of Canada Short Course, vol. 36*, pp.165–188.

Webster, J. D., Vetere, F., Botcharnikov, R. E., Goldoff, B., McBirney, A., & Doherty, A. L. (2015). Experimental and modeled chlorine solubilities in aluminosilicate melts at 1 to 7000 bars and 700 to 1250 C: Applications to magmas of Augustine Volcano, Alaska. *American Mineralogist*, **100**(2-3), 522–535.

Whalen, J. B., Currie, K. L. & Chappell, B. W. (1987). A-type granites: geochemical characteristics, discrimination and petrogenesis. *Contributions to Mineralogy and Petrology* **95**, 407–419. https://doi.org/10.1007/BF00402202.

White, R. W., Powell, R., & Clarke, G. L. (2002). The interpretation of reaction textures in Fe-rich metapelitic granulites of the Musgrave Block, central Australia: constraints from mineral equilibria calculations in the system K2O–FeO–MgO–Al2O3–SiO2–H2O–TiO2–Fe2O3. *Journal of metamorphic Geology*, **20**(1), 41–55.

White, R. W., Powell, R. O. G. E. R., Holland, T. J. B., Johnson, T. E. & Green, E. C. R. (2014). New mineral activity–composition relations for thermodynamic calculations in metapelitic systems. *Journal of Metamorphic Geology* **32**(3), 261–286. https://doi.org/10.1111/jmg.12071.

Whitney, D. L., & Evans, B. W. (2010). Abbreviations for names of rock-forming minerals. *American mineralogist*, **95**(1), 185–187.

Wilke, S., Klahn, C., Bolte, T., Almeev, R. & Holtz, F. (2015). Experimental investigation of the effect of Ca, Fe and Ti on cotectic compositions of the rhyolitic system. *European Journal of Mineralogy* **27**(2), 147–159. https://doi.org/10.1127/ejm/2015/0027-2423.

Williams, M. A., Kelsey, D. E. & Rubatto, D. (2022). Thorium zoning in monazite: a case study from the Ivrea–Verbano zone, NW Italy. *Journal of Metamorphic Geology* **40**(6), 1015–1042. https://doi.org/10.1111/jmg.12656.

Xia, B., Zhang, L. & Bader, T. (2014). Zircon U–Pb ages and Hf isotopic analyses of migmatite from the 'paired metamorphic belt'in Chinese SW Tianshan: constraints on partial melting associated with orogeny. *Lithos* **192-195**, 158–179. https://doi.org/10.1016/j.lithos.2014.02.003.

Yakymchuk, C. (2023). Prograde zircon growth in migmatites. *Journal of Metamorphic Geology*, **41**(5), 719–743.

Yakymchuk, C. & Acosta-Vigil, A. (2019). Geochemistry of phosphorus and the behavior of apatite during crustal anatexis: insights from melt inclusions and nanogranitoids. *American Mineralogist* **104**(12), 1765–1780. https://doi.org/10.2138/am-2019-7054.

Yakymchuk, C. & Brown, M. (2014). Behaviour of zircon and monazite during crustal melting. *Journal of the Geological Society* **171**(4), 465–479. https://doi.org/10.1144/jgs2013-115.

Yakymchuk, C. & Brown, M. (2019). Divergent behaviour of Th and U during anatexis: implications for the thermal evolution of orogenic crust. *Journal of Metamorphic Geology* **37**(7), 899–916. https://doi.org/10.1111/jmg.12469.

Yakymchuk, C., Clark, C. & White, R. W. (2017). Phase relations, reaction sequences and petrochronology. *Reviews in Mineralogy and Geochemistry* **83**(1), 13–53. https://doi.org/10.2138/rmg.2017.83.2.

Yakymchuk, C., Kirkland, C. L. & Clark, C. (2018). Th/U ratios in metamorphic zircon. *Journal of Metamorphic Geology* **36**(6), 715–737. https://doi.org/10.1111/jmg.12307.

Yang, G., Chen, R. X., Zheng, Y. F., Xia, Q. X., Yu, Y. J., Li, K. & Zha, X. P. (2023). Multiple episodes of zircon growth during Anatectic metamorphism of metasedimentary rocks in collisional Orogens: constraints from felsic Granulites in the bohemian massif. *Journal of Earth Science* **34**(3), 609–639. https://doi.org/10.1007/s12583-021-1487-y.

Yu, S., Li, S., Zhang, J., Peng, Y., Somerville, I., Liu, Y. & Li, Y. (2019). Multistage anatexis during tectonic evolution from oceanic subduction to continental collision: a review of the north Qaidam UHP Belt, NW China. *Earth-Science Reviews* **191**, 190–211. https://doi.org/10.1016/j.earscirev.2019.02.016.

Zajacz, Z., Halter, W., Malfait, W. J., Bachmann, O., Bodnar, R. J., Hirschmann, M. M. & Webster, J. D. (2005). A composition-independent quantitative determination of the water content in silicate glasses and silicate melt inclusions by confocal Raman spectroscopy. *Contributions to Mineralogy and Petrology* **150**, 631–642. https://doi.org/10.1007/s00410-005-0040-9.

Zeng, L., Liang, F., Asimow, P., Chen, F., & Chen, J. (2009). Partial melting of deeply subducted continental crust and the formation of quartzofeldspathic polyphase inclusions in the Sulu UHP eclogites. *Chinese Science Bulletin*, **54**(15), 2580–2594.

Zhang, Z. M., Shen, K., Sun, W. D., Liu, Y. S., Liou, J. G., Shi, C. & Wang, J. L. (2008). Fluids in deeply subducted continental crust: petrology, mineral chemistry and fluid inclusion of UHP metamorphic veins from the Sulu orogen, eastern China. *Geochimica et Cosmochimica Acta* **72**(13), 3200–3228. https://doi.org/10.1016/j.gca.2008.04.014.

Zhang, Q. Q., Gao, X. Y., Chen, R. X. & Zheng, Y. F. (2020). Granulites record the tectonic evolution from collisional thickening to extensional thinning of the Tongbai orogen in Central China. *Journal of Metamorphic Geology* **38**(3), 265–295. https://doi.org/10.1111/jmg.12522.

Zhang, X. Z., Wang, Q., Wyman, D., Kerr, A. C., Dan, W. & Qi, Y. (2022). Tibetan plateau insights into> 1100° C crustal melting in the quaternary. *Geology* **50**(12), 1432–1437. https://doi.org/10.1130/G50387.1.

Zhang, G., Wu, C., Wang, Y., Zhang, L. & Webb, A. A. G. (2024). Rapid heating (<2 ma) to ultrahigh-temperature metamorphism via asthenospheric upwelling. *Science Advances* **10**(24), eadl4381. https://doi.org/10.1126/sciadv.adl4381.

Zou, L., Guo, J. H., Zhang, L. F., Huang, G. Y., Jiao, S. J., Tian, Z. H. & Liu, P. H. (2024). Paleoproterozoic ultrahigh-temperature mafic granulites with a high-pressure prograde path from the Alxa block: implications on the tectonic evolution of the Khondalite Belt, North China craton. *Journal of Metamorphic Geology* **42**(4), 551–581. https://doi.org/10.1111/jmg.12764.

Journal of Petrology, 2025, **66**, egaf053
https://doi.org/10.1093/petrology/egaf053
Perspectives in Petrology